



**Faculty of Electrical Technology and Engineering**

**DEVELOPMENT OF FLOATOVOLTAICS FOR WATER QUALITY  
MONITORING SYSTEM**

UNIVERSITI TEKNIKAL MALAYSIA MELAKA

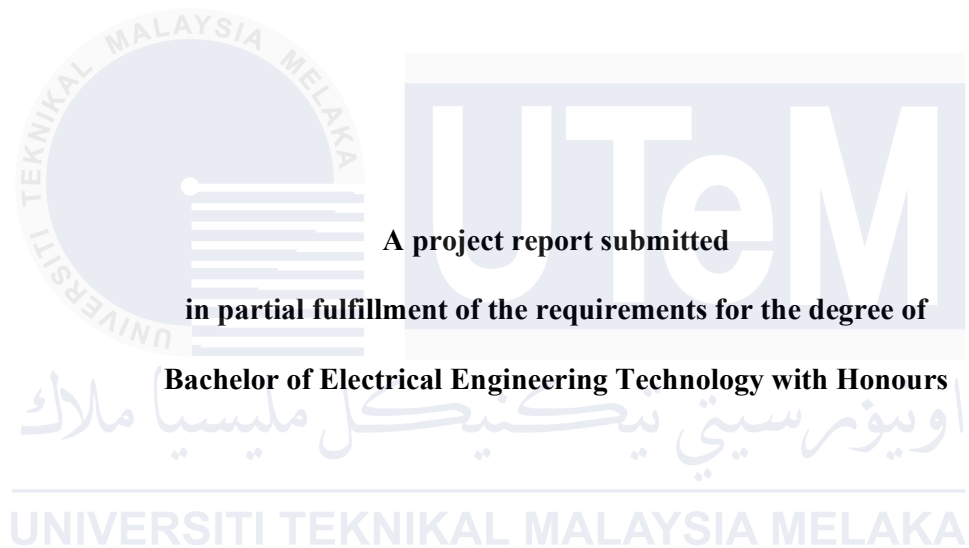
**MUHAMMAD ADIB BIN NORDIN**

**Bachelor of Electrical Engineering Technology with Honours**

**2024**

**DEVELOPMENT OF FLOATOVOLTAICS FOR WATER QUALITY  
MONITORING SYSTEM**

**MUHAMMAD ADIB BIN NORDIN**



**Faculty of Electrical Technology and Engineering**

**UNIVERSITI TEKNIKAL MALAYSIA MELAKA**

**2024**

## DECLARATION

I hereby declare that this project report entitled "Development of Floatovoltaics for Water Quality Monitoring System" is the outcome of my own research, except where references are cited. This project report has not been submitted for any other degree, nor is it being concurrently submitted for any other degree.



Signature :

Student Name : MUHAMMAD ADIB BIN NORDIN

Date : 26/01/2025

UNIVERSITI TEKNIKAL MALAYSIA MELAKA

## APPROVAL

I hereby declare that I have checked this project report and in my opinion, this project report is adequate in terms of scope and quality for the award of the degree of Bachelor of Electrical Engineering Technology with Honours.



Signature : TS. DR. SUZIANA BINTI AHMAD

Date : 26/01/2025

UNIVERSITI TEKNIKAL MALAYSIA MELAKA



## DEDICATION

*This work is dedicated to my parents, lecturers, friends, and siblings for their encouragement, support, understanding, and assistance in completing this final project.*



## ABSTRACT

Continuous water quality monitoring is essential for safeguarding aquatic ecosystems and ensuring potable water supplies. However, traditional methods based on manual sampling and laboratory analysis are both labor-intensive and expensive. Existing continuous monitoring systems often require grid connections or frequent battery replacements, hindering the deployment in remote water bodies. This project investigates the development of floatovoltaic (floating solar panel) powered water quality monitoring systems. A self-contained system that integrates floatovoltaics for energy generation, a suite of water quality sensors, a data acquisition system, and wireless data transmission capabilities was proposed. By integrating solar energy generation with an ESP32-based water quality monitoring system, the setup leverages renewable energy to power sensors for measuring key water parameters such as pH, total dissolved solids (TDS), and temperature. Floating solar panels provide a dual-purpose solution by not only generating clean energy but also potentially reducing water evaporation and algae growth in water bodies. The experimental setup aims to analyze the performance and reliability of the floating solar panel in powering the water quality monitoring system, ensuring an efficient and eco-friendly approach. This integrated system demonstrates the potential of renewable energy in advancing environmental monitoring technologies, contributing to sustainable development goals.

## ***ABSTRAK***

Pemantauan kualiti air yang berterusan adalah penting untuk melindungi ekosistem akuatik dan memastikan bekalan air yang boleh diminum. Walau bagaimanapun, kaedah tradisional berdasarkan persampelan manual dan analisis makmal adalah intensif buruh dan mahal. Sistem pemantauan berterusan sedia ada selalunya memerlukan sambungan grid atau penggantian bateri yang kerap, menghalang penggunaan di badan air terpencil. Projek ini menyiasat pembangunan sistem pemantauan kualiti air berkuasa floatovoltaic (panel suria terapung). Sistem serba lengkap yang menyepadukan floatovoltaics untuk penjanaan tenaga, set penerima kualiti air, sistem pemerolehan data dan keupayaan penghantaran data tanpa wayar telah dicadangkan. Dengan menyepadukan penjanaan tenaga suria dengan sistem pemantauan kualiti air berasaskan ESP32, persediaan memanfaatkan tenaga boleh diperbaharui kepada penerima kuasa untuk mengukur parameter air utama seperti pH, jumlah pepejal terlarut (TDS) dan suhu. Panel solar terapung menyediakan penyelesaian dwiguna dengan bukan sahaja menjana tenaga bersih tetapi juga berpotensi mengurangkan penyejatan air dan pertumbuhan alga dalam badan air. Persediaan eksperimen bertujuan untuk menganalisis prestasi dan kebolehpercayaan panel solar terapung dalam menjanakan sistem pemantauan kualiti air, memastikan pendekatan yang cekap dan mesra alam. Sistem bersepadu ini menunjukkan potensi tenaga boleh diperbaharui dalam memajukan teknologi pemantauan alam sekitar, menyumbang kepada matlamat pembangunan mampan.

## ACKNOWLEDGEMENTS

First and foremost, all praise is due to Allah SWT for granting me the ability and strength to complete my Final Year Project on the Development of floatovoltaics for water quality monitoring.

I would like to extend my deepest gratitude to my supervisor, TS. Dr. Suziana Binti Ahmad, for her invaluable guidance, wisdom, and patience throughout the duration of this project.

My utmost appreciation goes to my parents and family members for the unwavering love and prayers during my period of study.

Finally, I would like to thank all the staff at UTEM, my fellow colleagues and classmates, the faculty members, and everyone else who has been cooperative and helpful, even if not mentioned by name here.

## TABLE OF CONTENTS

	PAGE
DECLARATION	
APPROVAL	
DEDICATIONS	
ABSTRACT	i
ABSTRAK	ii
ACKNOWLEDGEMENTS	iii
TABLE OF CONTENTS	iv
LIST OF FIGURES	ix
LIST OF SYMBOLS	xv
LIST OF ABBREVIATIONS	xvi
LIST OF APPENDICES	xvii
 <b>CHAPTER 1                      INTRODUCTION</b>	 <b>18</b>
1.1      Project Background	18
1.2      Problem Statement	19
1.3      Project Objective	20
1.4      Scope of Project	20
 <b>CHAPTER 2                      LITERATURE REVIEW</b>	 <b>21</b>
2.1      Introduction	21
2.2      Renewable Energy	21

2.2.1	Solar energy	22
2.2.2	Wind Energy	25
2.2.3	Tidal Energy	26
2.2.4	Wave Energy	27
2.3	Solar PV System	30
2.3.1	Floating solar PV panel	31
2.3.2	Ground-mounted solar PV panel	33
2.3.3	Roof-mounted solar PV panel	34
2.4	Microcontrollers for water quality monitoring system	35
2.4.1	ESP32	36
2.4.2	ESP8266	37
2.4.3	Arduino Uno	38
2.4.4	Raspberry Pi	39
2.5	Water quality monitoring system	40
2.5.1	The pH of water	40
2.5.2	Temperature of water	41
2.5.3	Total Dissolved Solids (TDS) level in water	42
2.5.4	Turbidity of water	43
2.5.5	Oxygen level in water	44
2.6	Comparison of water quality monitoring system based on previous paper	45
2.7	Floating solar powered water quality monitoring system	47
2.8	Summary	55
<b>CHAPTER 3</b>	<b>METHODOLOGY</b>	<b>57</b>
3.1	Introduction	57
3.2	Flow chart of the the overall project development	57
3.2.1	Flowchart of solar PV sytem	59
3.2.2	Flowchart of water quality system	61
3.3	Block diagram of the floatovoltaics for water quality monitoring system development	63
3.4	Development of solar PV system	64
3.4.1	Block diagram of solar PV system	65
3.4.2	Components for solar PV system	66
3.4.3	Hardware setup for solar PV system	67
3.4.4	Measurement setup for solar PV system	68

3.5	Development of water quality system	69
3.5.1	Block diagram of the water quality system	69
3.5.2	Components and hardware setup in water quality system	71
3.5.3	Hardware setup	72
3.6	Floating mechanism for floating solar PV system	74
3.7	Software design for monitoring system development	76
3.7.1	Block diagram of monitoring system	76
3.7.2	Software used for monitoring system	77
3.8	Development of floatovoltaics for water quality monitoring	78
3.8.1	Componenet and hardware setup for the final product	79
3.8.2	Circuit design for the overall system	82
3.8.3	Real time hardware setup	83
3.9	Gantt Chart of the project (PSM 1)	86
3.10	Gantt Chart of the project (PSM 2)	87
3.11	Summary	88
<b>CHAPTER 4</b>	<b>RESULTS AND DISCUSSIONS</b>	<b>89</b>
4.1	Introduction	89
4.2	Data collected from solar PV system	90
4.3	Analysis for solar PV system	100
4.4	Data from floating solar power generation	102
4.5	Data tested from Water Quality Sensor	106
4.6	Data collected at Location 1 (Urban Reforestation)	112
4.7	Data collected at Location 2 (Taman Rimba)	114
4.8	Data collected at Location 3 (Tasik Ayer Keroh)	116
4.9	Analysis for pH, TDS and Temperature	119
4.10	Analysis for Solar	123
4.11	Analysis of Battery Capacity	127
4.12	Monitoring system	128
4.13	Summary	129
<b>CHAPTER 5</b>	<b>CONCLUSION AND RECOMMENDATIONS</b>	<b>130</b>
5.1	Conclusion	130
5.2	Future works	131
<b>REFERENCES</b>		<b>132</b>
<b>APPENDICES</b>		<b>139</b>

## LIST OF TABLES

<b>TABLE</b>	<b>TITLE</b>	<b>PAGE</b>
Table 2.1	Water quality monitoring system based on previous paper	45
Table 3.1	Component used in solar PV system	66
Table 3.2	Component used in water quality system	71
Table 3.3	Software for monitoring system	77
Table 4.1	Data collected for a week	90
Table 4.2	Analysis of power efficiency of the solar PV	100
Table 4.3	Solar generation at Urban Reforestation	102
Table 4.4	Data collected for temperature	106
Table 4.5	Data collected for TDS	108
Table 4.6	Data collected for pH	110
Table 4.7	Solar measurement at Location 1	112
Table 4.8	Water sample at Location 1	113
Table 4.9	Solar measurement at Location 2	114
Table 4.10	Water sample at Location 2	115
Table 4.11	Solar measurement at Location 3	116



<b>Table 4.12 Water sample at Location 3</b>	<b>117</b>
<b>Table 4.13 Summary of the pH analysis</b>	<b>119</b>
<b>Table 4.14 Summary of Tds analysis</b>	<b>121</b>
<b>Table 4.15 Summary of Temperature analysis</b>	<b>122</b>



## LIST OF FIGURES

FIGURE	TITLE	PAGE
Figure 2.1	Global solar direct normal distribution condition[3].	22
Figure 2.2	Global solar PV capacity from 2011-2021[3].	23
Figure 2.3	Working operation of solar energy[2]	24
Figure 2.4	World trends in renewable energy[4]	25
Figure 2.5	Potential Basin Area and Maximum Tidal Range at Various Locations in the Gulf of Kutch[7].	26
Figure 2.6	Oscillating water column working principle[9].	28
Figure 2.7	Pelamis(a), AquaBuoy(b) and Lysekil WEC (c), (d) [10].	29
Figure 2.8	Typical layout of floating PV system[13]	31
Figure 2.9	A small-scale FPV system illustration (left part) with the land-based system (right)[14].	32
Figure 2.10	Uneven tilt for the adjacent solar arrays[15]	33
Figure 2.11	Possible installation of solar panel on roof building[18].	34
Figure 2.12	ESP32 microcontrollers[20]	36
Figure 2.13	NodeMCU eps8266[22]	37

<b>Figure 2.14 Arduino UNO[24]</b>	<b>38</b>
<b>Figure 2.15 Rasberry Pi[26]</b>	<b>39</b>
<b>Figure 2.16 Smart pH sensor[28]</b>	<b>40</b>
<b>Figure 2.17 DS18B20 Temperature Sensor[31].</b>	<b>41</b>
<b>Figure 2.18 TDS sensor diagram[33]</b>	<b>42</b>
<b>Figure 2.19 Wiring diagram for analog turbidity sensor[34]</b>	<b>43</b>
<b>Figure 2.20 Oxygen sensor[37]</b>	<b>44</b>
<b>Figure 2.21 LoRaWan network architecture[27]</b>	<b>47</b>
<b>Figure 2.22 Structure design[27]</b>	<b>48</b>
<b>Figure 2.23 Whole setup based on Wemos chip and a multiplexer [39]</b>	<b>49</b>
<b>Figure 2.24 Conceptual framework for Water Quality Monitoring.[41]</b>	<b>51</b>
<b>Figure 2.25 Flow chart for Water Quality Assessment using ML[41].</b>	<b>51</b>
<b>Figure 2.26 Hardware design[42]</b>	<b>52</b>
<b>Figure 2.27 Blynk dashboard[42]</b>	<b>53</b>
<b>Figure 2.28 High level IoWT architecture [43]</b>	<b>54</b>
<b>Figure 2.29 IoWT domain model [43]</b>	<b>55</b>
<b>Figure 3.1 Flowchart of overall system</b>	<b>58</b>

<b>Figure 3.2 Flowchart of solar PV system</b>	<b>60</b>
<b>Figure 3.3 Flowchart of water quality system</b>	<b>62</b>
<b>Figure 3.4 Block diagram of the overall system</b>	<b>63</b>
<b>Figure 3.5 Solar PV system block diagram</b>	<b>65</b>
<b>Figure 3.6 Real life setup for solar PV system</b>	<b>67</b>
<b>Figure 3.7 Connection of solar PV system</b>	<b>68</b>
<b>Figure 3.8 Block diagram of the water quality system</b>	<b>70</b>
<b>Figure 3.9 ph sensor connection</b>	<b>72</b>
<b>Figure 3.10 TDS sensor connection</b>	<b>73</b>
<b>Figure 3.11 Temperature sensor connection.</b>	<b>74</b>
<b>Figure 3.12 Floating mechanism for floating solar PV system</b>	<b>75</b>
<b>Figure 3.13 Block diagram of monitoring system</b>	<b>76</b>
<b>Figure 3.14 Final product of the project</b>	<b>78</b>
<b>Figure 3.15 (a)Top view, (b)Front view, (c)Side view, (d)Perspective view</b>	<b>79</b>
<b>Figure 3.16 Layout of the electronic items used.</b>	<b>80</b>
<b>Figure 3.17 Connection of the electronic items</b>	<b>81</b>
<b>Figure 3.18 Wiring diagram for the overall system</b>	<b>82</b>

<b>Figure 3.19 Hardware setup at location 1</b>	<b>83</b>
<b>Figure 3.20 Hardware setup at location 2</b>	<b>84</b>
<b>Figure 3.21 Hardware setup at location 3</b>	<b>85</b>
<b>Figure 4.1 Voltage graph at day 1</b>	<b>91</b>
<b>Figure 4.2 Current graph at day 1</b>	<b>91</b>
<b>Figure 4.3 Voltage graph at day 2</b>	<b>92</b>
<b>Figure 4.4 Current graph at day 2</b>	<b>92</b>
<b>Figure 4.5 Voltage graph at day 3</b>	<b>93</b>
<b>Figure 4.6 Current graph at day 3</b>	<b>93</b>
<b>Figure 4.7 Voltage graph at day 4</b>	<b>94</b>
<b>Figure 4.8 Current graph at day 4</b>	<b>95</b>
<b>Figure 4.9 Voltage graph at day 5</b>	<b>95</b>
<b>Figure 4.10 Current graph at day 5</b>	<b>96</b>
<b>Figure 4.11 Voltage graph at day 6</b>	<b>96</b>
<b>Figure 4.12 Current graph at day 6</b>	<b>97</b>
<b>Figure 4.13 Voltage graph at day 7</b>	<b>97</b>
<b>Figure 4.14 Current graph at day 7</b>	<b>98</b>

<b>Figure 4.15 Voltage compared with <math>V_{mp}</math> graph</b>	<b>99</b>
<b>Figure 4.16 Current compared with <math>I_{mp}</math> graph</b>	<b>100</b>
<b>Figure 4.17 Average power compared with rated power graph</b>	<b>101</b>
<b>Figure 4.18 Voltage Vs Time</b>	<b>103</b>
<b>Figure 4.19 Current Vs Time</b>	<b>104</b>
<b>Figure 4.20 Power Vs Time</b>	<b>105</b>
<b>Figure 4.21 Temperature measurement graph</b>	<b>106</b>
<b>Figure 4.22 Temperature test setup</b>	<b>107</b>
<b>Figure 4.23 TDS measurement graph</b>	<b>108</b>
<b>Figure 4.24 TDS test setup</b>	<b>109</b>
<b>Figure 4.25 pH measurement graph</b>	<b>110</b>
<b>Figure 4.26 pH test setup</b>	<b>111</b>
<b>Figure 4.27 Graph Analysis of pH</b>	<b>119</b>
<b>Figure 4.28 Graph Analysis for TDS</b>	<b>120</b>
<b>Figure 4.29 Graph Analysis of Temperature</b>	<b>121</b>
<b>Figure 4.30 Graph Voltage A Vs Power A</b>	<b>123</b>
<b>Figure 4.31 Graph Current A Vs Power A</b>	<b>123</b>

<b>Figure 4.32 Graph Voltage B Vs Power B</b>	<b>124</b>
<b>Figure 4.33 Graph Current B Vs Power B</b>	<b>124</b>
<b>Figure 4.34 Graph Voltage C Vs Power C</b>	<b>125</b>
<b>Figure 4.35 Graph Current C Vs Power C</b>	<b>126</b>
<b>Figure 4.36 Blynk app interface</b>	<b>128</b>



## LIST OF SYMBOLS

% - Percentage

-

-

-



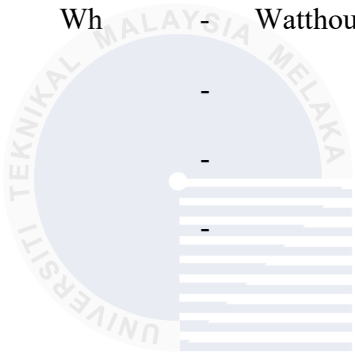
اونيورسيتي تيكنيكل مليسيا ملاك

UNIVERSITI TEKNIKAL MALAYSIA MELAKA



## LIST OF ABBREVIATIONS

$V$	-	Voltage
$I$	-	Current
$P$	-	Power
Ah	-	Amperehour
Wh	-	Watt-hour



اونيورسيتي تېكنيكل مليسيا ملاك

UNIVERSITI TEKNIKAL MALAYSIA MELAKA

## LIST OF APPENDICES

APPENDIX	TITLE	PAGE
	<b>Appendix A Solar panel specification</b>	<b>139</b>
	<b>Appendix B Solar Charge Contrroller specification</b>	<b>139</b>
	<b>Appendix C Battery specification</b>	<b>140</b>
	<b>Appendix D ESP32 Active Mode</b>	<b>140</b>
	<b>Appendix E TDS sensor arduino coding</b>	<b>141</b>
	<b>Appendix F pH sensor arduino coding</b>	<b>142</b>
	<b>Appendix G Temperature sensor arduino coding</b>	<b>143</b>
	<b>Appendix H Full system coding</b>	<b>144</b>

## CHAPTER 1

### INTRODUCTION

#### 1.1 Project Background

Traditional water quality monitoring relies on stationary systems that draw power from the grid. These systems are expensive to install and maintain, especially in remote locations, and the fixed positions limit the data that can be collected, providing an incomplete picture of water quality. Floatovoltaics, a combination of floating solar panels and environmental sensors, offers a compelling alternative.

This project centers around developing a water quality monitoring system powered by floatovoltaics. The system would utilize various sensors to gather real-time data on crucial water quality parameters like temperature, pH, dissolved oxygen, and conductivity. This data would then be transmitted wirelessly for immediate analysis and visualization. The successful implementation of this project has the potential to significantly transform water quality monitoring practices. By harnessing floatovoltaic technology, the project proposes a more sustainable, cost-effective, and wider-reaching approach to safeguarding our vital water resources.

## 1.2 Problem Statement

Ensuring the health of our water resources is critical, and traditional water quality monitoring systems often face limitations. These systems frequently rely on unreliable grid connections or battery backups, which can be expensive and environmentally harmful. Fossil fuel dependence for grid power and battery production contributes to greenhouse gas emissions. Therefore, solar-powered floating panels offer a promising solution that aligns with Sustainable Development Goal (SDG) 7: Affordable and Clean Energy. By harnessing the sun's clean energy, these panels can provide a sustainable power source for monitoring equipment. This eliminates reliance on non-renewable resources and minimizes the carbon footprint of monitoring operations. Additionally, floating panels efficiently utilize underutilized space on water bodies, maximizing sun exposure for power generation. However, implementing this solution requires innovative engineering. Water-resistant and weatherproof monitoring equipment needs to be developed to withstand the challenges of a freshwater environment (SDG 14: Life Below Water). Furthermore, efficient energy management systems are crucial to optimize power generation and usage, ensuring continuous monitoring even during fluctuating environmental conditions. By addressing these challenges, solar-powered floating panels can become a game-changer for water quality monitoring. This approach offers a reliable, cost-effective, and environmentally friendly way to safeguard our water resources, contributing significantly to achieving multiple Sustainable Development Goals set forth by the United Nations.

### 1.3 Project Objective

The primary objective of this project is to design, develop, and implement a novel approach to harness solar energy while concurrently monitoring water quality using floating solar panels. Specifically, the project aims to:

1. To develop solar energy generation using floating solar panels for water quality monitoring.
2. To implement water quality monitoring system using ESP32, pH sensor, TDS sensor and temperature sensor.
3. To analyze the floating solar panel for water quality monitoring system data experiments setup.

### 1.4 Scope of Project

The scope of this project are as follows:

- a) Developing a comprehensive system architecture to seamlessly integrate floating solar panels with the ESP8266 microcontroller and a range of sensors, including pH, total dissolved solids (TDS), and temperature sensors, for effective water quality monitoring.
- b) Ensuring the integration of floating solar panels with appropriately designed energy storage solutions to provide reliable and uninterrupted power for the continuous operation of water quality monitoring devices.
- c) Addressing the long-term sustainability and scalability of the project by considering its implications within the broader context of environmental conservation, efficient resource utilization, and effective management strategies.

## **CHAPTER 2**

### **LITERATURE REVIEW**

#### **2.1 Introduction**

Monitoring water quality is essential to preserving aquatic habitats and guaranteeing the availability of clean drinking water. Conventional techniques for monitoring water quality can entail labor-intensive, costly, and time-consuming manual sample collection and laboratory analysis. Recent advancements in technology have led to the development of innovative solutions for continuous, real-time water quality monitoring. One such promising technology is floatovoltaics, which combines floating solar panels with environmental sensors. This project report explores the development of floatovoltaics for water quality monitoring systems. This section provides a literature review that examines existing research on floatovoltaics, water quality monitoring systems, and integration.

#### **2.2 Renewable Energy**

The world's population is growing, and technological improvements have led to an exponential increase in the need for energy. Despite the adverse effects on the environment and human health, fossil fuels remain the primary energy source. Burning fossil fuels emits significant quantities of greenhouse gases like carbon dioxide, methane, and nitrous oxide. Furthermore, with the rapid expansion of industrial and civil activities, it is expected that these emissions will increase in the future [1]. Here are the main types of renewable energy such as solar energy[2],[3], wind energy[4],[5], tidal energy[6],[7] and wave energy[8],[9],[10].

### 2.2.1 Solar energy

Global population expansion and technological advancements are raising energy consumption. Economically disadvantaged regions, commonly known as the Global South, encounter various obstacles, including restricted availability of clean water, energy, industrialization, and food security[2]. Because of its plentiful, clean, and cost-free reserves, solar energy is regarded as one of the most promising alternative energy sources[3]. To address the impacts of climate change and reduce the global carbon footprint, solar energy has become indispensable. Figure 2.1 illustrates the global distribution of direct normal solar radiation[3].

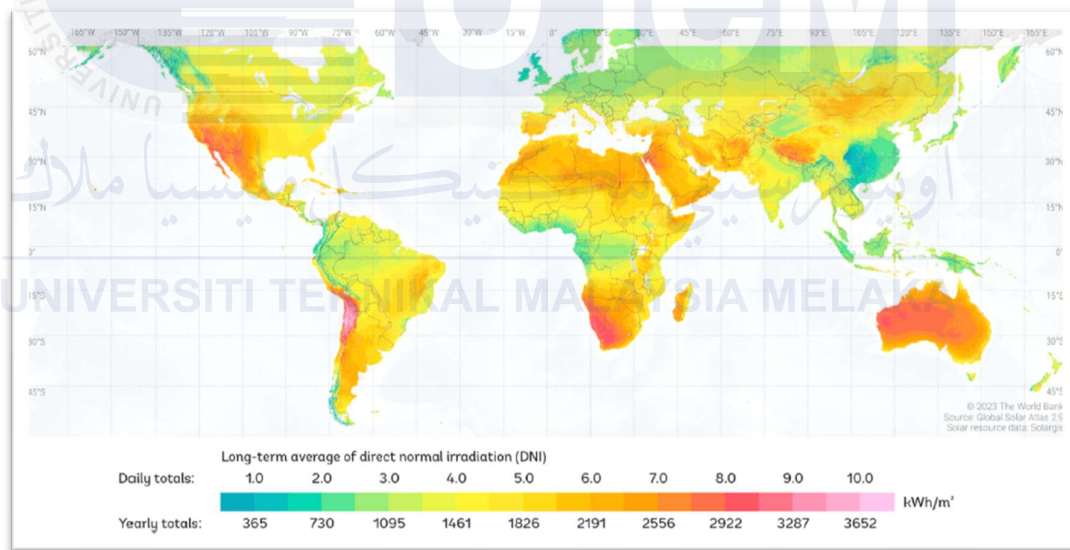


Figure 2.1 Global solar direct normal distribution condition[3].

Figure 2.1 presents the global distribution of direct normal solar irradiance. [3]. Solar energy is primarily utilized for providing thermal energy to consumers and generating electricity using photovoltaic (PV) cells, steam turbines, or alternative technologies,

following the capture of sunlight through various solar receivers. Figure 2.2 shows the global solar PV capacity from 2011 to 2021[3].

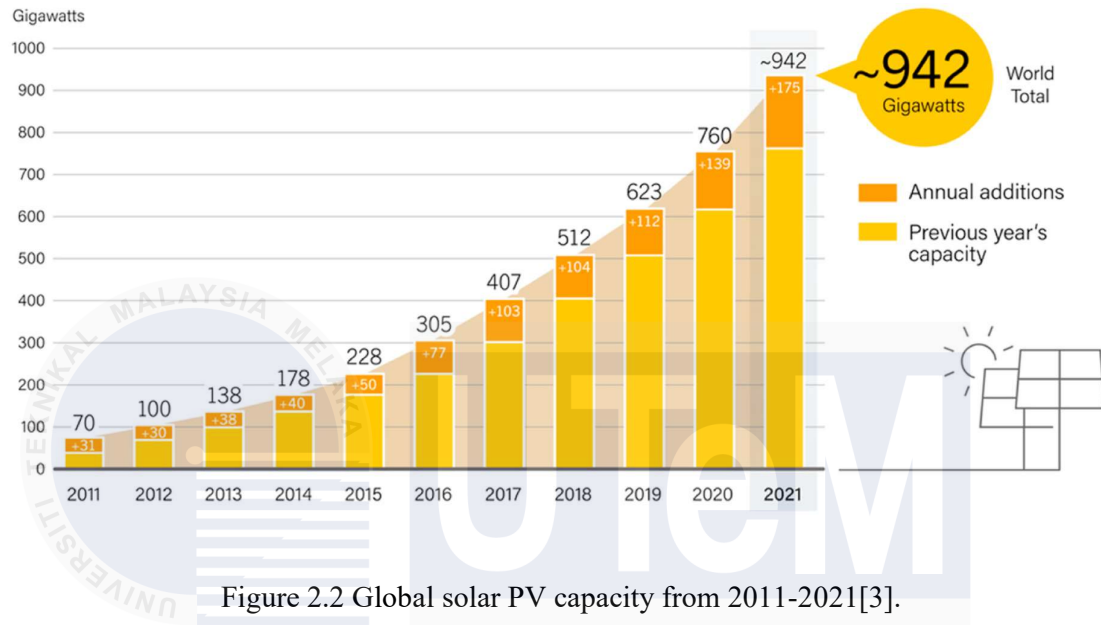


Figure 2.2 Global solar PV capacity from 2011-2021[3].

Figure 2.2 shows the global solar PV capacity trends from 2011 to 2021. Despite a notable growth in solar power output, the photovoltaic sector still needs specialists and technicians to use, design, and maintain the technologies[3]. The irregular and unpredictable nature of solar energy presents obstacles to the widespread adoption and commercialization of large-scale solar power generation, thus hindering the progress of solar energy development. The lack of supporting industries in Africa complicates the adoption of solar energy technologies, where photovoltaic technologies are not widely distributed. Adoption of solar energy, like the switch from animal to tractor power, can alter the production activities of farm families by offering a reliable supply of electricity. The working operation of solar energy presented in Figure 2.3 [2].



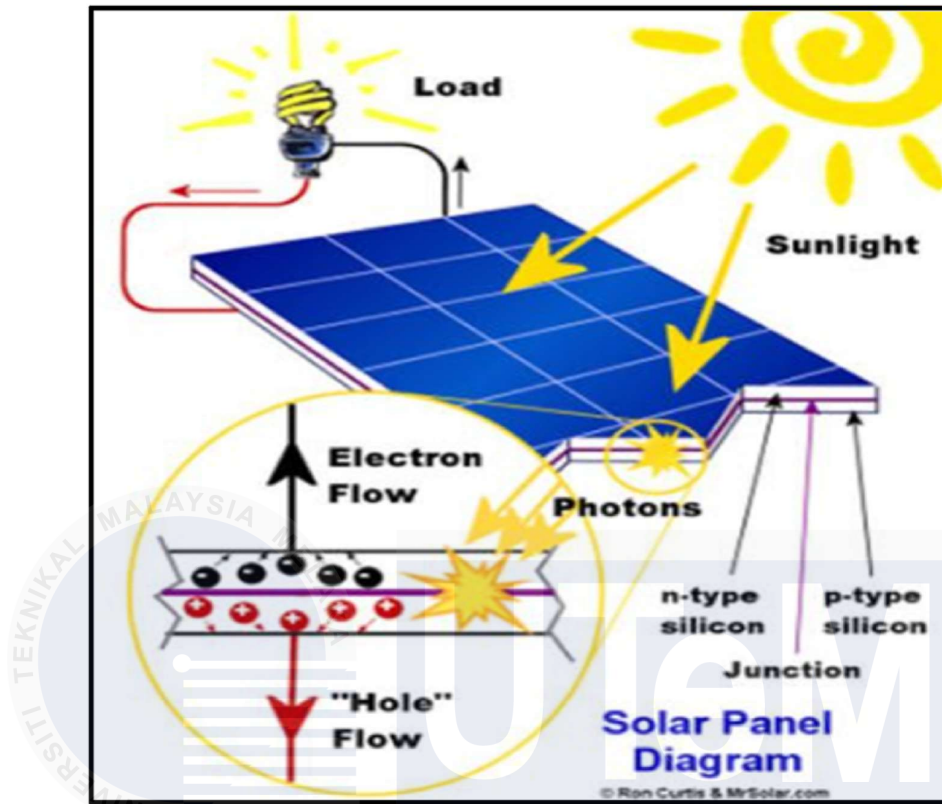


Figure 2.3 Working operation of solar energy[2]

Figure 2.3 illustrates the solar energy working operation[2]. Solar photovoltaic (PV) and solar thermal power generation are the two main types of solar power generation. Solar photovoltaic (PV) systems provide a decentralised solution that meets the demands of places without access to conventional energy by directly converting sunshine into power. Solar thermal systems harness heat from the sun to produce thermal energy for heating or electricity generation purposes[2]. Soiling, the buildup of dust particles on solar cell surfaces, can occur due to atmospheric dust. Weather conditions greatly influence the power output of photovoltaic (PV) systems, potentially leading to abrupt fluctuations in power production and increased operating costs .

### 2.2.2 Wind Energy

Wind energy is among the most widely adopted non-hydro renewable energy sources globally. Climate change stands out as a critical challenge confronting human civilization in the twenty-first century[4]. The rapid growth in wind energy shares is attributed to the decreasing Levelized Cost of Energy (LCOE) for wind farms and the global imperative to decarbonize our energy networks. Various countries are formulating extensive strategies to assess and forecast the potential for mitigating future global warming through the expansion of wind energy. The world trends in renewable energy shown in Figure 2.4 [4].

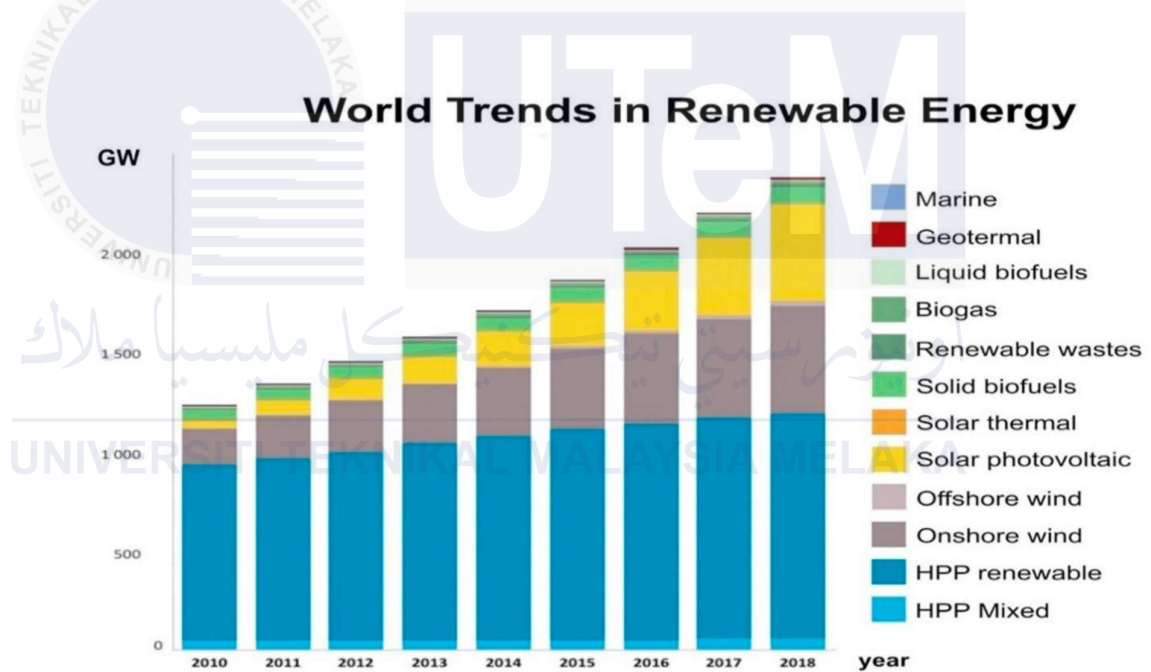


Figure 2.4 World trends in renewable energy[4]

Figure 2.4 illustrates that solar and wind energy generation are the most rapidly growing sectors of renewable energy (RE) [4]. Notably, wind energy has experienced particularly swift expansion in Europe. As the third-largest offshore market at the end of 2019, China was the nation with the largest installation of new offshore wind capacity (2.4

GW)[5]. China has an extensive wind energy potential, totaling over 4350 GW, making it one of the world's most significant resources.

### 2.2.3 Tidal Energy

The rise in electricity generation from renewable sources stems from the persistent demand for power, concerns over greenhouse gas emissions, and the dwindling availability of fossil fuels. As one of the first and most extensively explored new energy technologies, tidal power generation has matured into a reliable and competitive energy source[6]. Although there are obvious benefits to converting tidal energy into power, India's tidal energy resources are mainly unknown. In response to the unpredictability of solar and wind energy systems, some countries are exploring tidal energy systems for power generation. Figure 2.5 displays the probable basin area and maximum tidal range at various locations[7]

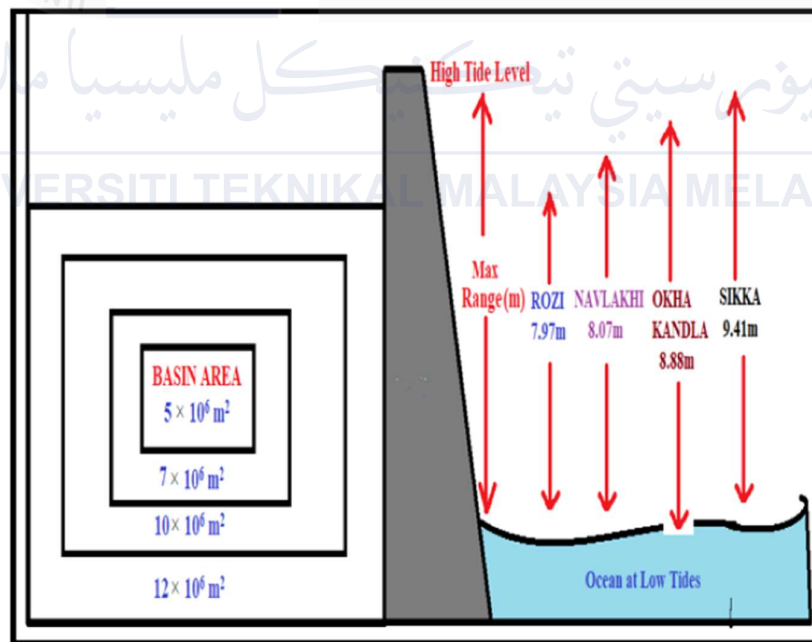


Figure 2.5 Potential Basin Area and Maximum Tidal Range at Various Locations in the Gulf of Kutch[7].

Figure 2.5 depicts the estimated basin area and maximum tidal range at various locations within the Gulf of Kutch [7]. There is still very little power produced worldwide from tidal energy. The integration of tidal energy within the larger framework of environmental value issues and regional economic growth is specifically addressed in this study. Modelling is the method utilised in the tidal energy system to develop the working framework for tidal power plants. Tidal energy stands out from other renewable sources due to its high predictability, relying mainly on the consistent movements of the sun, moon, and earth, which can be forecasted with significant accuracy well in advance. The ensuing fluctuations in power output and prediction precision pose significant obstacles to the effective allocation of grid assets[6].

#### **2.2.4 Wave Energy**

As the world grapples with the urgent challenges of climate change and increasing energy demand, there is a growing necessity for more reliable renewable energy sources. Wave energy stands out as having significant potential, estimated at around 32000 TWh/year of untapped capacity[8]. It represents a promising component of the renewable energy mix that warrants further development. However, wave energy converters face challenges with poor capacity factors in low-energy oceans or bays, as it are typically designed to harness energy from ocean waves. Figure 2.6 illustrates the operational concept of an oscillating water column[9]

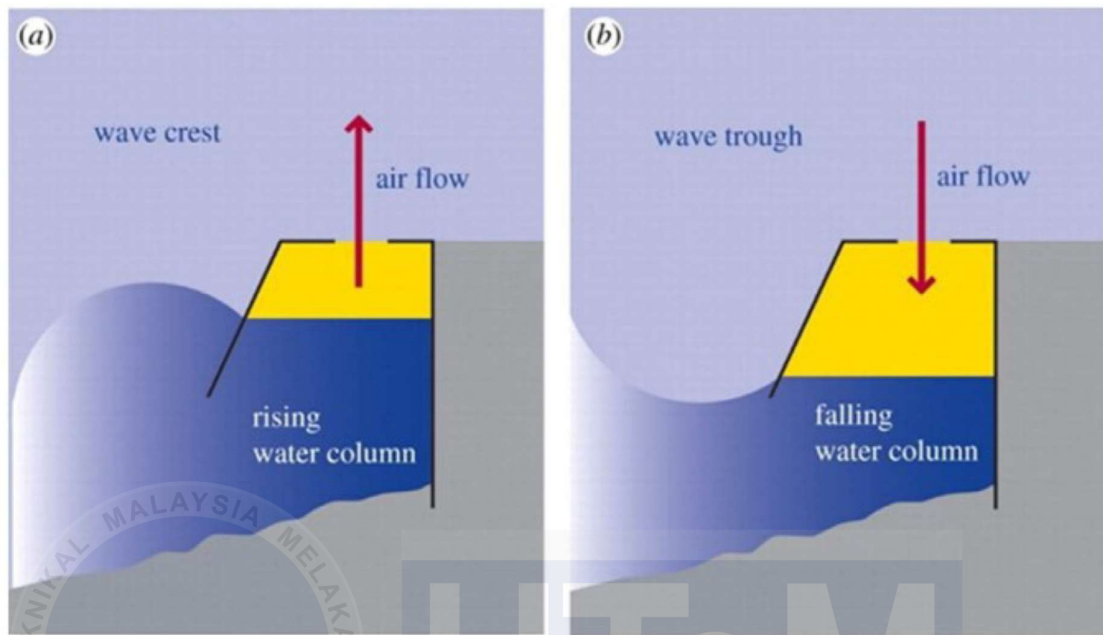


Figure 2.6 Oscillating water column working principle[9].

The operational mechanism of the oscillating water column is depicted in Figure 2.6[9]. Ocean energy encompasses various energy sources such as ocean currents, tides, waves, and temperature and salinity gradients, making it a captivating and versatile option.

The chosen indexes gave a more limited converter location pair possibility map, demonstrating that the wave resource was required but inadequate to choose viable locations.

Figure 2.7 shows three offshore wave energy converter (WEC) [10].

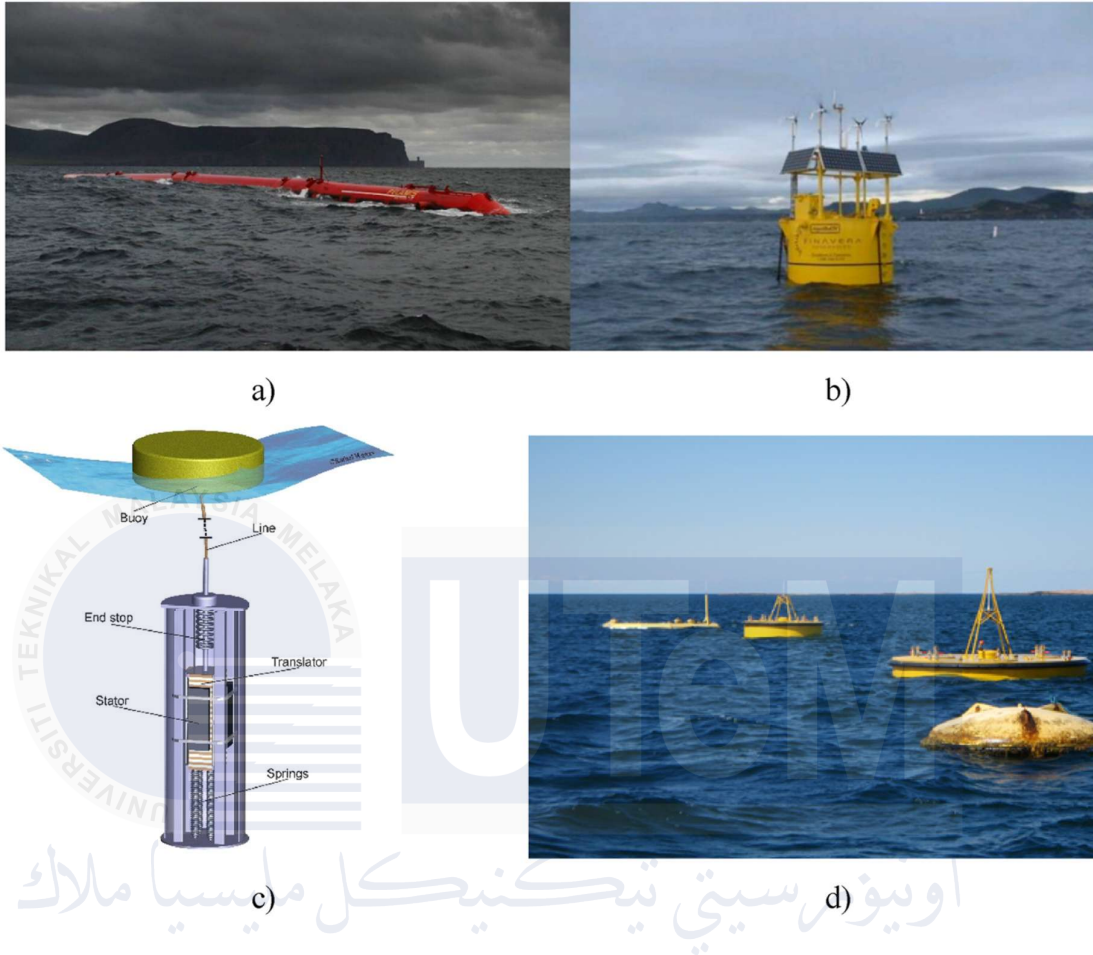


Figure 2.7 Pelamis(a), AquaBuoy(b) and Lysekil WEC (c), (d) [10].

The three offshore WEC is presented in Figure 2.7[10]. A sensitivity analysis was carried out to give a general picture of how different factors affected the price of energy. The rated power of the AquaBuoy is 250 kW, while the rated power of the Pelamis is 750 kW. The linear generator's stroke length determines the power generation of the Lysekil[10].

### 2.3 Solar PV System

Solar photovoltaic (PV) systems have gained considerable attention among scholars in recent decades as a favored renewable energy source. Essentially, a solar photovoltaic system is a mechanism designed to transform solar energy into electrical energy. It consists of one or more solar modules coupled to various electrical and mechanical components. For solar PV systems to operate economically, efficiently, and safely, the design must adhere to national and international power quality requirements while remaining dependable and affordable. The main limitations of solar photovoltaic (PV) systems include the expensive installation and relatively low power conversion efficiency, typically ranging from 9% to 17% [11]. Additionally, PV modules exhibit weather-dependent behavior and nonlinear characteristics. The International Renewable electricity Agency (IRENA) reports that between 2010 and 2016 there was a nearly 69% decrease in the levelized cost of electricity for solar photovoltaics [12]. 95% of continuously tracking systems indicate that south-facing slanted PV arrays track efficiently at midday[11]. Solar PV system can be classified into three major field such as floating [13], [14], ground [15], [16] and roof [17],[18]



### 2.3.1 Floating solar PV panel

Since photovoltaic (PV) power generating uses a clean and limitless energy source, compared to conventional power plants, it requires a bigger area per unit capacity. In response to land scarcity and rising costs, several nations, including Japan and Singapore, are strategically deploying floating photovoltaic (FPV) systems. Like conventional PV systems, a floating PV system is installed on top of water utilising floaters rather of utilising the land surface. These innovative installations utilize artificial water bodies, such as irrigation ponds, lakes, and reservoirs, for solar panel placement. Typical layout of floating PV system is shown in Figure 2.8 [13].

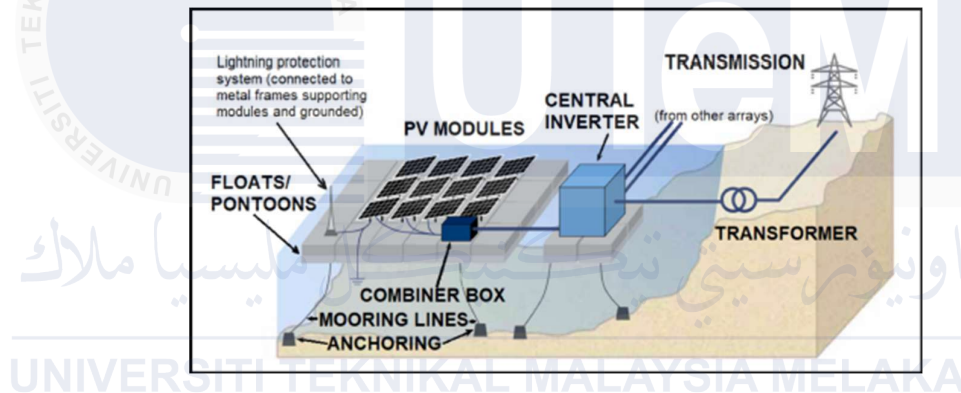


Figure 2.8 Typical layout of floating PV system[13]

An FPV system's overall design is similar to a typical GPV system, with the exception that, as Figure 2.8 illustrates, PV modules and frequently inverters are installed on a floating platform[13]. By blending with the surrounding water to become a part of the organic surroundings, FPV systems can offer aesthetic advantages. As an alternative to land, water surfaces can be utilised for solar plants, which will lessen the effect of temperature on photovoltaic cells and water evaporation. A small scale of FPV system and land-based system illustrate in Figure 2.9 [14].



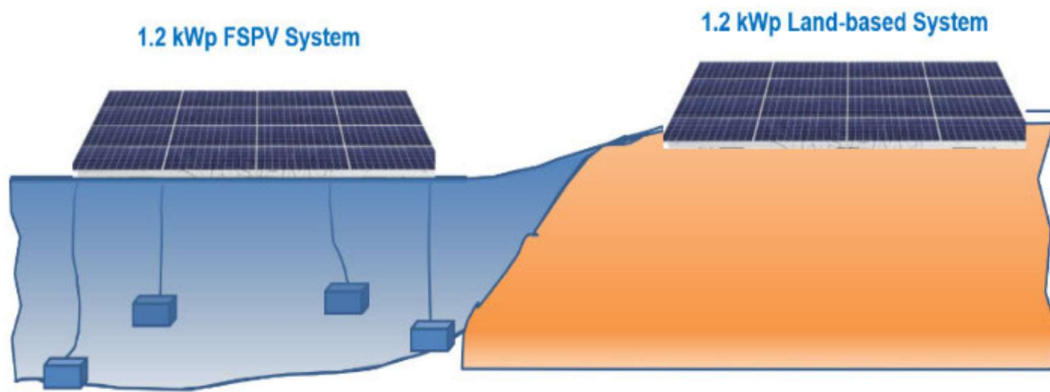


Figure 2.9 A small-scale FPV system illustration (left part) with the land-based system (right)[14].

Figure 2.9 presents a small scale of FPV system and land-based system[14]. It is possible to deploy FPV systems in manmade and natural reservoirs. Due to the high cost of buoyancy units for the PV modules, FPV installation was expensive. The cooling of the PV modules is a key factor in improving efficiency. Water cooling impact increases the solar panels' efficiency, which decreases with excessive heat. Because of the cooling impact and economical use of land, FPVs increase efficiency.

### 2.3.2 Ground-mounted solar PV panel

To generate electricity, photovoltaic modules (PV) are positioned in solar radiation at an angle that is sufficiently slanted to the ground. One of the most significant natural elements influencing photovoltaic performance is soiling, which has a long-term influence on the glass surface's deterioration and a significant reduction in the energy output of solar panels. The unequal tilt angle for the nearby solar arrays is seen in Figure 2.10[15].



Figure 2.10 Uneven tilt for the adjacent solar arrays[15]

Uneven tilt as seen in Figure 2.10 for the nearby solar arrays[15]. The ground-mounted solar panel was operated at tilt angles of  $25^{\circ}$  and  $45^{\circ}$ , and the wind directions were changed at intervals of  $30^{\circ}$  from  $0^{\circ}$  to  $180^{\circ}$ [16]. It has been noted that in many places, irregular structure frame systems, uneven ground conditions, and foundation flaws cause the tilt angle to vary or not be maintained constant for all solar arrays.

### 2.3.3 Roof-mounted solar PV panel

The use of solar photovoltaic (PV) on building rooftops has grown quickly all over the world since it is advantageous to produce solar electricity near energy users and doesn't require extra land. Solar panels installed on roofs are becoming more and more crucial to the construction of green energy structures[17]. From a structural standpoint, the roof-mounted solar panel arrays should be built to support the weight of the accumulated snow, wind forces exerted on the surface, and other dead loads, such as the electrical system and other attachments, in addition to the array's own weight. Figure 2.11 shows possible installation of solar panel on the roof of the building[18].

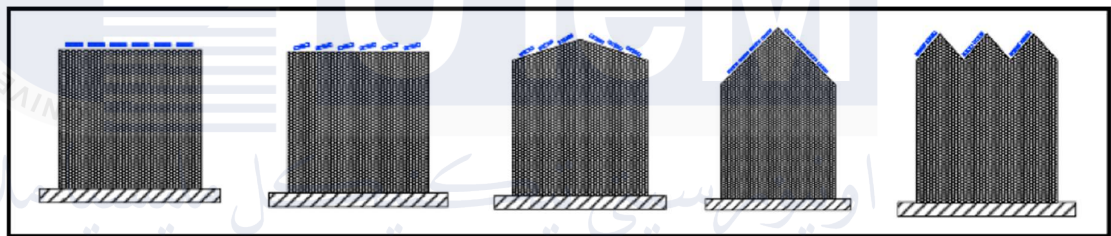


Figure 2.11 Possible installation of solar panel on roof building[18].

In Figure 2.11, PV systems are considered as attachments to the building exterior rather than as components of the building's structural structure[18]. The stability of rooftop solar photovoltaic systems and the accompanying structures is greatly impacted by wind forces. Building rooftop solar panels and supporting structures are subject to high wind loads, which are the main factor in load design. Solar panels on buildings must be designed to withstand wind pressures in a way that prevents damage to the PV module cover plate, the solar modules and the array supporting system. The biggest forces appeared in the unfavourable wind directions, where the most critical peak panel force coefficients were found[18].

## 2.4 Microcontrollers for water quality monitoring system

A microcontroller is a compact chip engineered to oversee designated functions within embedded systems. It amalgamates a processor, memory, and input/output components onto a single circuit. Widely employed in appliances, automobiles, and medical apparatus, microcontrollers excel at tailored tasks, boasting efficiency and reliability in real-time applications. Unlike general-purpose computers, its finely tuned for specific functions, making its adept at managing various electronic devices and machinery at a reasonable cost and energy consumption.

Functioning on a sequence of instructions stored in its memory, a microcontroller executes tasks in languages like C or assembly, dictating its interaction with electronic devices. Upon activation, it follows programmed code, encompassing activities such as data sensing, information processing, and actuator control. Continuously cycling through these instructions, it monitors peripheral inputs and adjusts outputs accordingly. The integrated design of a microcontroller ensures precise timing and effective management of real-time tasks, making it an ideal fit for embedded systems requiring specialized functions. Microcontroller can be classified into four major field such as ESP32 [19],[20], ESP8266 [21], [22]Arduino Uno [23],[24]and Raspberry Pi [25],[26].

### 2.4.1 ESP32

The ESP32 series of affordable, energy-efficient system-on-chip microcontrollers is driven by a dual-core Tensilica Xtensa LX6 microprocessor. These microcontrollers are fully integrated and come with built-in Bluetooth and Wi-Fi functionalities[19]. An ESP32 is a microcontroller with 38 pins that has integrated Wi-Fi connection, a digital analogue convertor (DAC), and an analogue digital convertor (ADC). In order to activate automatically, the ESP32 microcontrollers collect and interpret input from the sensors. Figure 2.12 shows the esp32[20].

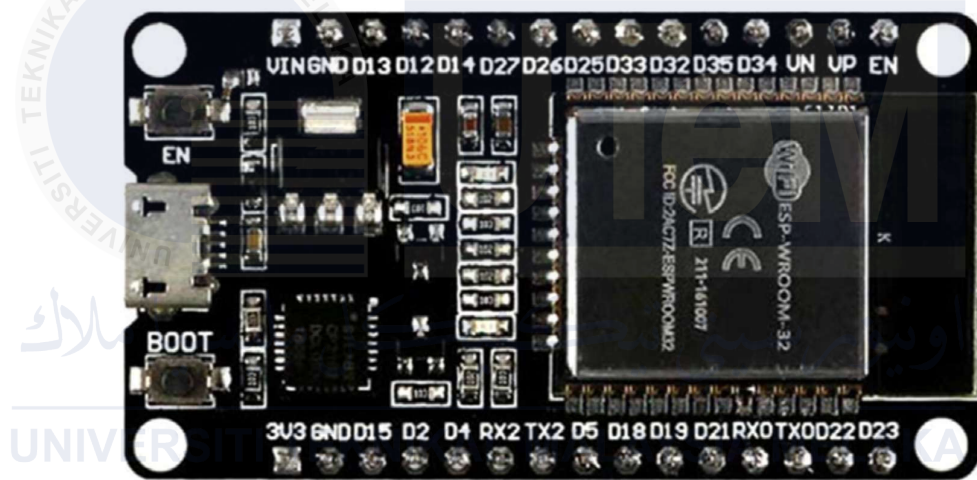


Figure 2.12 ESP32 microcontrollers[20]

The microcontrollers shown in Figure 2.12 is intended primarily for Internet of Things applications[20]. Any gadget may be remotely controlled thanks to a technology known as the Internet of Things (IoT). After that, Bluetooth was used to send the parameter data to the hardware.

#### 2.4.2 ESP8266

The ESP8266 efficient architecture enables competent processing of data, making it suitable for various IoT applications. Moreover, its low-power consumption characteristic is particularly appealing for battery-powered projects, ensuring extended operation[21].

Figure 2.13 show node MCU esp8266 board[22]

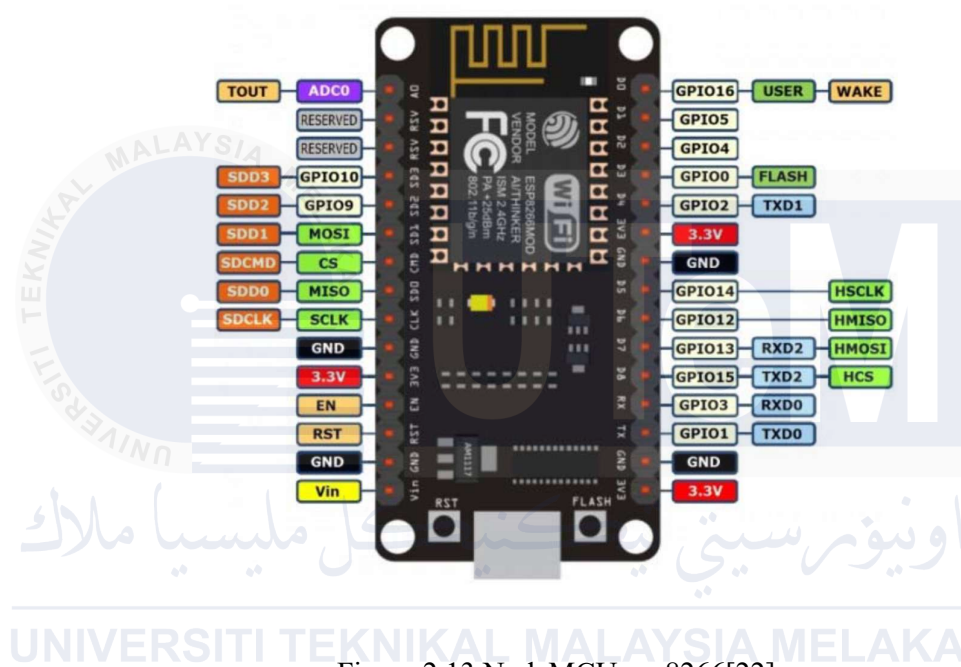


Figure 2.13 NodeMCU eps8266[22]

The node MCU esp8266 presented in Figure 2.13 [22]. In general, the quickest microcontroller was the ESP8266.

### 2.4.3 Arduino Uno

A microcontroller's function is to process signals in accordance with its functional model[23]. An extraordinarily potent and versatile microcontroller board is the Arduino Uno. Its digital and analog input/output (I/O) pins allow for versatile utilization, enabling connections to expansion boards (shields) and various circuits, opening numerous creative possibilities. Figure 2.14 shows the microcontroller Arduino UNO[24].

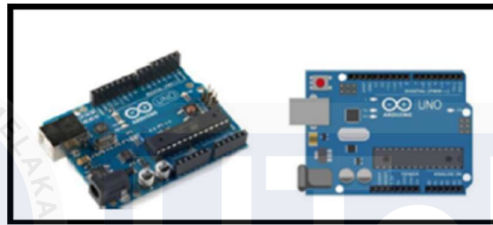


Figure 2.14 Arduino UNO[24]

The microcontroller Arduino UNO presented in Figure 2.14[24]. It uses a USB connection to connect to and communicate with the PC. It also features free software.



#### 2.4.4 Raspberry Pi

The Raspberry Pi is a single-board computer with desktop PC-like capabilities. The Raspberry Pi 3 Model B is a low-cost, internet-accessible microcontroller[25]. A variation of GNU/Linux, Raspbian is the operating system used by the Raspberry Pi. Additionally, it features a quad-core ARM Cortex CPU that supports multitasking. Figure 2.15 show the raspberry pi[26].

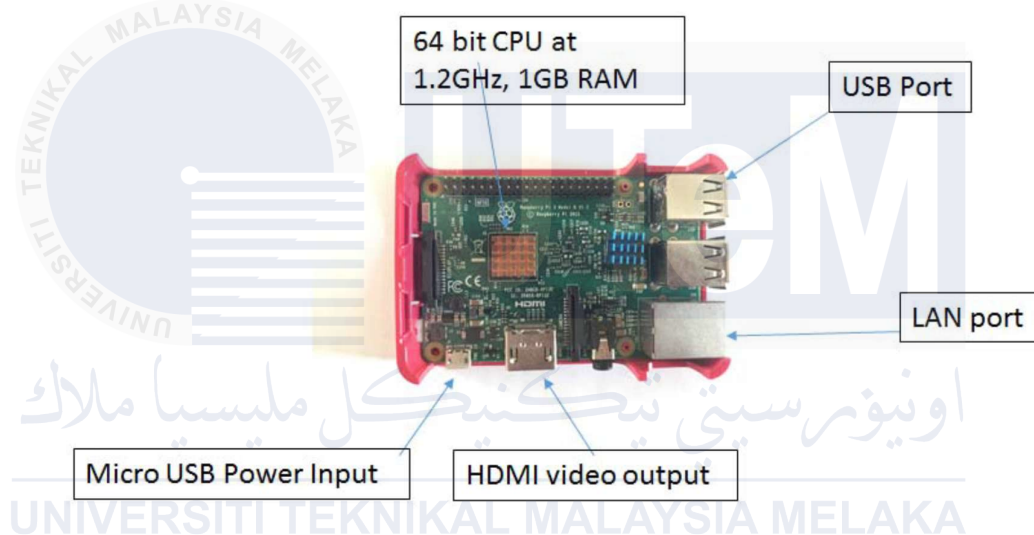


Figure 2.15 Raspberry Pi[26]

The raspberry pi presented in Figure 2.15 [26]The microcontroller is programmed with code in the Python programming language to carry out orders. Python has an easy-to-understand syntax[25].



## 2.5 Water quality monitoring system

Water, the nectar of life, is always in short supply and of low quality. Even if it's helpful, traditional techniques of assessing water quality are time-consuming and rare[27]. Systems for monitoring water quality (WQMS) are revolutionizing the industry by continuously delivering data in real time on a range of water quality indicators. This promotes enhanced water management techniques, early contaminant identification, and regulatory compliance[28]. This review delves deeply into the field of WQMS, examining the many kinds of sensors that are employed, the function of the Internet of Things (IoT), methods for analyzing data, and the various ways that WQMS is applied in various industries.

### 2.5.1 The pH of water

One of the most crucial physicochemical factors in water, pH has a big influence on the characteristics of the mixture. The pH is measured on a scale from 1 to 14, with 7 denoting neutral pH and values above and below 7 denoting bases and acids, respectively[29]. A real time smart pH sensor can be seen in Figure 2.16[28]



Figure 2.16 Smart pH sensor[28]

Figure 2.16 shows the real time smart pH sensor[28]. As a result, pH testing is essential for many different purposes, including food safety, water quality assessment, and biological and chemical process analysis[28]. In order to assess the quality of water, alkalinity testing is just as crucial as evaluating conductivity, color, turbidity, odor, and dissolved organic and inorganic elements.

### 2.5.2 Temperature of water

Water temperature is monitored via the DS18B20 sensor. The internal structure of the DS18B20 consists of four primary components: a temperature sensor, nonvolatile temperature alarm triggers TH and TL, configuration registers, and a 64-bit lithographic ROM[30]. The main benefit of the DS18B20 Temperature Sensor in Figure 2.17, is its small size, which makes it incredibly adaptable and appropriate for usage in a variety of scenarios[31].



Figure 2.17 DS18B20 Temperature Sensor[31].

Figure 2.17 shows the DS18B20 temperature sensor[31]. It can select the ideal water temperature based on the demands of the user. Over the course of a year, a thermistor can vary between  $0.02^{\circ}\text{C}$  and  $0.2^{\circ}\text{C}$ , depending on whether it is hermetically sealed or not[31]. High precision temperature measurement is possible with the DS18B20 temperature sensor since it can be set to vary the resolution between 9 and 12 bits, which corresponds to precise temperatures of  $0.5^{\circ}\text{C}$ ,  $0.25^{\circ}\text{C}$ ,  $0.125^{\circ}\text{C}$ , and  $0.0625^{\circ}\text{C}$ .

### 2.5.3 Total Dissolved Solids (TDS) level in water

One physical measure of water quality is total dissolved solids, or TDS. Two electrodes placed equally apart are inserted into the water to detect charge using a gravity sensor tds meter. Electroconductivity (EC) that travels between two probes in the solution may be measured from a distance to determine TDS. The TDS value increases with increasing EC value. A low cost TDS sensor diagram can be seen in Figure 2.18[33].

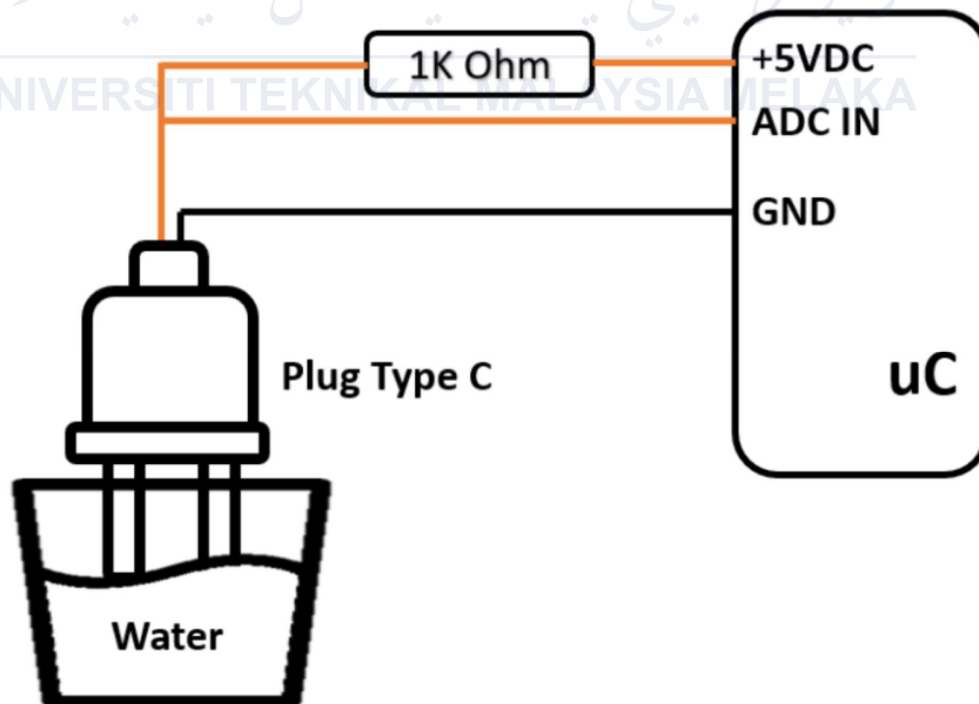


Figure 2.18 TDS sensor diagram[33]

Figure 2.18 shows the low cost TDS sensor diagram. Consumption water typically has a TDS value of 100–200 PPM[33]. The determination of the Total Dissolved Solids (TDS) value in water is influenced by its temperature.

#### 2.5.4 Turbidity of water

The buildup of organic debris results in the production of harmful gasses, which turbidizes the water. One important environmental factor that is taken into account while determining the quality of water is turbidity[34]. The amount of visible particles in the water is called turbidity. The turbidity sensor uses light rays to measure turbidity. The basic wiring diagram for analogue turbidity sensor can be seen in Figure 2.19[34].

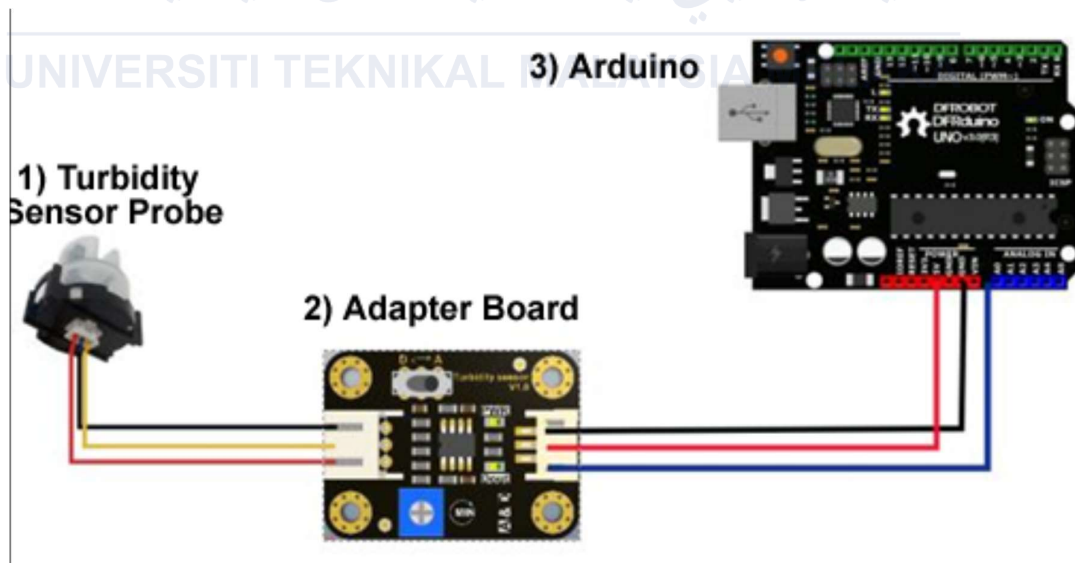


Figure 2.19 Wiring diagram for analog turbidity sensor[34]

Figure 2.19 show the wiring diagram for analogue turbidity sensor[34] The turbidity of the water decreases as the current value recorded by the sensor increases because the high resistance value is inversely proportional to the current. It can be said that the water is extremely clean and clear when the turbidity level is higher than 9 NTU. A turbidity level of 6 to 9 NTU is considered typical.potable water.

### 2.5.5 Oxygen level in water

The amount of dissolved oxygen in water is essential to fish growth and development. The majority of aquatic species depend on the dissolved oxygen in the water, therefore waterways with large concentrations of algae may have low levels of this element[36]. The oxygen meter indicated a dissolved oxygen value of 0.01 mg/l. Figure 2.20 presents the oxygen sensor[37].

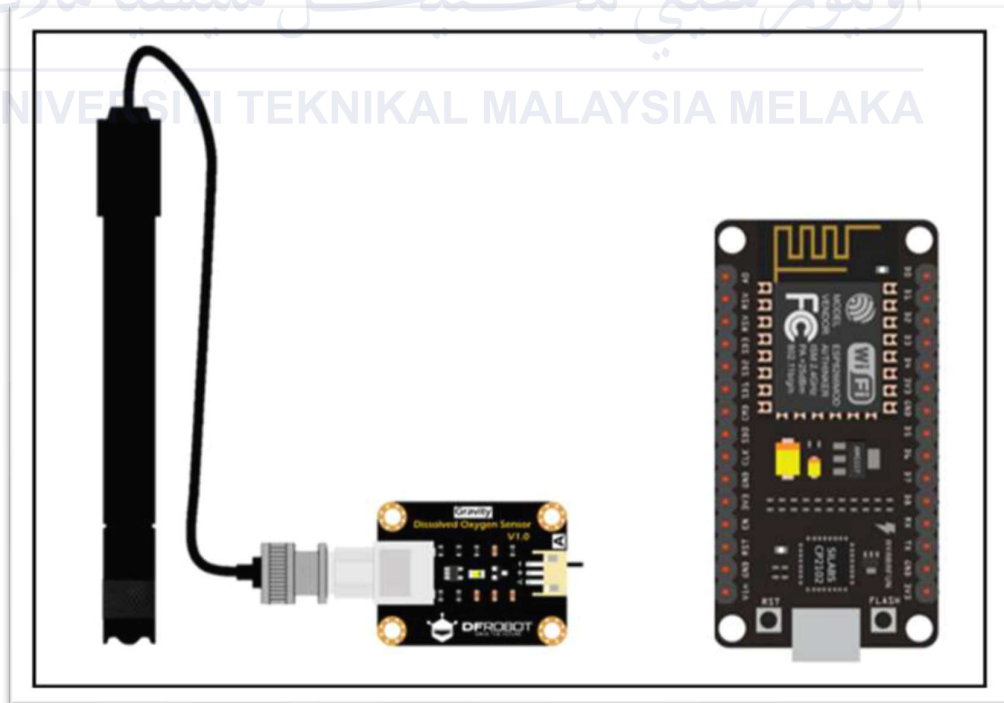


Figure 2.20 Oxygen sensor[37]

The oxygen sensor that measures the amount of oxygen in the water and transmits data to the Node MCU for processing can be seen in Figure 2.20[37]. The concentration of dissolved oxygen in water dictates the quantity of oxygen gas dissolved within it. The oxygen saturation voltage that the sensor produces ranges from 0 to 47 mV. The industrial dissolved oxygen sensor has a 32 mg/L measuring range[38].

## 2.6 Comparison of water quality monitoring system based on previous paper

The table presents a comparison of previous journals or research papers in terms of the methods and applications. Table 2.1 highlights the differences and similarities among these previous studies.

**Table 2.1 Water quality monitoring system based on previous paper**

No.	Author	Application	Objective	Method
1.	[27]	LoRaWan – long range wide area network	To develop a solar-powered IoT water quality monitoring system with sensors for pH, temperature, conductivity, turbidity, and GPS using a LoRa WAN network for communication.	-Turbidity sensor -pH sensor -Arduino nano -Temperature sensor -GPS module
2.	[39]	Freshwater biodiversity	To identify water quality parameters measurable by available IoT sensors and	-Conductivity sensor -TDS sensor -pH sensor

			develop a system to monitor them simultaneously.	
3.	[40]	Lakes	To developing a real-time water quality monitoring system for assessing the lakes surrounding UTHM.	-NodeMCU ESP32 -Turbidity sensor -Temperature sensor -pH sensor
4.	[41]	Drinking and irrigation	To construct a network for the gathering and tracking of water quality data in real time throughout Cape Town's water storage dams.	-Water sensor -remote cloud
5.	[42]	River	To designing a solar-powered IoT device for monitoring water quality.	-pH sensor -turbidity sensor -tds sensor -esp32 -blynk app
6.	[43]	Raw water resources	To create the Internet of Water Things (IoWT), a new web-based system for managing and monitoring water resources.	-Temperature sensor -level sensor -pluviometer

## 2.7 Floating solar powered water quality monitoring system

Based on previous related papers, several research had been conducted on floating solar powered water quality monitoring system. The first works presented by Lakshmikantha et al. ,2021 presents IoT based smart water quality monitoring system[27]. This research suggests a solar-powered, IoT-based system for monitoring water quality, employing LoRaWAN technology. Its aim is to develop and explore solutions for monitoring pH, temperature, turbidity, conductivity, and GPS data accessible through the Cayenne LPP cloud service. Testing had been conducted on the water in front of the Department of Electronics and Communications Engineering at Rajamangala University of Technology Thanyaburi. Different wireless connectivity methods, including LoRaWAN and LPWAN, will be assessed for data transmission. Additionally, the system will include a solar panel for recharging the battery, extending its operational time by 36 hours. Error analysis indicates that the monitoring system's accuracy is below 5%. Figure 2.21 and Figure 2.21, shows the LoRaWAN network architecture and structure design .

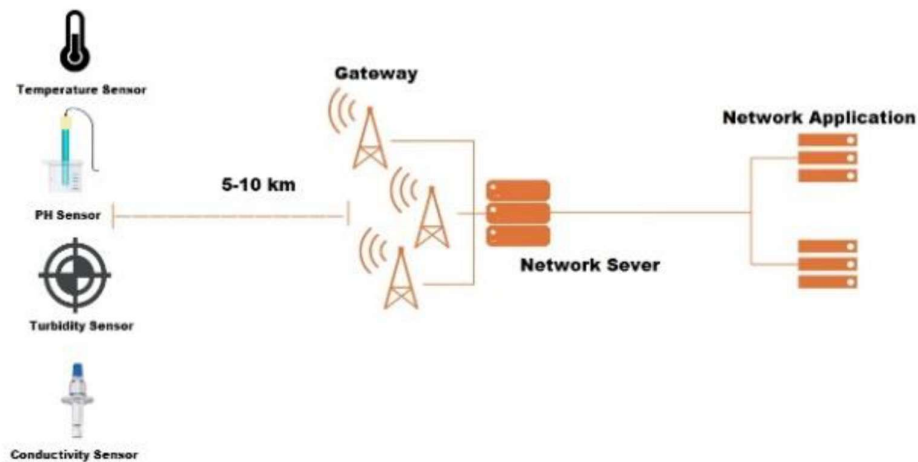


Figure 2.21 LoRaWan network architecture[27]



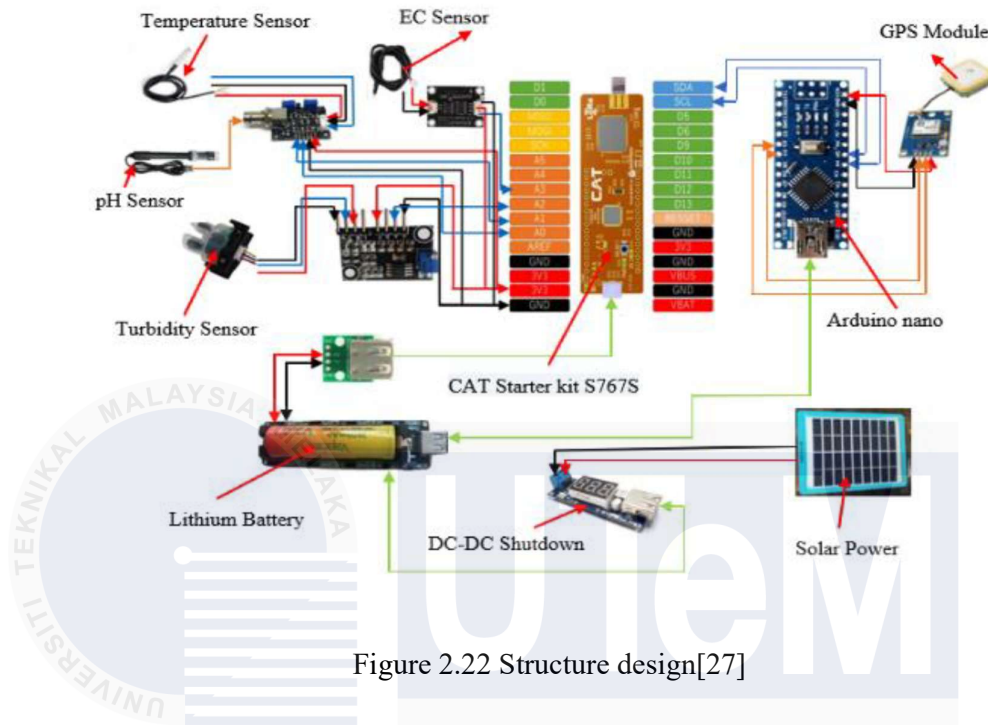


Figure 2.22 Structure design[27]

Next research is from Wang et al. ,2022 presents real-time water quality monitoring and estimation in AIoT for freshwater biodiversity conservation[39]. This study investigates the impact of declining water quality on freshwater biodiversity. The complex interrelationships between water quality metrics and the influence on various taxonomic groups make it challenging to comprehensively understand this issue. While traditional laboratory testing remains the primary method for many chemical and biological indicators, limitations exist due to the scarcity of diverse Internet-of-Things (IoT) sensors. This research proposes a novel approach leveraging recent advancements in Artificial Intelligence (AI) and IoT, termed AIoT, to enable real-time water quality monitoring and enhance biodiversity protection. A thorough literature review identified the ten most crucial water quality metrics affecting freshwater biodiversity. Subsequently, a generic methodology was developed to assess the interdependencies between IoT-measurable and non-measurable characteristics.

Historical water quality monitoring data was utilized to construct Gaussian Regression Neural Network (GRNN) and Multivariate Polynomial Regression (MPR) models. These models were then compared with traditional field water sampling, laboratory studies, and an IoT-based monitoring system along an urban river in Hong Kong. The GRNN model effectively distinguished abnormal parameter increases from normal conditions, while the MPR model, specifically at degree 8, demonstrated high coefficients of determination (exceeding 0.81) for key pollutants such as NO<sub>3</sub>-N, BOD<sub>5</sub>, PO<sub>4</sub>, and NH<sub>3</sub>-N, indicating strong predictive accuracy. These findings suggest that AIoT-powered water quality monitoring holds significant promise for real-time assessments and improved freshwater biodiversity protection strategies. Figure 2.23 shows whole setup based on Wemos chip and a multiplexer .

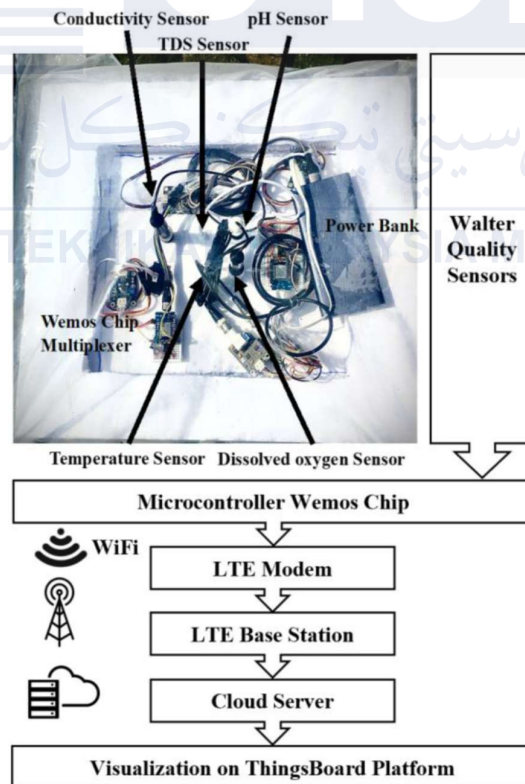


Figure 2.23 Whole setup based on Wemos chip and a multiplexer [39]

The process of collecting water samples from various sources, measuring different parameters, and comparing its against established standards is complex and challenging, particularly in adhering to guidelines during transportation and measurement. Ajayi et al. (2022) presented a study introducing a network for monitoring and evaluating water quality for drinking and irrigation purposes[41]. This study proposes a network architecture aimed at gathering real-time data on water parameters and employs Machine Learning (ML) tools to automatically assess the suitability of water samples for drinking and irrigation purposes. The proposed monitoring network is built upon LoRa technology and is designed with consideration for the land's topology. Simulations conducted using Radio Mobile revealed that a partial mesh network topology is the most appropriate choice. Given the limited availability of large, publicly accessible datasets on drinking and irrigation water, specific datasets were created for training ML models. Three ML models—Random Forest (RF), Logistic Regression (LR), and Support Vector Machine (SVM)—were assessed for the effectiveness in classifying water quality. The findings showed that Logistic Regression outperformed the other models for drinking water classification, while Support Vector Machine proved to be more suitable for irrigation water classification. Additionally, recursive feature elimination was employed with the three ML models to identify the water parameters that most significantly influenced the accuracy of each model's classification. Figure 2.24 and Figure 2.25 represent conceptual framework , flowchart and land structure.

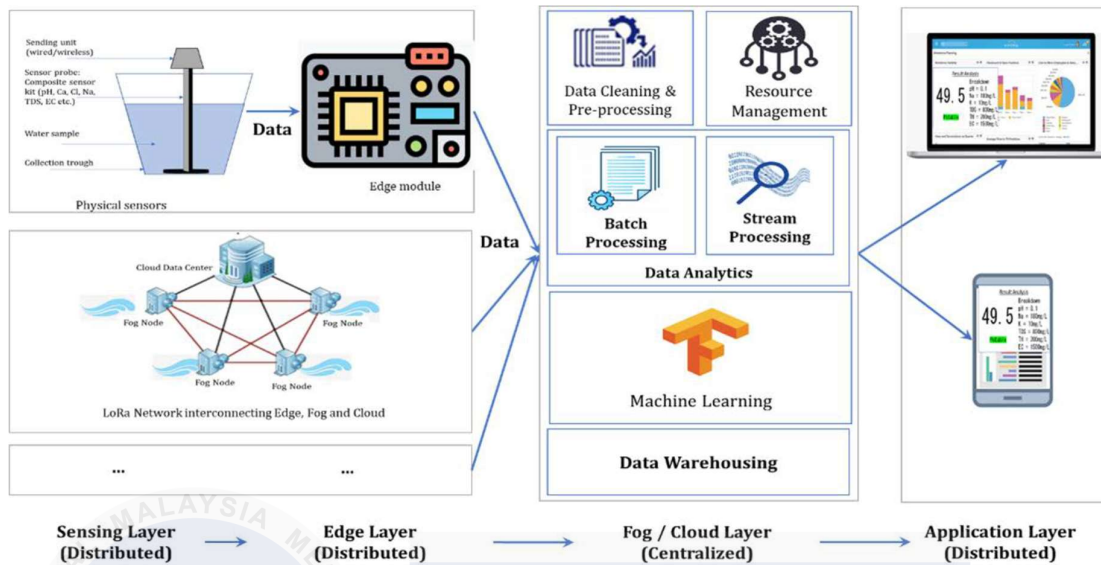


Figure 2.24 Conceptual framework for Water Quality Monitoring.[41]

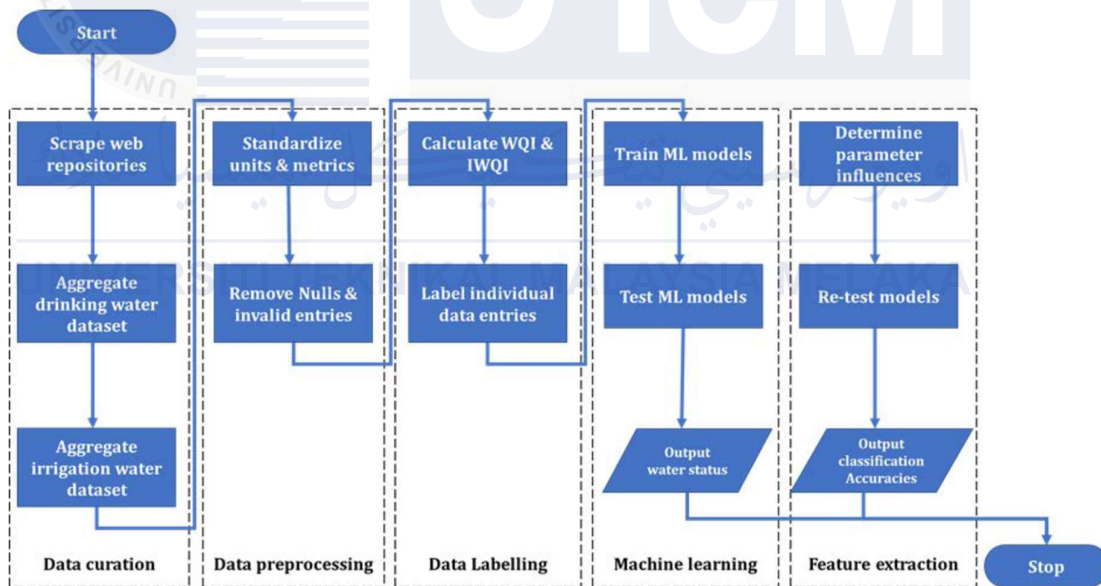


Figure 2.25 Flow chart for Water Quality Assessment using ML[41].

Further in research is by Bahri et al. ,2023 presents solar powered smart water monitoring system based on IoT and blynk platform[42]. This paper presents a solar-powered smart water monitoring system utilizing IoT technology. Water, a crucial and

abundant natural resource, is indispensable for human daily needs. Ensuring water purity is vital and a collective obligation. Contaminated water is the root cause of numerous infectious diseases, resulting in millions of deaths annually. This study concentrates on evaluating the water quality of the Melor River in Kelantan and creating a solar-powered IoT-based water quality monitoring system. The device, fueled by a solar array, is equipped with sensors for measuring turbidity, pH, and total dissolved solids (TDS). Real-time water parameter data is transmitted to a data center via an ESP32 microprocessor and sensors. Water quality can be monitored using the Blynk application on a smartphone through IoT development. Analysis demonstrated that the solar-powered system requires 34 hours for a full battery charge. Findings indicated that the river's water quality was satisfactory, with TDS content readings below 300 ppm, pH levels falling within the acceptable range of 4-11, and the water appearing cloudy. Hardware design and blynk dashboard can be seen in Figure 2.26 and Figure 2.27.

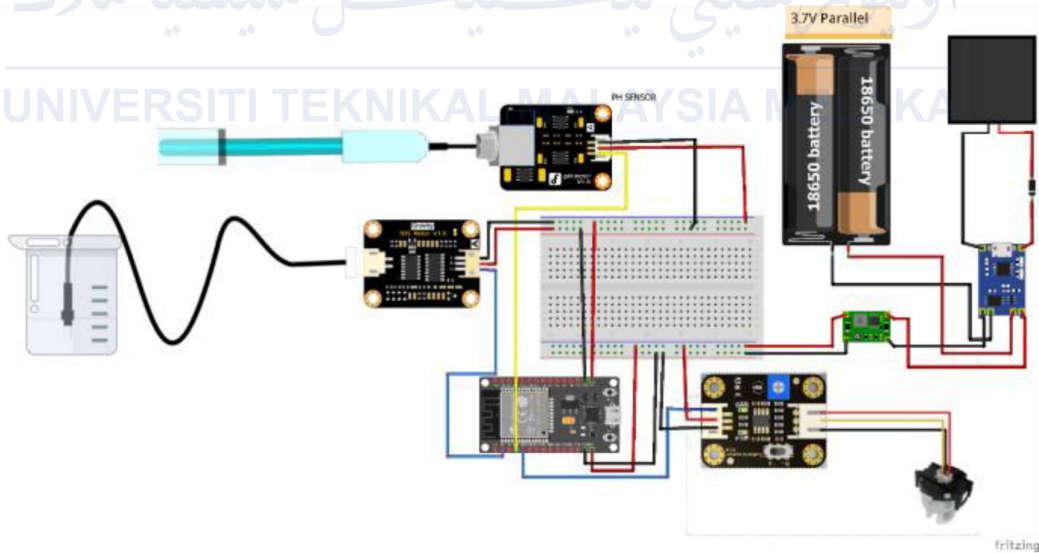


Figure 2.26 Hardware design[42]

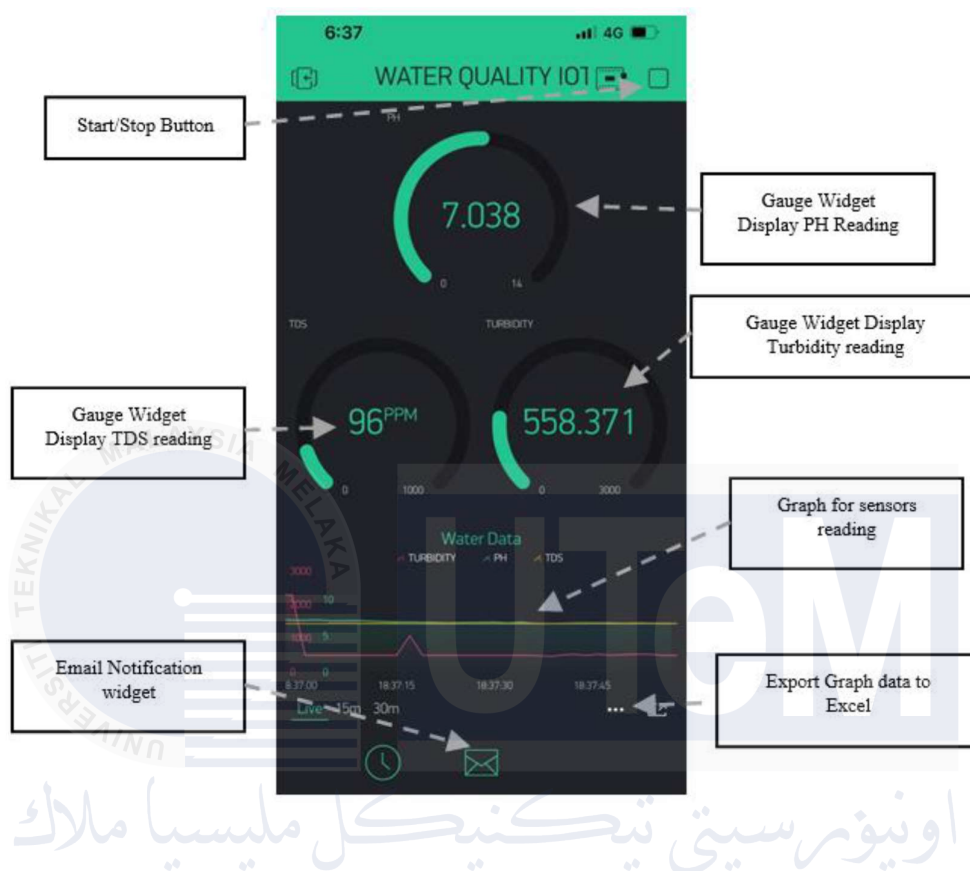


Figure 2.27 Blynk dashboard[42]

The last research is by Junior et al. ,2022 presents a remote raw water monitoring and control system[43]. This study endeavors to develop an innovative online system for monitoring and managing water resources, named the Internet of Water Things (IoWT). The proposed system is crafted to oversee and regulate raw water resources by leveraging a platform based on server-less architecture and the Internet of Things Architectural Reference Model. This platform underwent testing in a simulation environment using various electronic devices to validate its performance. The system captures raw water data from tubular wells, each equipped with a level sensor, temperature sensor, and rain gauge. Data is collected every minute by an electronic device and transmitted hourly to the IoWT system. Analysis of the data revealed that the amount of memory allocated to functions minimally impacts



efficiency. In a real-world scenario, the IoWT system connects a device installed in a water well to the platform, with data transmitted via a 3G network for processing. This approach demonstrates significant potential as a complementary tool for monitoring raw water and assisting in decision-making for water resource management. The high level IoWT architecture, internet of water things architecture and IoWT domain model can be seen in Figure 2.28, and Figure 2.29.

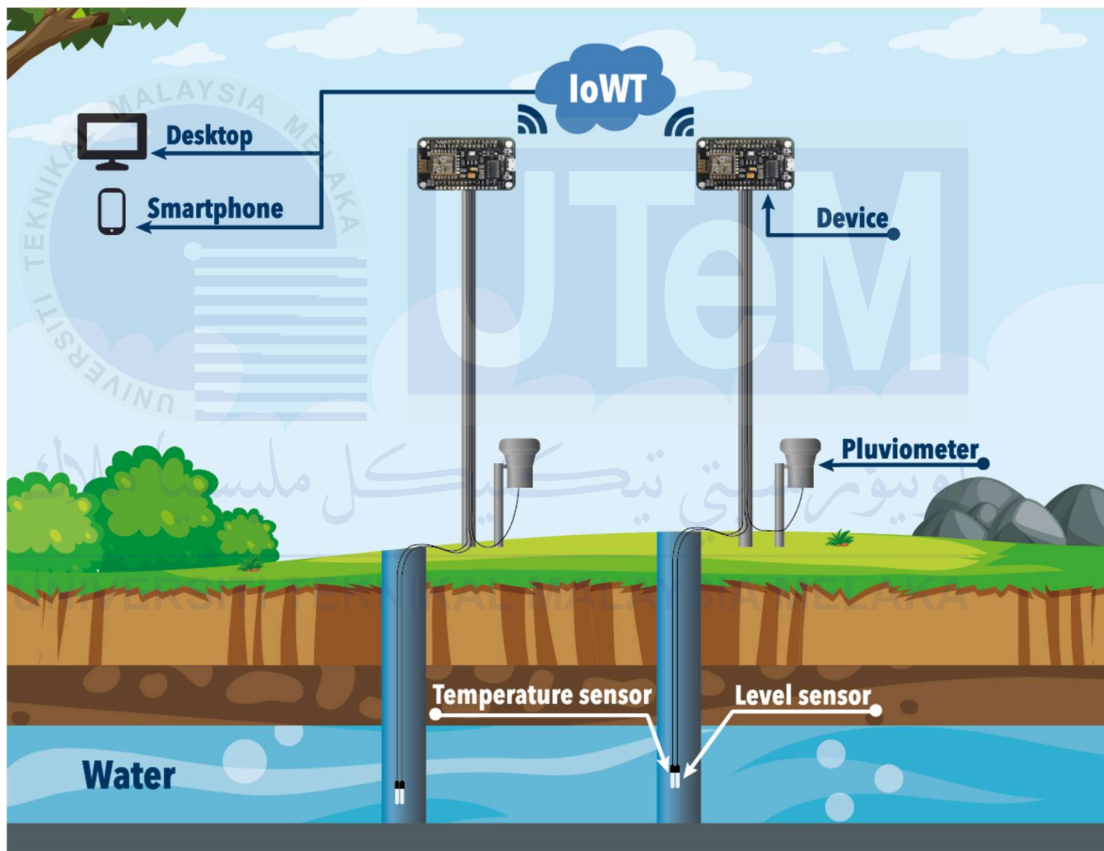


Figure 2.28 High level IoWT architecture [43]

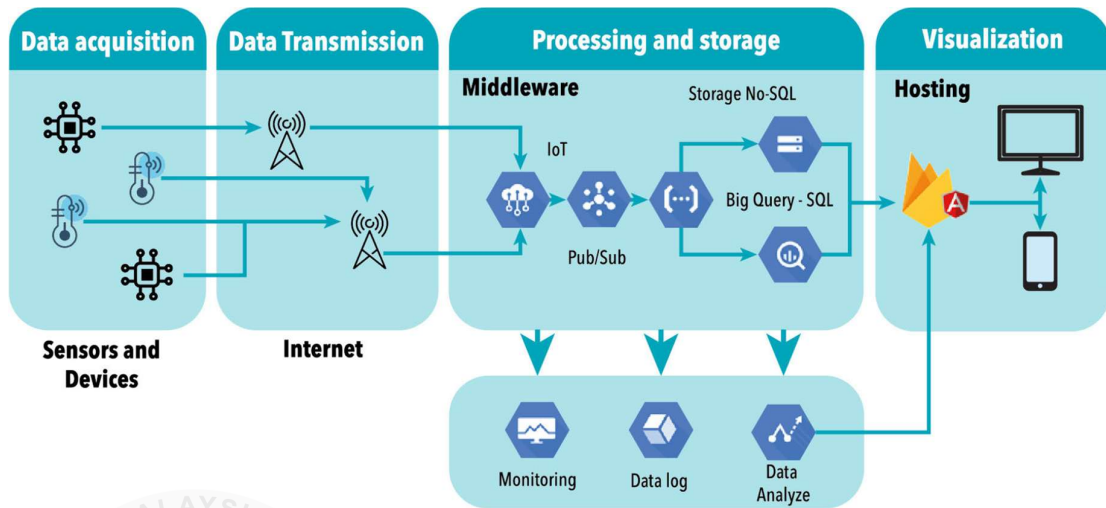


Figure 2.29 IoWT domain model [43]

## 2.8 Summary

Renewable energy sources like solar, wind, tidal, and wave energy are gaining global traction due to rising energy demands and environmental concerns over fossil fuels. Solar energy, in particular, stands out for its abundance, cleanliness, and cost-effectiveness. However, challenges such as sunlight intermittent and lack of supporting industries hinder widespread adoption, especially in regions like Africa. Nonetheless, solar energy offers decentralized solutions crucial for economically disadvantaged areas and has the potential to revolutionize energy production, similar to the shift from animal to tractor power in agriculture. Solar and wind energy sectors are experiencing rapid growth globally, particularly in Europe and China, contributing to energy mix diversification and climate change mitigation. Solar PV systems, comprising various components, offer reliable energy conversion, with ground-mounted, roof-mounted, and floating PV systems each presenting unique advantages and challenges. Despite initial high costs, floating PV panels are chosen for efficient water surface use and land use mitigation.



Microcontrollers, essential for embedded systems, integrate a processor, memory, and input/output components on a single chip, excelling in real-time, efficient, and reliable applications. Its operate based on instructions stored in memory, executing tasks such as data sensing, information processing, and actuator control. The major microcontroller types discussed include ESP32, ESP8266, Arduino Uno, and Raspberry Pi. The ESP32, with its dual-core processor, integrated Wi-Fi and Bluetooth, and efficient handling of sensor data, stands out for its affordability and energy efficiency. Given its advanced features and suitability for the Internet of Things (IoT) applications, the ESP32 was chosen for the water quality monitoring system.

Water quality monitoring systems (WQMS) provide real-time data on various water quality parameters, enhancing water management, early contaminant detection, and regulatory compliance. This review examines key sensors used in WQMS, including those for measuring pH, temperature, total dissolved solids (TDS), turbidity, and dissolved oxygen. The pH sensor measures the acidity or alkalinity of water, crucial for numerous applications such as food safety and chemical analysis. The DS18B20 temperature sensor offers high-precision temperature measurements, vital for maintaining optimal conditions for various processes. The TDS sensor measures the total dissolved solids in water, indicating water purity. Despite the importance of turbidity and dissolved oxygen sensors, the pH sensor, TDS sensor, and temperature sensor were chosen for the water quality monitoring system due to the critical role in assessing essential water quality parameters.

## CHAPTER 3

### METHODOLOGY

#### 3.1 Introduction

In this chapter, the intricate details of the research and methodology employed in the development of the Floatovoltaics Water Quality Monitoring System. This section serves as a comprehensive guide, detailing the steps, procedures, and methodologies utilized throughout the project's lifecycle. From inception to implementation, the methodology chapter forms the backbone of our project, ensuring adherence to a systematic workflow and facilitating seamless progression towards our objectives.

#### 3.2 Flow chart of the the overall project development

The flowchart outlines the process for developing a water quality monitoring system powered by photovoltaics. The system is designed to assess water quality in real-time. The process begins with establishing a suitable location for the solar panels and selecting the appropriate type of solar panels to generate electricity. Subsequently, a water quality monitoring system is chosen, followed by the selection of a monitoring system type.

After selecting the system components, the flowchart depicts the setup phase. This phase involves setting up the solar PV system, the water quality system, and the monitoring system. Following each setup step, there is a testing phase to ensure proper functionality before proceeding to the next step. Once all the components are set up and tested, the system is ready to perform real-time water quality testing. This includes measurement and data collection. The flowchart of the overall project development can be seen in Figure 3.1.

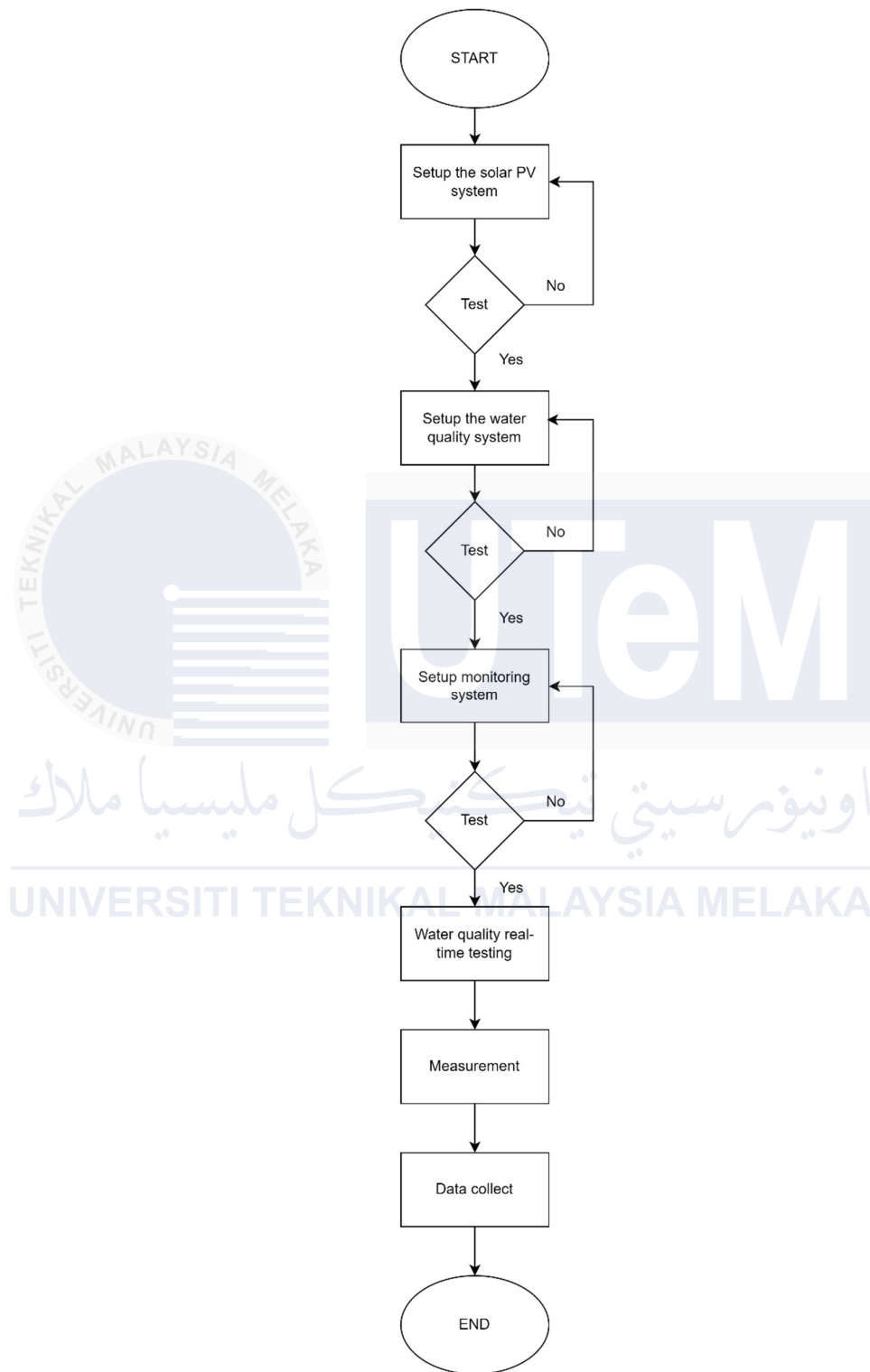


Figure 3.1 Flowchart of overall system

### 3.2.1 Flowchart of solar PV sytem

The flowchart outlines the process for developing a water quality monitoring system powered by photovoltaics. The system is designed to assess water quality in real-time. The process begins with establishing a suitable location for the solar panels and selecting the appropriate type of solar panels to generate electricity. Subsequently, a sealed lead acid battery is chosen to store the electrical energy generated by the solar panels. A voltage regulator is then selected to convert the voltage from the battery to a level suitable for powering the water quality monitoring system.

After selecting the system components, the flowchart depicts the setup phase. This phase involves setting up the solar PV system, the sealed lead acid battery, and the voltage regulator. Following each setup step, there is a testing phase to ensure proper functionality before proceeding to the next step. Once all the components are set up and tested, the system is ready to perform real-time water quality testing. This includes measurement and data collection. The flowchart of solar PV system can be seen in Figure 3.2.

UNIVERSITI TEKNIKAL MALAYSIA MELAKA

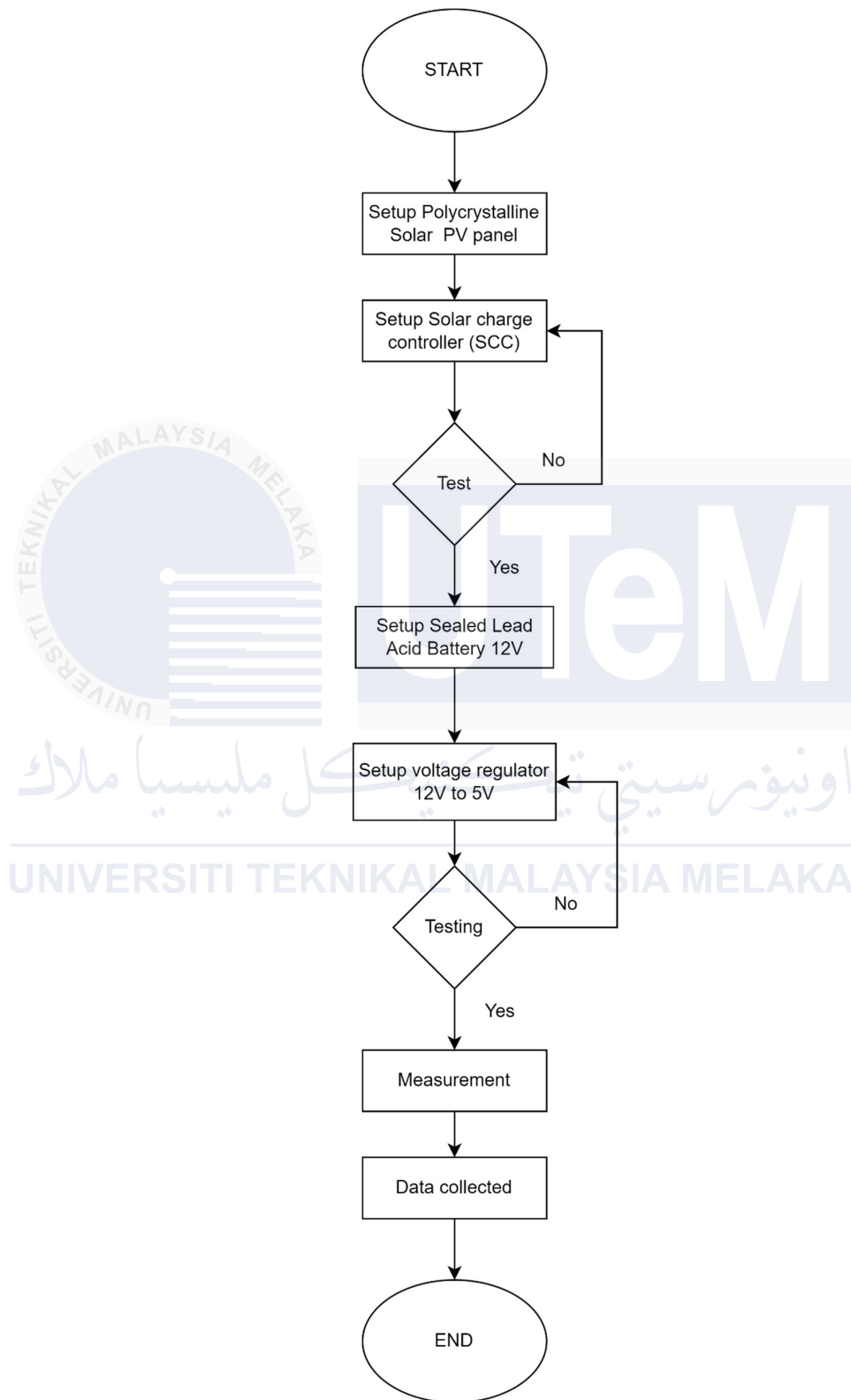


Figure 3.2 Flowchart of solar PV system

### 3.2.2 Flowchart of water quality system

The flowchart outlines the process for developing a water quality monitoring system powered by photovoltaics. The system is designed to assess water quality in real-time. The first step involves setting up the microcontroller, which is an ESP32 in this case. Then, the pH sensor is set up. The flowchart shows a decision point here - if the setup is successful, it proceeds to testing the setup. If not, it likely means going back and troubleshooting the setup of the pH sensor.

The process repeats for the turbidity sensor and the TDS sensor. Each sensor setup is followed by a testing phase to ensure the sensor is functioning properly before proceeding to the next component. This iterative process of setup and testing ensures that each part of the system is working correctly before moving on to the next step. Once all the sensors are set up and tested successfully, the system is ready to measure and collect data from the water body. The flowchart as seen in Figure 3.3

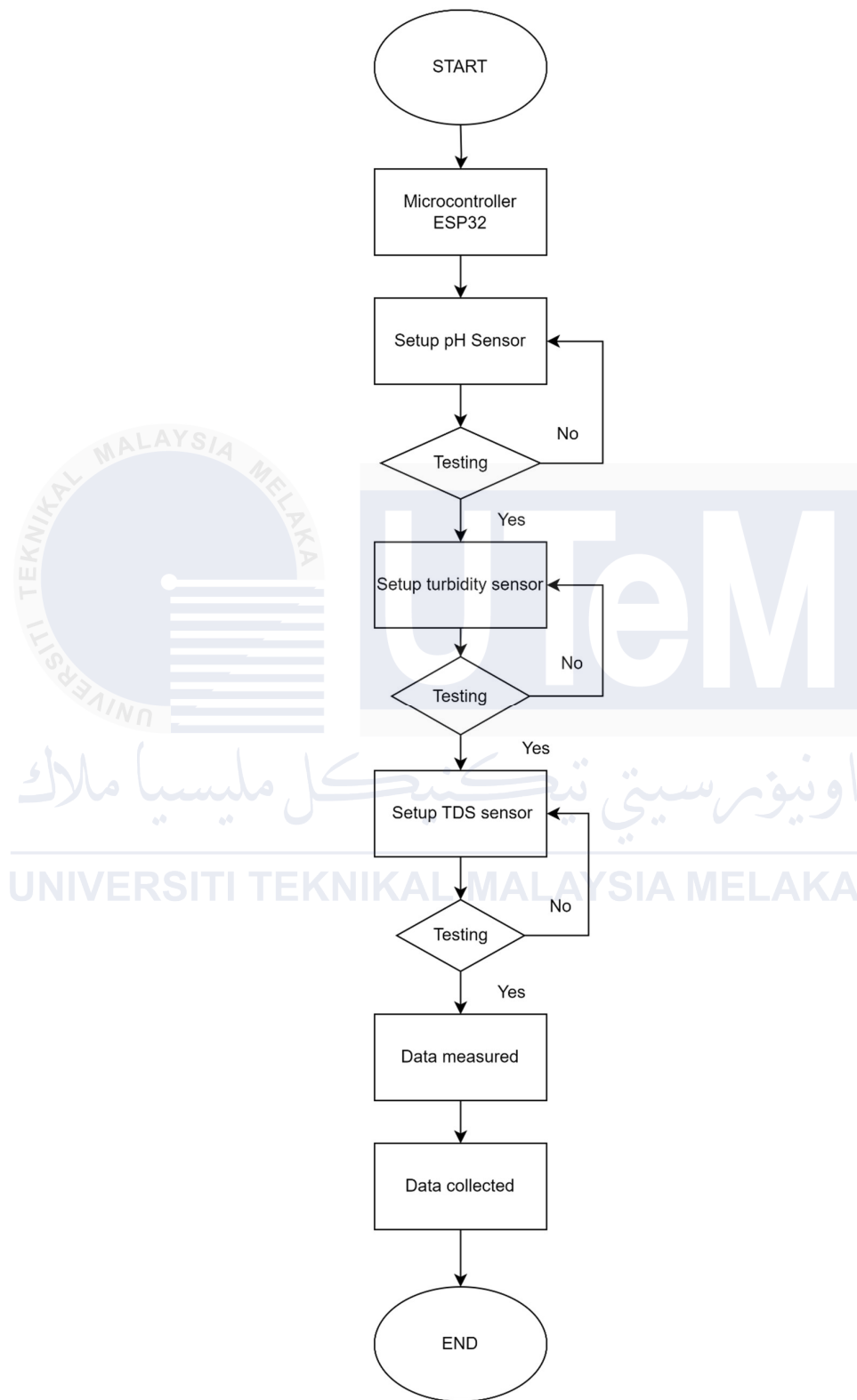


Figure 3.3 Flowchart of water quality system

### 3.3 Block diagram of the floatovoltaics for water quality monitoring system development

The overall system consists of a solar PV system, water quality system and monitoring system. Figure 3.4 shows the block diagram of overall system in the project development.

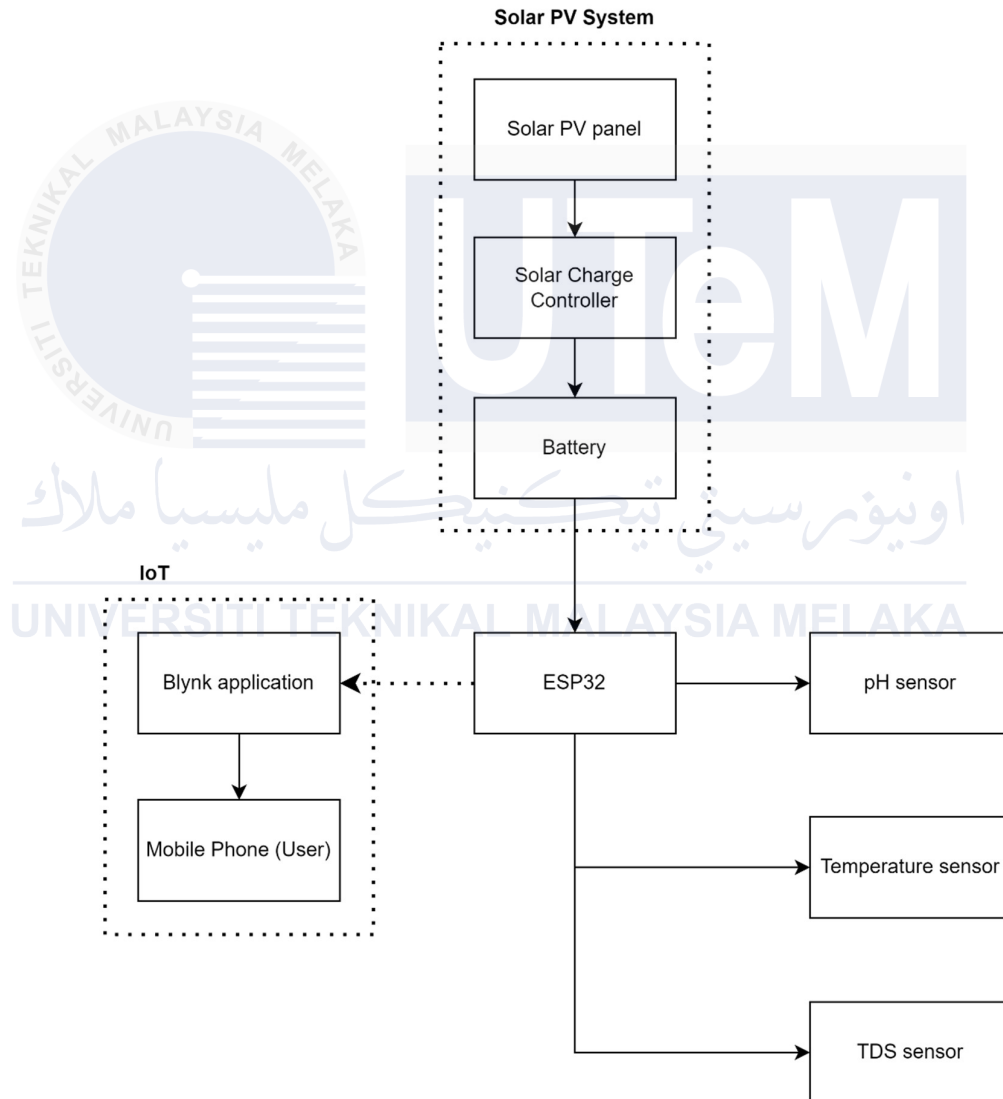


Figure 3.4 Block diagram of the overall system



The water quality monitoring system consists of an ESP32 microcontroller, a pH sensor, a temperature sensor, and a TDS sensor. The ESP32 microcontroller coordinates the entire system and collects data from the sensors. The pH sensor measures the acidity or alkalinity of the water. The temperature sensor measures the water temperature, and the TDS sensor measures the total dissolved solids in the water

The collected data is then transmitted to a mobile phone application (Blynk app) through the ESP32 microcontroller, likely over Wi-Fi or cellular connection. This allows a user to monitor the water quality remotely in real-time.

### **3.4 Development of solar PV system**

The development methodology for solar panels can be broken down into several key stages. First, research focuses on understanding the conversion of sunlight into electricity through photovoltaic materials. This involves selecting and optimizing materials like silicon for maximum efficiency. Then, design takes center stage, where engineers create the physical structure of the panel, considering factors like cell layout, electrical connections, and weatherproofing. Next, fabrication translates the design into a functional product, involving processes like cell formation, interconnection, and lamination. Finally, rigorous testing ensures the panel meets performance and durability standards, guaranteeing a reliable source of clean energy. This development cycle is constantly evolving as researchers strive to improve efficiency, reduce costs, and create more sustainable solar panel technologies.

### 3.4.1 Block diagram of solar PV system

The solar power supply system employs solar panels to produce DC electricity. A solar charge controller is responsible for regulating this electricity to charge the battery safely. The battery stores the DC power and provides energy to the voltage regulators, which lower the voltage from 12VDC to 3.3VDC for the appliances. Managing the entire system is the ESP32, which can integrate sensor data, including readings from pH, TDS, and temperature sensors, to monitor different parameters. The block diagram of the solar power supply system is illustrated in Figure 3.5.

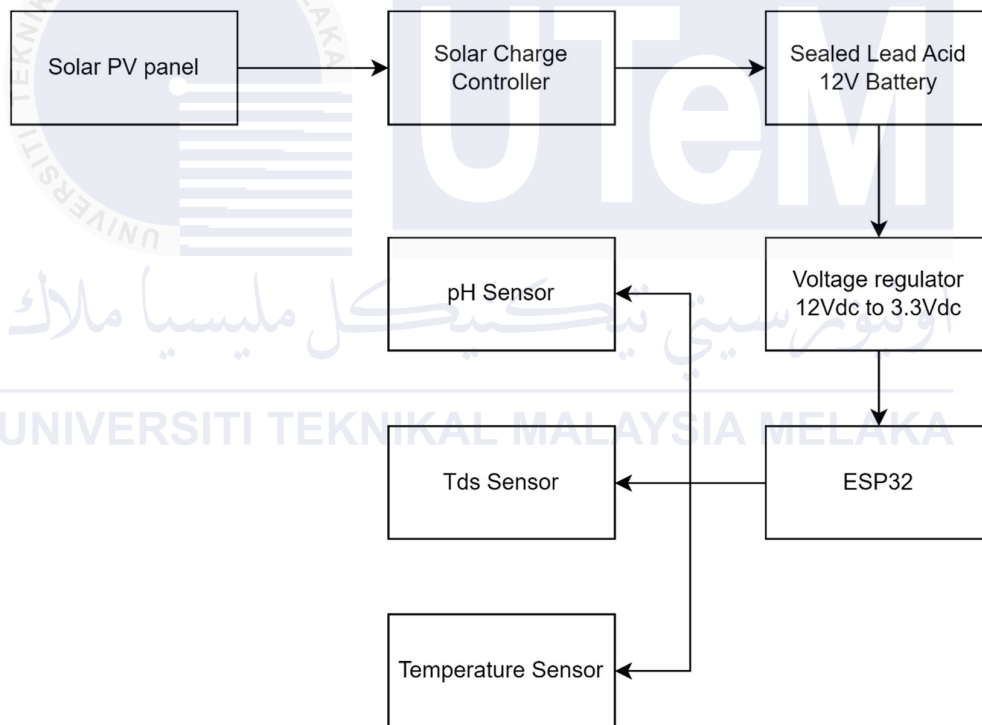





Figure 3.5 Solar PV system block diagram

### 3.4.2 Components for solar PV system

The solar PV system is a combination of some components and its functions like a team. The solar panel captures sunlight, converting it to DC electricity. The solar charge controller, the system's guard, regulates this current for safe battery charging. Finally, the battery acts as storage, saving excess energy for use at night or during low sunlight. The components used can be seen in Table 3.1.

Table 3.1 Component used in solar PV system

No	Type	Quantity	Model	Price
1.	Polycrystalline solar PV panel	1		RM 30.00
2.	Solar charge controller (SCC)	1		RM33.00
3.	Sealed Lead Acid Battery	1		RM36.50

### 3.4.3 Hardware setup for solar PV system

Several methods exist for measuring a solar PV system's performance. One common approach is to use a multimeter to measure the solar panel's output voltage and current. The solar panel converts sunlight into electricity, which flows to a solar charge controller. This controller safeguards the battery from overcharging, while the battery stores the electricity generated by the solar panel. Figure 3.6 presents the real-life setup of the solar PV system.



Figure 3.6 Real life setup for solar PV system

The positive and negative terminals of the battery are connected to the solar charge controller. The solar PV panel is also connected to the solar charge controller. To measure current, the multimeter is connected in series with the solar PV panel, and to measure voltage, it is connected in parallel with the panel. Additionally, the load is connected to the solar charge controller.

### 3.4.4 Measurement setup for solar PV system

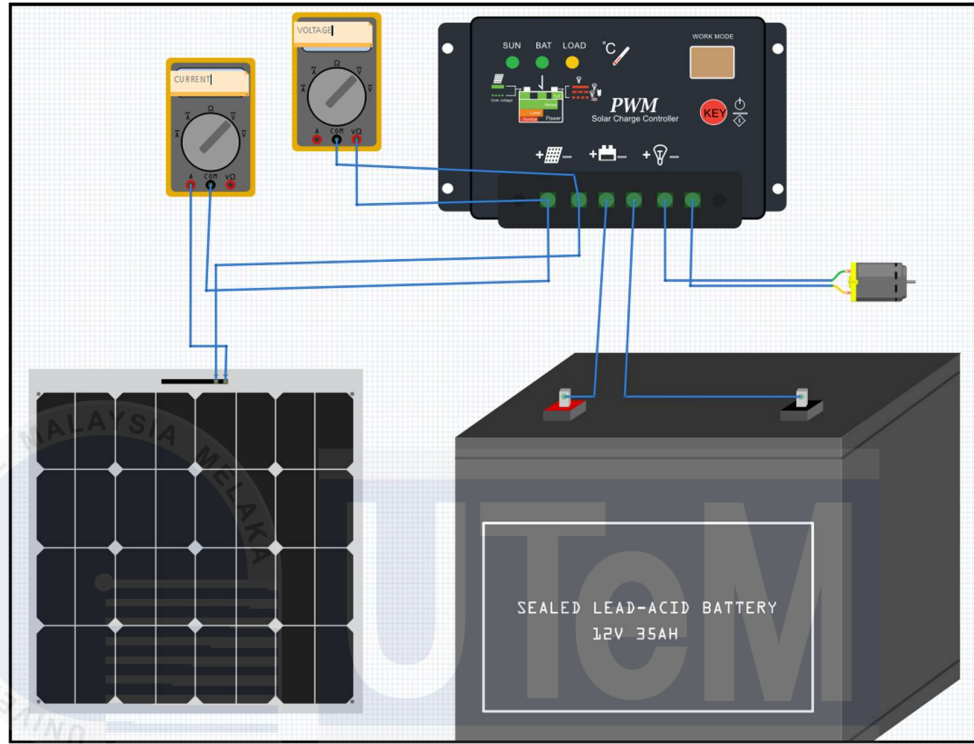


Figure 3.7 Connection of solar PV system

From Figure 3.7, the positive and negative terminal of the battery is connected to the solar charge controller (SCC). Then the solar PV panel is connected to the SCC and the multimeter is connected either in series with the solar PV panel to measure current or in parallel with the solar PV panel to measure voltage. Lastly the load is connected to the SCC. The multimeter range is set to 20V for the voltage and 10A for the current. The output power and average power from solar PV panel can be calculated using the formula below. The obtained result is represented in chapter 4.

$$\text{Output power, } P = I \times V \quad (3.1)$$

$$\text{average power, } \Delta P = \frac{P1 + P2 + P3}{3} \quad (3.2)$$

### 3.5 Development of water quality system

This system, akin to the automatic fish tank cleaner, centers around a microcontroller for its operation. An ESP32 microcontroller acts as the brain, gathering and interpreting critical data. Unlike obstacle detection in the cleaner, this system focuses on water quality parameters. Three specialized sensors work in concert to achieve this: a pH sensor continuously monitors water acidity, a TDS sensor measures total dissolved solids, and a temperature sensor tracks temperature fluctuations. These factors all significantly impact the health of aquatic environments. The ESP32 processes this comprehensive data, potentially transmitting it wirelessly for remote monitoring. This allows for convenient tracking of water quality trends, ensuring optimal conditions for various aquatic applications, from fish tanks and hydroponics to even swimming pools.

#### 3.5.1 Block diagram of the water quality system

An ESP32 microcontroller acts as the central processing unit, receiving data from three sensors: a pH sensor to measure acidity, a TDS sensor to gauge total dissolved solids, and a temperature sensor. The ESP32 then processes this sensor data and transmits it wirelessly via its built-in Wi-Fi module. By connecting to the Blynk app, a popular IoT platform, the data can be visualized on user smartphone or tablet. The app can even be configured to send alerts if water quality readings deviate from desired levels. This system offers a convenient and informative way to monitor water quality in various applications like aquariums, pools, or wells. From Figure 3.8, the block diagram depicts a wireless water quality monitoring system.

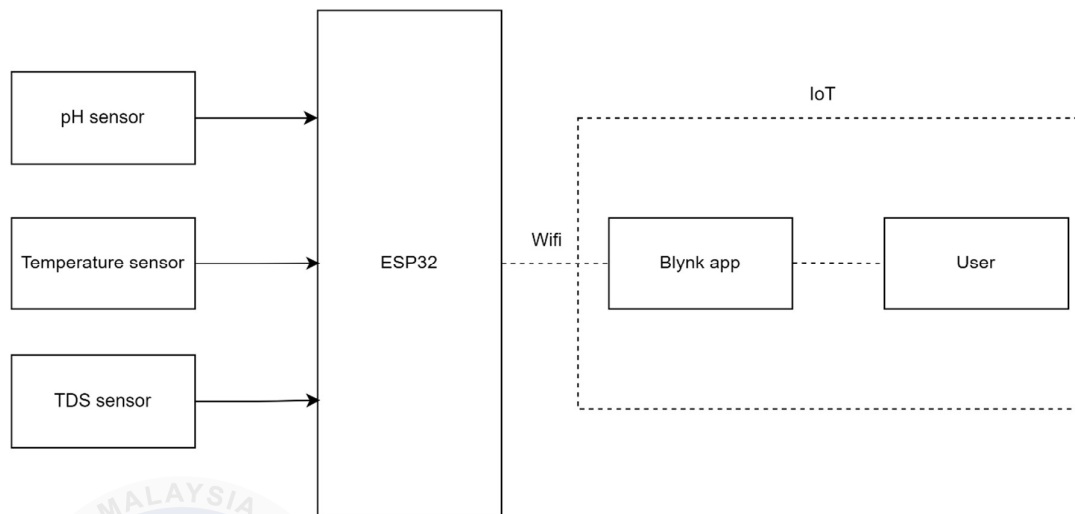
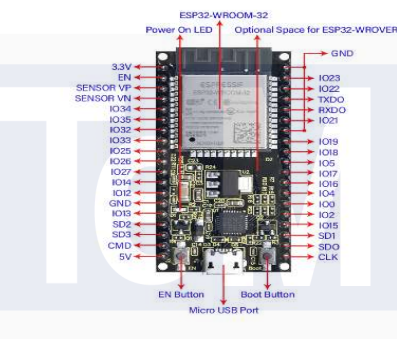




Figure 3.8 Block diagram of the water quality system


### 3.5.2 Components and hardware setup in water quality system

The water quality system is composed of various components, each essential for the system's functioning. The overall cost of these element totals RM86.40, as specified in Table 3.2.

Table 3.2 Component used in water quality system

Bil	Type	Quantity	Component	Price
1.	ESP32	1		RM15.00
2.	pH Sensor	1		RM36.50
3.	TDS Sensor	1		RM26.40



4.	Temperature Sensor	1		RM8.50
----	--------------------	---	--	--------

### 3.5.3 Hardware setup

The water quality system is intricately designed around an ESP32 microcontroller, which serves as the central hub for data acquisition and analysis. Integral to its functionality are sensors specifically tailored for assessing key parameters such as pH, TDS (Total Dissolved Solids), and temperature. These sensors collectively provide a comprehensive snapshot of the aquatic environment, offering insights into crucial aspects of water quality. The pH sensor plays a pivotal role in monitoring acidity levels, a critical factor in sustaining a healthy aquatic ecosystem. Similarly, the TDS sensor provides invaluable information on the concentration of dissolved substances, offering a nuanced understanding of water purity.

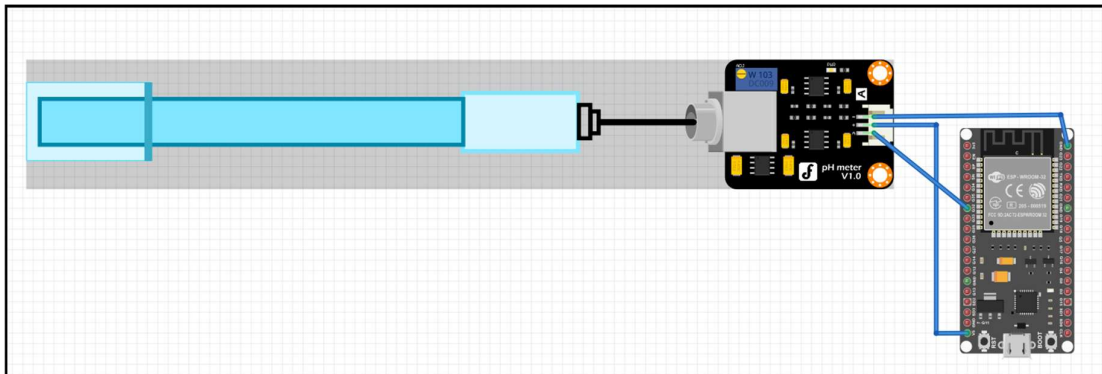
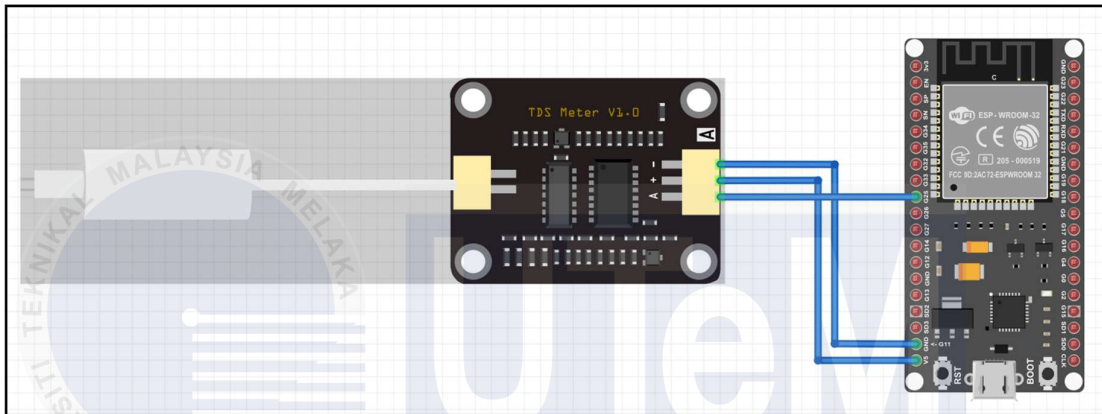


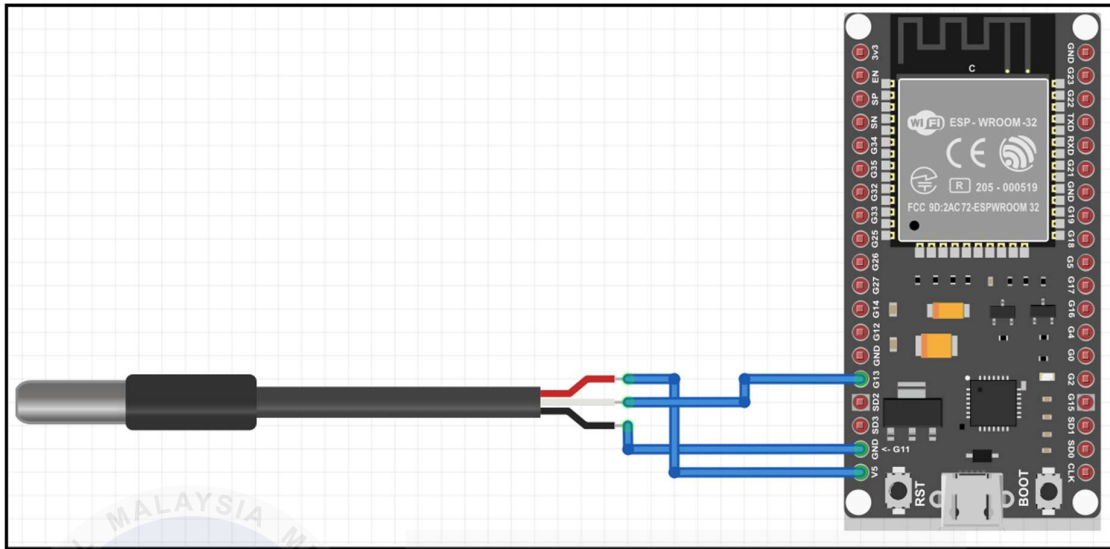
Figure 3.9 ph sensor connection

Figure 3.9 show the connection of the pH sensor is illustrated using Fritzing. The sensor's functionality has been successfully validated using an Arduino Uno board. For comprehensive instructions on interfacing with the pH sensor, in the coding as provided in **Appendix F**.



**Figure 3.10 TDS sensor connection**

In Figure 3.10, the connection of the TDS sensor is depicted using Fritzing. The sensor's functionality has been successfully validated using an Arduino Uno board. For detailed instructions on interfacing with the TDS sensor, in the coding as provided in **Appendix E**.



**Figure 3.11 Temperature sensor connection.**

Figure 3.11 illustrates the wiring setup of the temperature sensor as depicted using Fritzing. The sensor's functionality has been effectively verified through testing with an Arduino Uno board. The coding as in **Appendix G** shows guidance on how to interface with the temperature sensor

### **3.6 Floating mechanism for floating solar PV system**

Deploying a floating solar photovoltaic (FPV) system involves several critical steps to ensure the stability, efficiency, and longevity of the installation. First, the design of the floating structure is determined, typically utilizing pontoon-based structures or modular floats made from high-density polyethylene (HDPE) due to its buoyancy and durability. The floating arrays are configured with appropriate tilt angles and spacing to maximize solar energy capture. Anchoring and mooring systems are then implemented to secure the floating structure; these may include traditional anchors, mooring lines, or piles, depending on the water body's characteristics. Material selection is crucial, with HDPE used for floats, aluminum or galvanized steel for support structures, and stainless steel for mooring

components, ensuring resistance to UV radiation, water, and corrosion. Electrical connections are designed to be waterproof and robust, incorporating floating or onshore inverters and careful cable management to withstand environmental conditions. Additionally, environmental impact assessments are conducted to minimize ecological disruption, and all necessary regulatory permits are obtained. This comprehensive approach ensures a stable, efficient, and environmentally compliant FPV system installation. The visual representation of the basic design is drawn in tinkercad can be found in Figure 3.12.

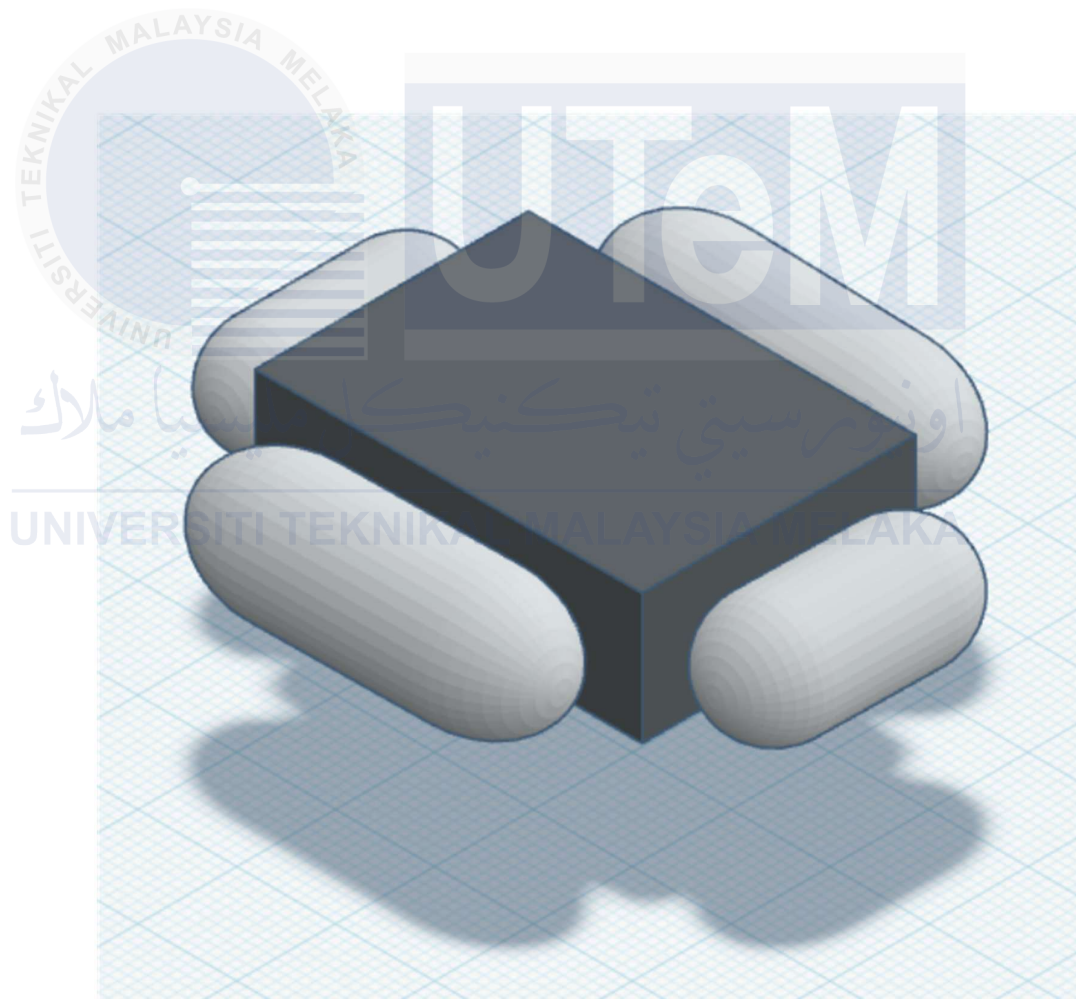


Figure 3.12 Floating mechanism for floating solar PV system

### 3.7 Software design for monitoring system development

The software design for the IoT water quality monitoring system utilizes the Arduino IDE and the Blynk application. The Arduino IDE is employed for writing, compiling, and uploading code to the ESP32 microcontroller. This code includes the logic for reading sensor data and handling wireless communication. The Blynk application offers a user-friendly interface for monitoring the device via a smartphone, enabling users to receive real-time updates on the system's status.

#### 3.7.1 Block diagram of monitoring system

This block diagram illustrates a fundamental software design for a monitoring system. At the heart of the system is the ESP32 microcontroller, which acts as the central control unit. The system gathers sensor data and sends it to a designated platform the Blynk application facilitating real-time monitoring and analysis of the environment. This data transmission is usually carried out over Wi-Fi. Figure 3.13 presents the block diagram of the monitoring system.

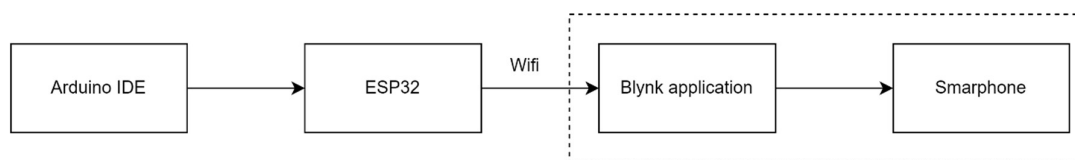
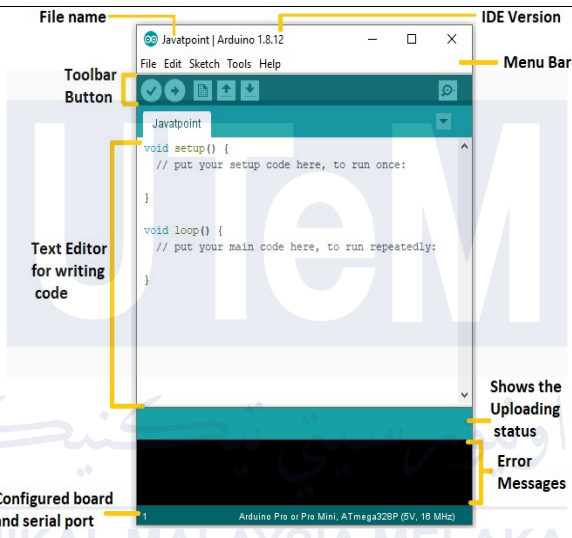



Figure 3.13 Block diagram of monitoring system

### 3.7.2 Software used for monitoring system

The monitoring system includes two essential software components, each integral to the system's functionality. As detailed in Table 3.3, all costs associated with these software components are covered, making its free of charge.

**Table 3.3 Software for monitoring system**

Bil.	Type	Quantity	Model	Price
1.	Ardino IDE	1		FREE
2.	Blynk application	1		FREE



### 3.8 Development of floatovoltaics for water quality monitoring

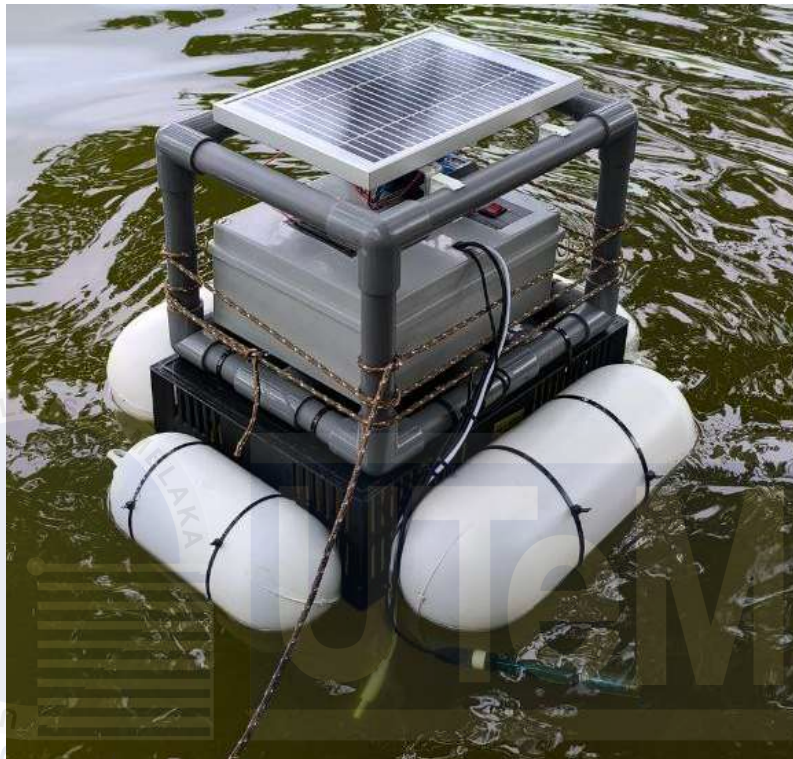
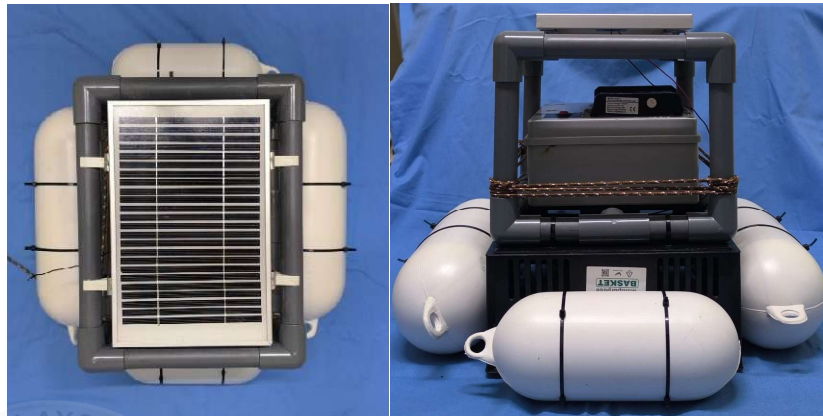


Figure 3.14 Final product of the project

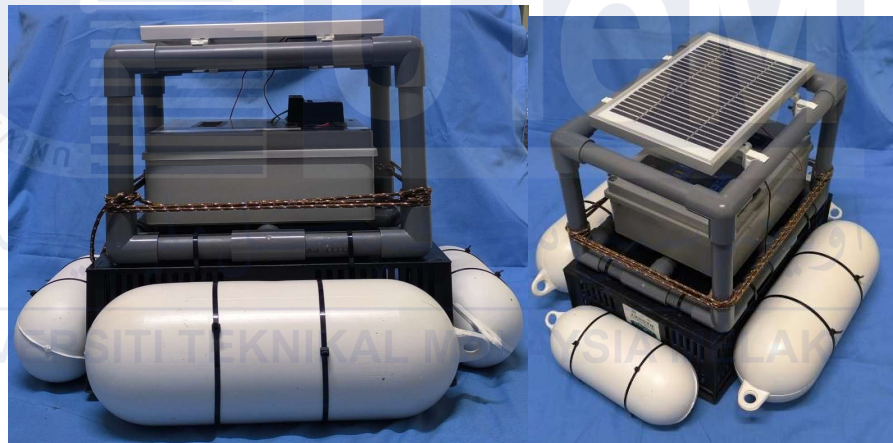
Figure 3.14 shows the final product for this project. With the goal of addressing renewable energy generation and water resource management, the finished device combines floatovoltaics (floating solar panels) with an integrated water quality monitoring system. Solar panels installed on floating platforms placed on bodies of water, such as lakes, ponds, or reservoirs, are known as floatovoltaics. In addition to producing renewable energy, these systems minimize algae development, minimize water evaporation, and maximize panel efficiency by using natural cooling from the water's surface.

### 3.8.1 Component and hardware setup for the final product



(a)

(b)



(c)

(d)

Figure 3.15 (a)Top view, (b)Front view, (c)Side view, (d)Perspective view

As shown in Figure 3.15, the things that makes it float are 4 buoys that have been attached to each side of the platform. A frame of PVC pipe created to secure the system from animal threat and sliding out into the water. Figure 3.16 shows the details of the system connection in the box.



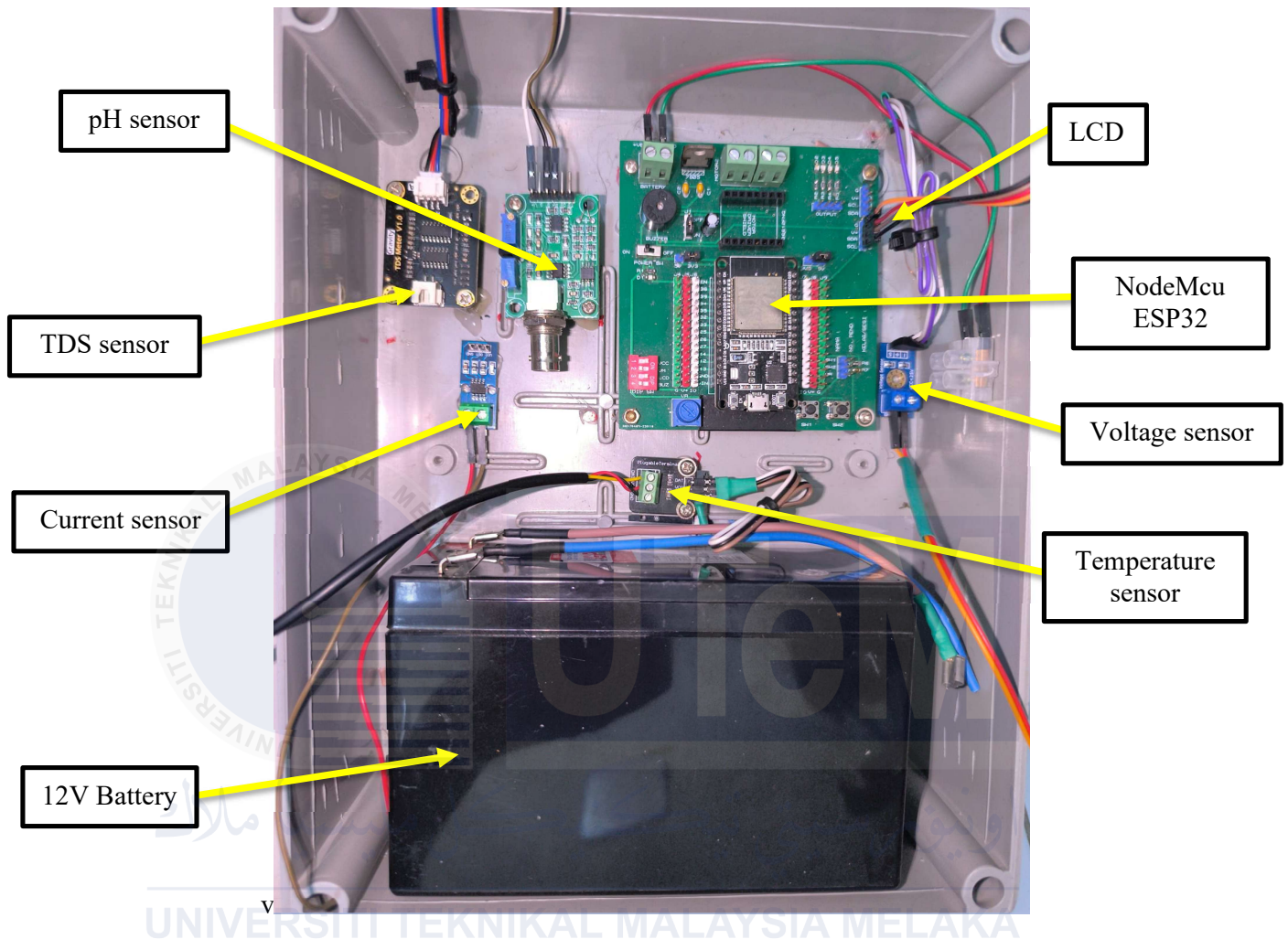


Figure 3.16 Layout of the electronic items used.

Figure 3.16 shows the arrangement of components used in the junction box without any connection to the esp32. The components include the power supply, sensors and indicator for this product. As for the complete arrangement with the connection to esp32 can be seen in Figure 3.17.

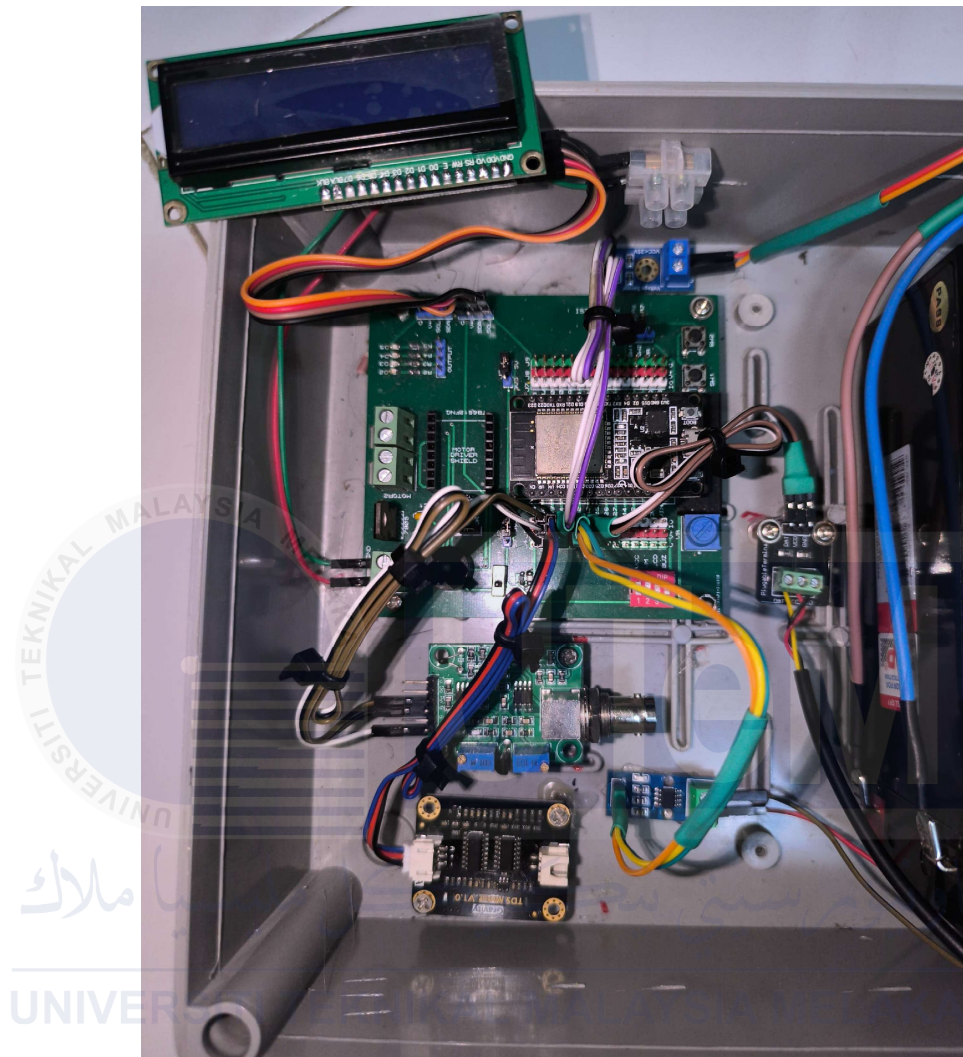


Figure 3.17 Connection of the electronic items

Figure 3.17 illustrate the connection of the components to the esp32 for the system. The pH sensor, tds sensor and temperature sensor are the water quality sensor while current sensor and voltage sensor is used to read current and voltage of the solar panel.

### 3.8.2 Circuit design for the overall system

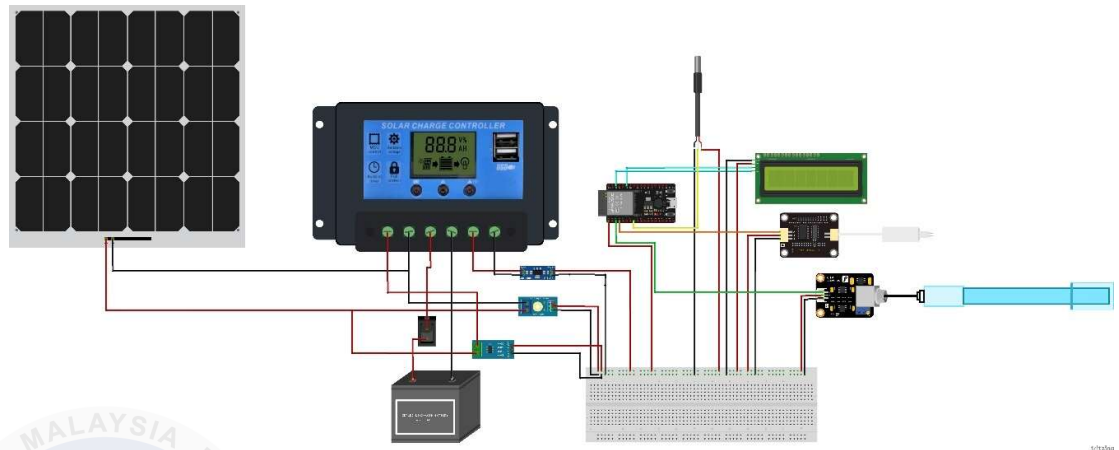


Figure 3.18 Wiring diagram for the overall system

In Figure 3.18, the connection diagram for all components used in the project is illustrated using Fritzing software. This diagram serves as a visual representation of the hardware integration required for the development of the floatovoltaics with a water quality monitoring system. The setup combines multiple sensors such as TDS, pH, temperature, voltage, and current sensors successfully connected to the ESP32 microcontroller. These sensors are interfaced with the ESP32 to provide accurate and real-time data monitoring, which is accessible via the Blynk application. All the information about the coding and pinout for each sensor can be seen in Appendix H.

### 3.8.3 Real time hardware setup

#### A. Location 1 (Urban Reforestation, Bukit Beruang, Melaka)



Figure 3.19 Hardware setup at location 1

Figure 3.19 Hardware setup at location 1 Figure 3.19 illustrates the hardware setup of the floatovoltaics with the water quality monitoring system deployed at **Location 1**. This setup showcases the integration of all components, including the TDS, pH, temperature, voltage, and current sensors, mounted alongside the floatovoltaic system on a calm water surface. Despite the water's calm state, the high level of contaminants highlights potential challenges for aquatic life and environmental quality in the area. Weather conditions during the deployment were overcast with signs of imminent rain, which posed a unique challenge for the floatovoltaic system.



**B. Location 2 (Taman Rimba, Taman Tasik Utama, Ayer Keroh, Melaka)**



Figure 3.20 Hardware setup at location 2

Figure 3.20 illustrates the hardware setup of the floatovoltaics with the water quality monitoring system deployed at **Location 2**. This setup highlights the integration of components, including the TDS, pH, temperature, voltage, and current sensors, working in tandem with the floatovoltaic system on a calm water surface. The calm water conditions contribute to stable sensor readings, ensuring accurate data collection. The deployment occurred on a sunny day, providing optimal conditions for the floatovoltaic system. This location's unique feature is its aquaculture activity, which benefits from the integrated monitoring system.

### C. Location 3 (Tasik Ayer Keroh, Ayer Keroh, Melaka)



Figure 3.21 Hardware setup at location 3

Figure 3.21 depicts the hardware setup of the floatovoltaics with the water quality monitoring system deployed at **Location 3**. This deployment showcases the system's ability to operate in dynamic conditions, with real-time data measurements recorded and analyzed to assess both water quality and energy generation. The water is exceptionally crystal clear, yet visibility to the bottom is limited, indicating significant depth. Location 3 is characterized by a large water body with significant human activity, including recreational and aquaculture-related operations. The presence of many visitors and ongoing activities introduces potential variations in water quality due to waste or disturbances, making continuous monitoring crucial.

### 3.9 Gantt Chart of the project (PSM 1)

Progress	WEEK												
	1	2	3	4	5	6	7	8	9	10	11	12	13
Psm briefing													
Install & Use Mendeley													
Paper/journal download													
Literature review													
Problem statement													
Objective													
Abstract													
Scope													
Introduction													
Methodology													
Chapter 1 -obj, problem statement													
Chapter 2- literature review													
Chapter 3 - methodology													
Chapter 4 - result													
Chapter 5 - Conclusion													
Past paper presentation													
Hardware/simulation													
work progress presentation													
Report submission													
Slide presentation submission													
PSM1 presentation													

### 3.10 Gantt Chart of the project (PSM 2)

Progress	WEEK												
	1	2	3	4	5	6	7	8	9	10	11	12	13
Buy Component													
Data Acquisition													
Analyse Data													
Project simulation													
Record Result													
Present Data to SV													
Improved Data													
Hardware Setup													
Project Tested Finalized													
Update Chapter 3 - methodology													
Update Chapter 4 – Result													
Update Chapter 5 – conclusion													
Report & poster discussion													
Report & poster finalized													
Report & poster submission													
Final PSM2 presentation													



### 3.11 Summary

This chapter details the proposed methodology for developing and designing the project, leveraging electrical, software, and mechanical design expertise. The project's problems and requirements have been analyzed to achieve the desired outcome. Consequently, this project will function successfully by incorporating all the knowledge gained from prior research and projects. The setup for solar PV system has been completed. The measurement for voltage and current of the solar PV system using hardware setup for 7-days have been done. The obtained results and analysis can be seen in Chapter 4.

A floating solar panel system equipped with water quality monitoring capabilities was successfully deployed and tested in three diverse locations, each presenting unique environmental challenges. From turbid waters with low sunlight to clear but rough waters with heavy human activity, the system demonstrated its adaptability and resilience. Regardless of the location, the system consistently provided accurate data on water quality parameters like TDS, pH, and temperature, while simultaneously generating solar energy to power the monitoring equipment. These findings highlight the system's potential as a valuable tool for sustainable aquaculture practices and effective water resource management across various environmental conditions. The obtained results and analysis can be seen in Chapter 4.

## CHAPTER 4

### RESULTS AND DISCUSSIONS

#### 4.1 Introduction

This chapter presents the findings obtained from the data collected over a 7-day period using the solar PV panel. The collected data will be analyzed to assess the performance of the floatovoltaic system for water monitoring applications. The observed trends, power generation efficiency, and any challenges encountered during the experiment will be discussed. Finally, based on the results, recommendations for future improvements and potential applications will be provided.

## 4.2 Data collected from solar PV system

Table 4.1 Data collected for a week

	Time	Voltage (V)	Current (A)	Power (W)	Average power (W)
Day 1	8:00	12.8	0.4	5.12	3.54
Friday	12:00	11.8	0.31	3.66	
26/4/24	16:00	10.2	0.18	1.84	
Day 2	8:00	11.8	0.3	3.54	4.53
Saturday	12:00	13.2	0.43	5.68	
27/4/24	16:00	11.6	0.28	3.25	
Day 3	8:00	12.6	0.37	4.66	4.42
Sunday	12:00	13.6	0.45	6.12	
28/4/24	16:00	11.3	0.25	2.83	
Day 4	8:00	12.3	0.35	4.31	4.67
Monday	12:00	13.1	0.43	5.63	
29/4/24	16:00	11.6	0.28	3.25	
Day 5	8:00	12.8	0.4	5.12	4.65
Tuesday	12:00	13.5	0.45	6.08	
30/4/24	16:00	11.2	0.3	3.36	
Day 6	8:00	12.5	0.36	4.50	4.24
Wednesday	12:00	11.6	0.27	3.13	
1/5/2024	16:00	12.8	0.39	4.99	
Day 7	8:00	12.4	0.37	4.59	4.59
Thursday	12:00	13.5	0.45	6.08	
2/5/2024	16:00	11.5	0.27	3.11	

Table 4.1 shows the data collected from solar PV system in a week. This table summarizes electrical measurements captured over a seven-day period. Daily readings were taken at three consistent time points: 8:00 AM, 12:00 PM, and 4:00 PM. For each time point, voltage (V), current (A), and instantaneous power (W) were recorded. The table additionally calculates an average power (W) for three days.

A. Day 1: Friday 26/4/2024

Figure 4.1, shows the graph voltage at day 1 beginning at around 12.8V at 8:00 and ending at approximately 10.2V at 16:00. Figure 4.2 shows minor fluctuations throughout the day, with an overall increase followed by a decrease. It starts at approximately 0.4A at 8:00, decrease at around 0.31A at 12:00, and then drops to about 0.18A by 16:00.

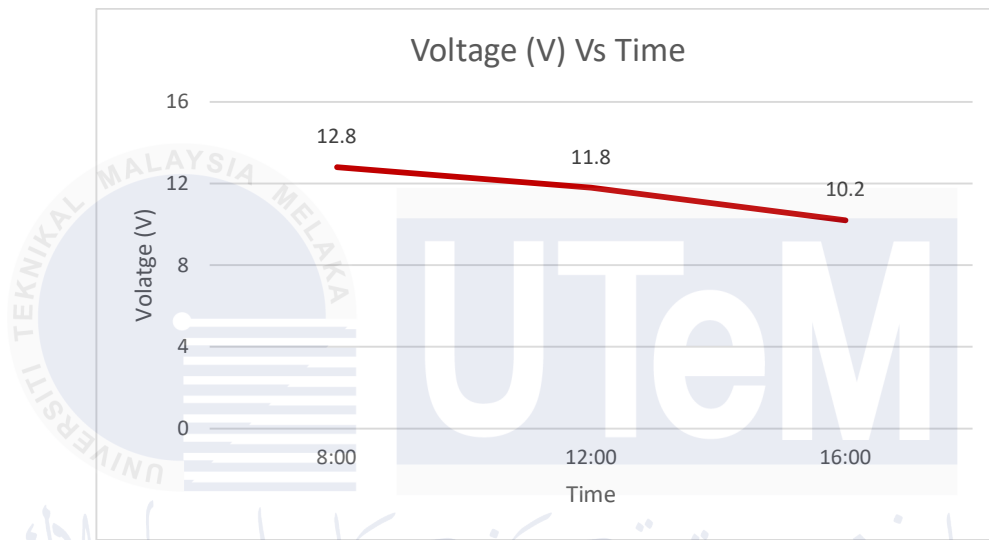


Figure 4.1 Voltage graph at day 1

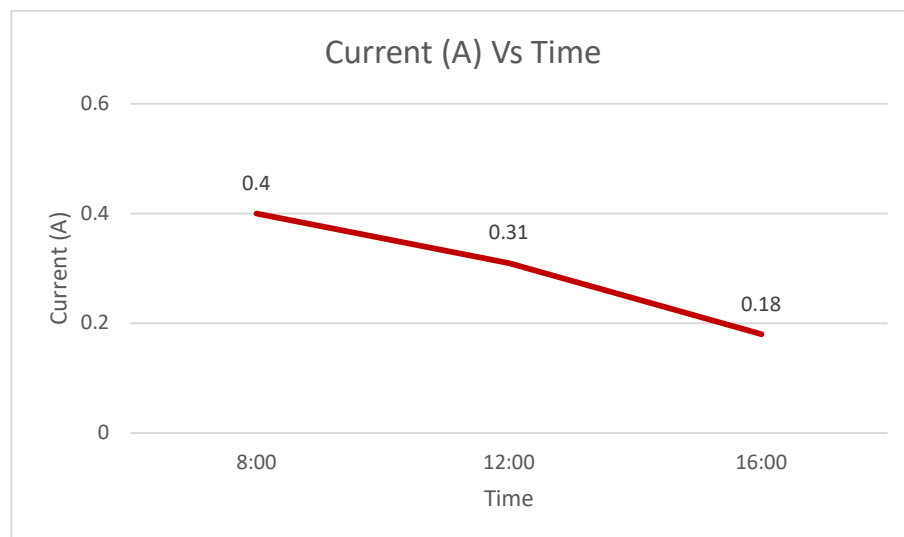


Figure 4.2 Current graph at day 1

B. Day 2: Saturday 27/4/2024

The voltage graph (Figure 4.3) beginning at around 11.8V at 8:00 and ending at approximately 11.6V at 16:00. Figure 4.2 shows minor fluctuations throughout the day, with an overall increase followed by a decrease. It starts at approximately 0.3A at 8:00, peaks at around 0.43A at 12:00, and then drops to about 0.28A by 16:00.

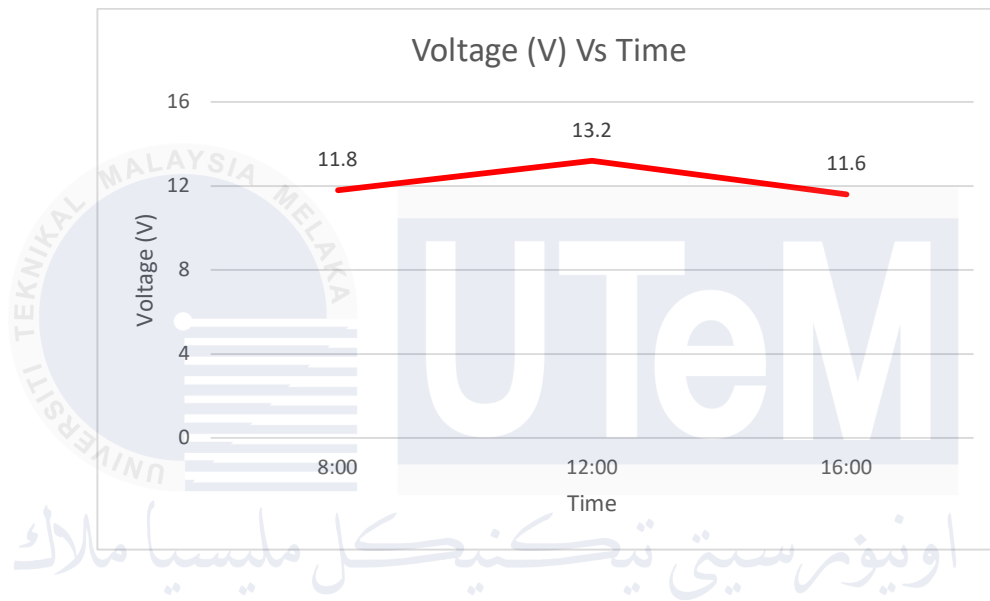


Figure 4.3 Voltage graph at day 2

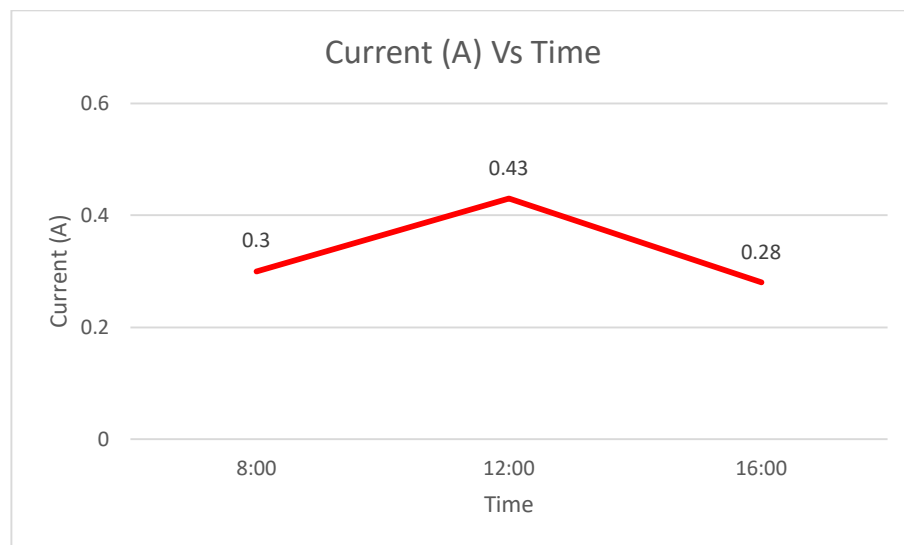


Figure 4.4 Current graph at day 2

### C. Day 3: Sunday 28/4/2024

The voltage graph (Figure 4.5), beginning at around 12.6V at 8:00 and ending at approximately 11.3V at 16:00. This graph resembles the one from the previous day, likely due to similar weather conditions. The current graph as seen in Figure 4.6 shows minor fluctuations throughout the day, with an overall increase followed by a decrease. It starts at approximately 0.37A at 8:00, peaks at around 0.45A at 12:00, and then drops to about 0.25A by 16:00.

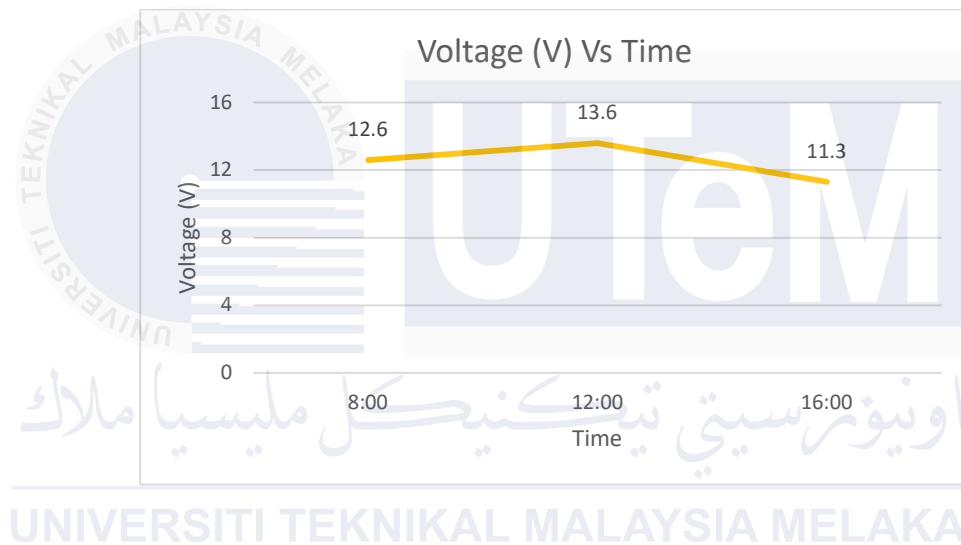


Figure 4.5 Voltage graph at day 3

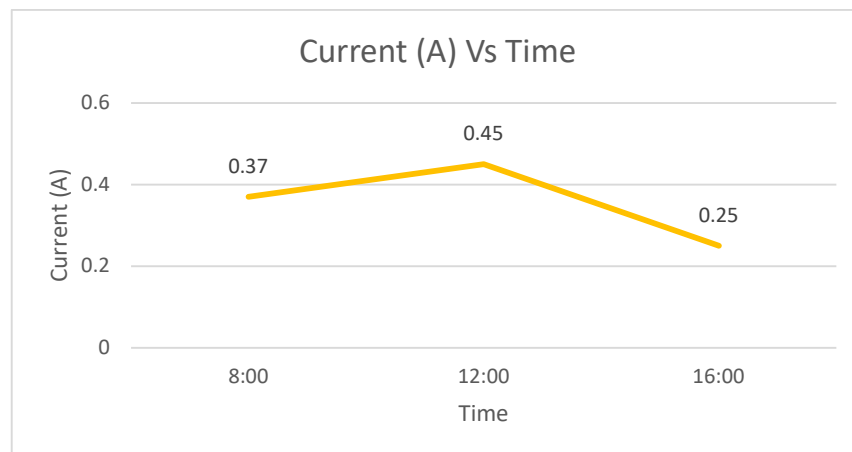


Figure 4.6 Current graph at day 3

#### D. Day 4: Monday 29/4/2024

The voltage graph (Figure 4.7), beginning at around 12.3V at 8:00 and ending at approximately 11.6V at 16:00. The current graph as seen in Figure 4.8 shows minor fluctuations throughout the day, with an overall increase followed by a decrease. It starts at approximately 0.35A at 8:00, peaks at around 0.43A at 12:00, and then drops to about 0.28A by 16:00. This graph resembles the one from the previous day, likely due to similar weather conditions.

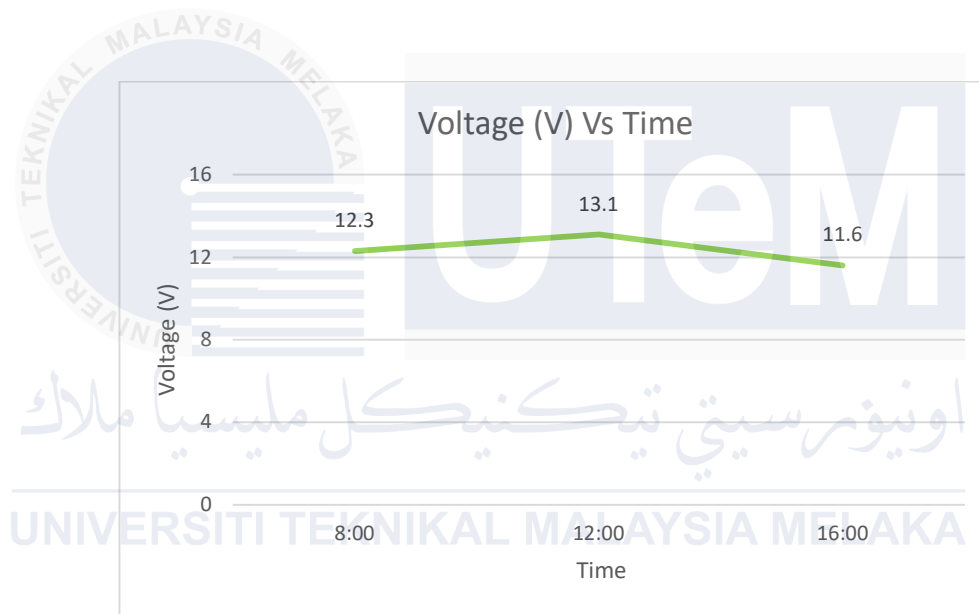


Figure 4.7 Voltage graph at day 4

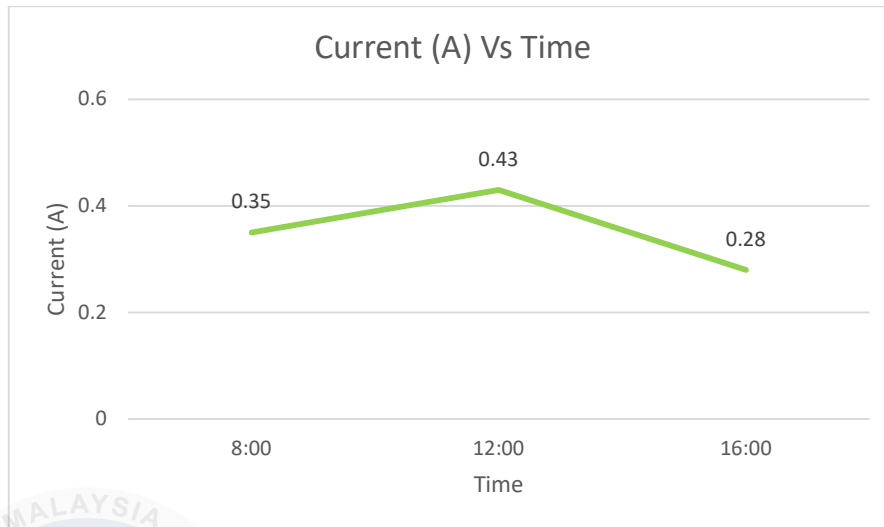


Figure 4.8 Current graph at day 4

E. Day 5: Tuesday 30/4/2024

In Figure 4.9 exhibits a gradual decline from around 12.8 volts at 8:00 AM to approximately 11.2 volts at 4:00 PM. This pattern is similar to the previous day's graph, suggesting consistent weather conditions. Figure 4.10 shows slight variations throughout the day. It initially increases from about 0.4 amps at 8:00 AM to a peak of around 0.45 amps at 12:00 PM before decreasing to approximately 0.3 amps by 4:00 PM.

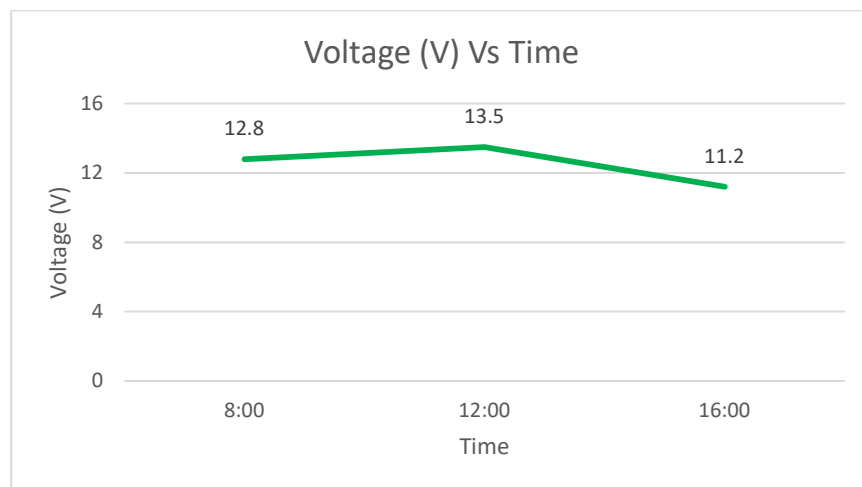


Figure 4.9 Voltage graph at day 5



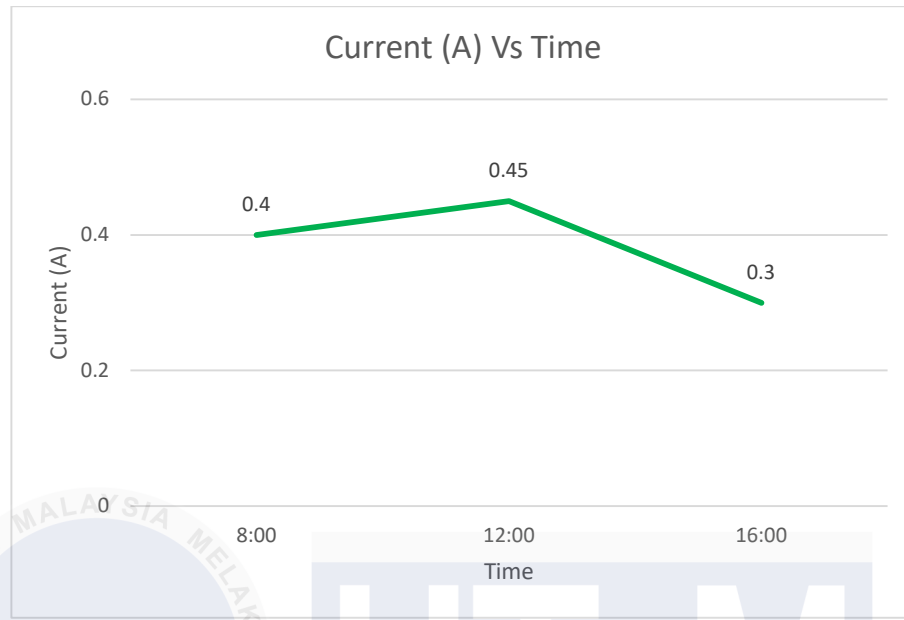


Figure 4.10 Current graph at day 5

F. Day 6: Wednesday 1/5/2024

Figure 4.11 shows the voltage graph, which starts at around 12.5V at 8:00 and ends at about 12.8V at 16:00. Figure 4.12 displays the present graph, which exhibits slight variations throughout the day, with an overall increase followed by a decline. By 8:00, it is at around 0.36A, by 12:00, it is at about 0.27A, and by 16:00, it is at about 0.39A.

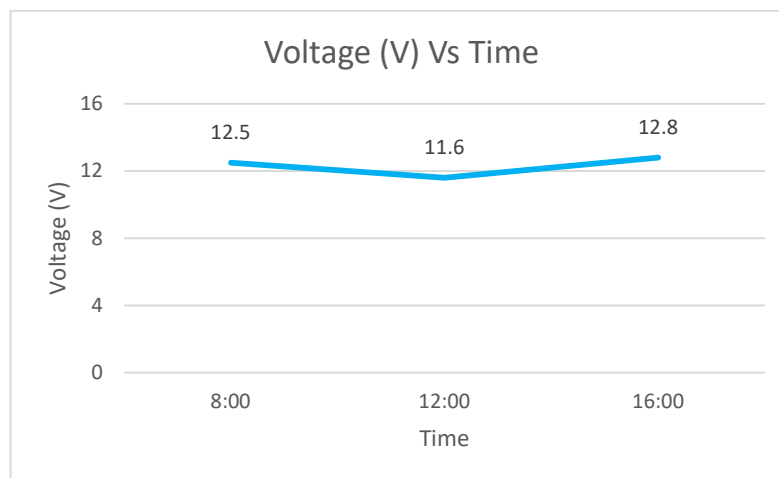


Figure 4.11 Voltage graph at day 6

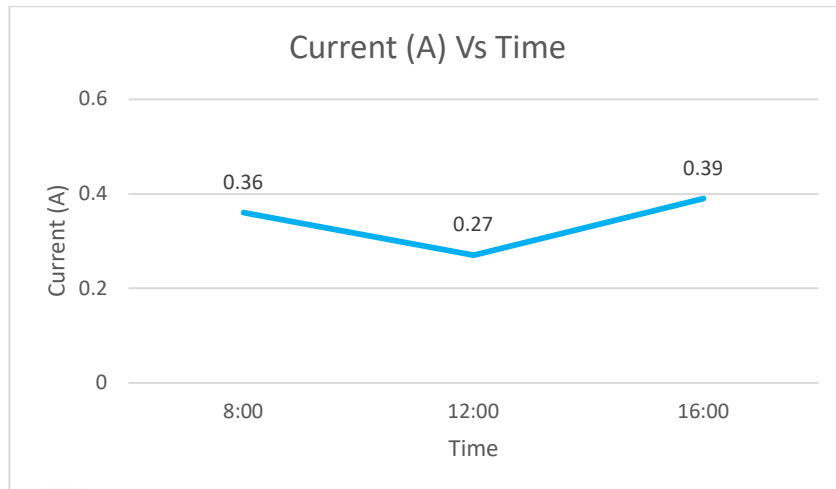


Figure 4.12 Current graph at day 6

G. Day 7: Thursday 2/5/2024

Figure 4.13 shows a gradual decline over the course of the day, starting at approximately 12.4V at 8:00 and ending around 11.5V by 16:00. Figure 4.14 demonstrates minor fluctuations, with an overall increase followed by a decrease. The current starts at about 0.37A at 8:00, peaks at 0.45A around noon, and then drops to approximately 0.27A by 16:00. This pattern closely mirrors that of the previous day, likely due to similar weather conditions.

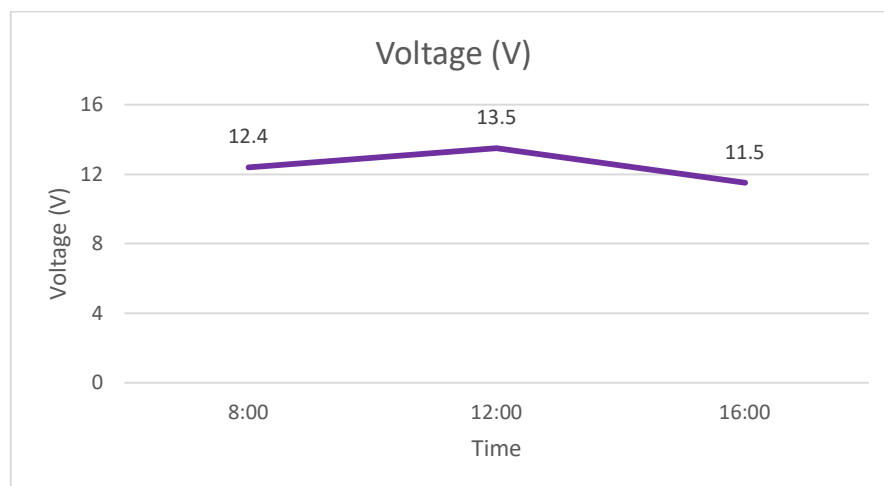


Figure 4.13 Voltage graph at day 7

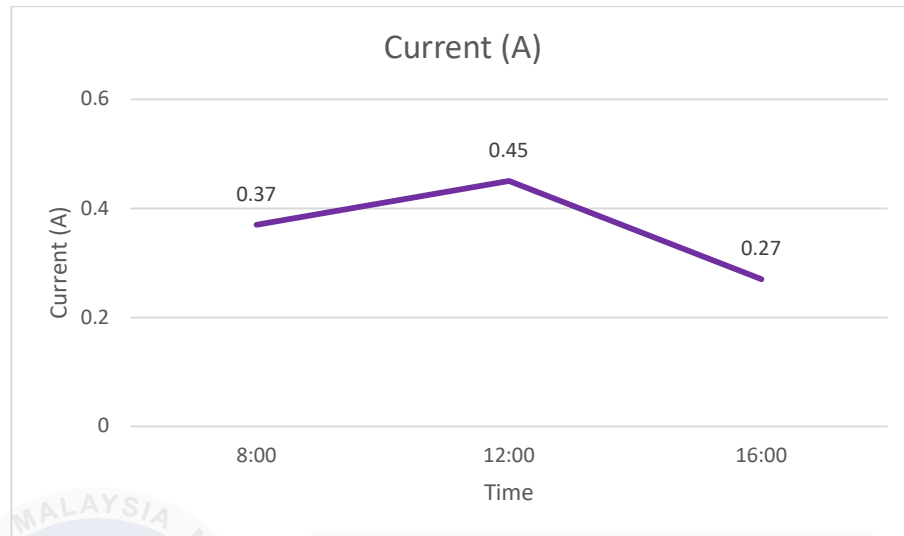


Figure 4.14 Current graph at day 7

The x-axis represents time from 8:00 AM to 4:00 PM, while the y-axis shows voltage ranging from 10V to 14V. Each series has a distinct color. Series 1, starting at 12.8V, peaks at 13.6V before noon, then sharply drops to 10.2V by 4:00 PM. Series 2 begins at 11.8V, peaks at 13.2V at noon, and returns to 12V by 4:00 PM. Series 3 starts at 12.3V, reaches 13.5V before noon, and drops to 12.3V by 4:00 PM. Series 4, starting at 12.4V, peaks at 13.1V at noon, and ends at 12.1V by 4:00 PM. Series 5 begins at 12.6V, peaks at 13.2V, and falls to 11.6V by 4:00 PM. Series 6 starts at 12.2V, dips to 11.6V, and rises to 12.8V by 4:00 PM. Series 7, starting at 12.5V, peaks at 13.1V, and drops to 11.2V by 4:00 PM. The  $V_{mp}$  line is a constant reference at 12V. The graph highlights the voltage behavior over time, with most series peaking around noon and decreasing later, except Series 6, which shows a rise towards the end. This comparison provides insights into the performance characteristics of the different series relative to the reference voltage. From Figure 4.15, the voltage at maximum power ( $V_{mp}$ ) compared with the voltage from each day.

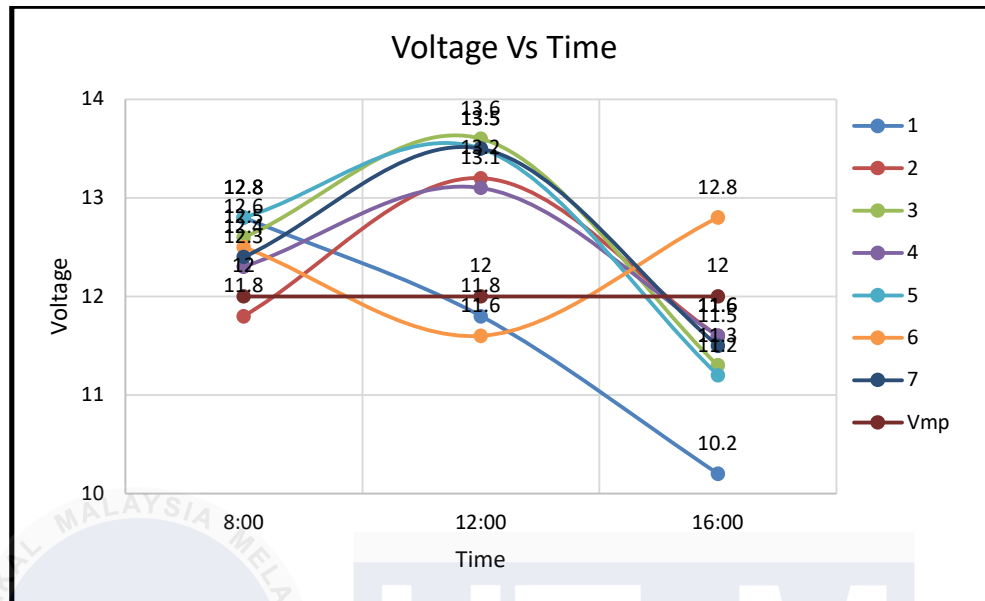


Figure 4.15 Voltage compared with Vmp graph

The current data analysis across seven days shows distinct fluctuations throughout the day, with the x-axis representing time from 8:00 AM to 4:00 PM and the y-axis displaying current values ranging from 0.2A to 0.5A. Each day's data is represented by a different color, and the  $I_{sc}$  line, fixed at 0.4A, serves as a reference. On Day 1, the current starts at 0.42A, peaks just before noon at 0.45A, and then sharply declines to 0.25A by 4:00 PM, showing a notable drop of 0.15A from the  $I_{sc}$ . Day 2 starts lower at 0.3A, gradually rises to 0.43A by noon, and settles at 0.39A by 4:00 PM, with a slight deviation of -0.01A. Day 3 experiences a similar pattern, beginning at 0.35A, reaching a peak of 0.45A before noon, and then dropping to 0.27A by 4:00 PM, which results in a -0.13A difference from the reference current. On Day 4, the current fluctuates from 0.36A to 0.42A at noon, then drops to 0.28A, showing a difference of -0.12A. Day 5 starts at 0.4A, peaks at 0.42A, and declines to 0.3A by 4:00 PM, with a difference of -0.1A from the  $I_{sc}$ . Day 6 follows an irregular pattern, beginning at 0.37A, dipping to 0.27A around noon, and then increasing to 0.39A by 4:00 PM, resulting in a minimal difference of -0.01A. Lastly, Day 7 starts at 0.42A, peaks

slightly higher at 0.43A, and then drops to 0.27A by 4:00 PM, showing a difference of -0.13A from the reference. This comparison underscores the variability in current behavior, with most days showing a decrease after peaking around noon, while Day 6 demonstrates a rise towards the end of the day. The  $I_{sc}$  line serves as a clear benchmark for understanding these fluctuations in the solar panel's performance over time.

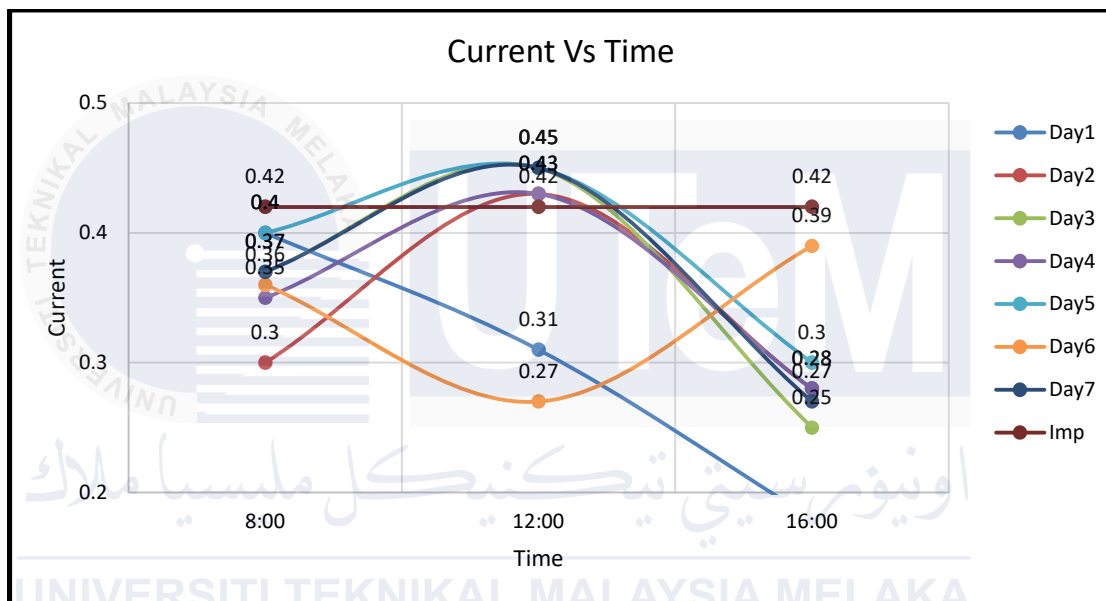


Figure 4.16 Current compared with  $I_{mp}$  graph

### 4.3 Analysis for solar PV system

Table 4.2 Analysis of power efficiency of the solar PV

Day	average power (W)	rated power (W)	differnet	% different
1	3.54	5	1.46	70.76
2	4.46	5	0.54	89.24
3	4.47	5	0.53	89.45
4	4.44	5	0.56	88.81
5	4.72	5	0.28	94.35
6	4.06	5	0.94	81.24
7	4.59	5	0.41	91.8

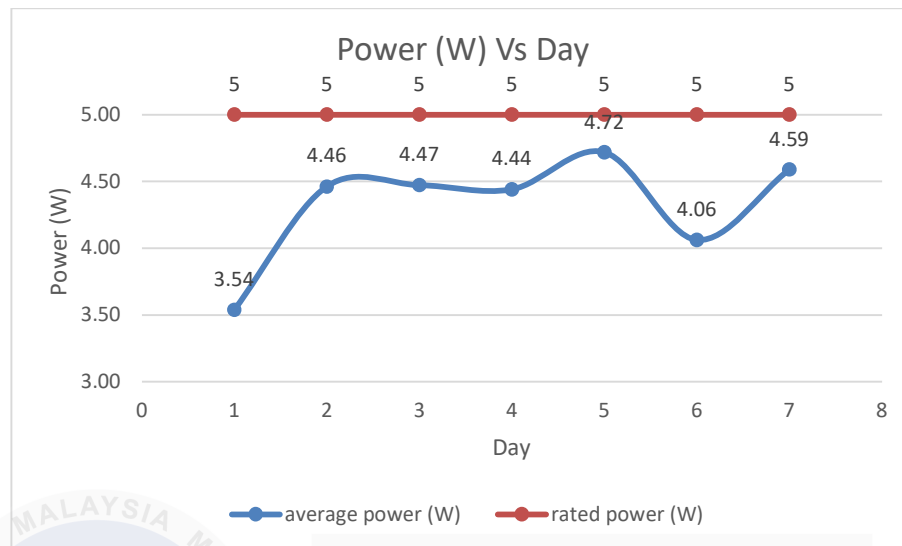


Figure 4.17 Average power compared with rated power graph

The comparison between average power calculated from the measured value with the specification power can be seen Figure 4.17 . The x-axis represents the days from 1 to 7, while the y-axis shows power in watts, ranging from 3.5W to 5W. The blue line represents the average power, which fluctuates throughout the week. It starts at 3.54W on Day 1, rises significantly to 4.46W on Day 2, and remains relatively stable around 4.44W to 4.72W from Day 3 to Day 5, with the highest value on Day 5. There is a noticeable drop to 4.06W on Day 6, followed by a rise to 4.59W on Day 7. In contrast, the orange line representing the rated power stays constant at 5W across all days. This comparison shows that the average power output is consistently below the rated power, highlighting variations in performance and consistency of the power output over the week.

#### 4.4 Data from floating solar power generation

Table 4.3 Solar generation at Urban Reforestation

Time	Voltage, V	Current, A	Power, W
8:00	10.86	0.2	2.17
9:00	10.92	0.26	2.84
10:00	10.89	0.25	2.72
11:00	11.53	0.34	3.92
12:00	12.11	0.41	4.97
13:00	11.93	0.4	4.77
14:00	11.74	0.38	4.46
15:00	11.62	0.36	4.18
16:00	11.55	0.34	3.93
17:00	11.23	0.3	3.37
18:00	10.54	0.29	3.06

Table 4.3 shows the data collection of solar power generation for a day at Urban Reforestation, Bukit Beruang, Melaka. The data is recorded hourly from 8 AM to 6 PM. It includes measurements of voltage, current, and calculated power output. The analysis for each measurement across time can be seen in Figure 4.18, Figure 4.19 and Figure 4.20.

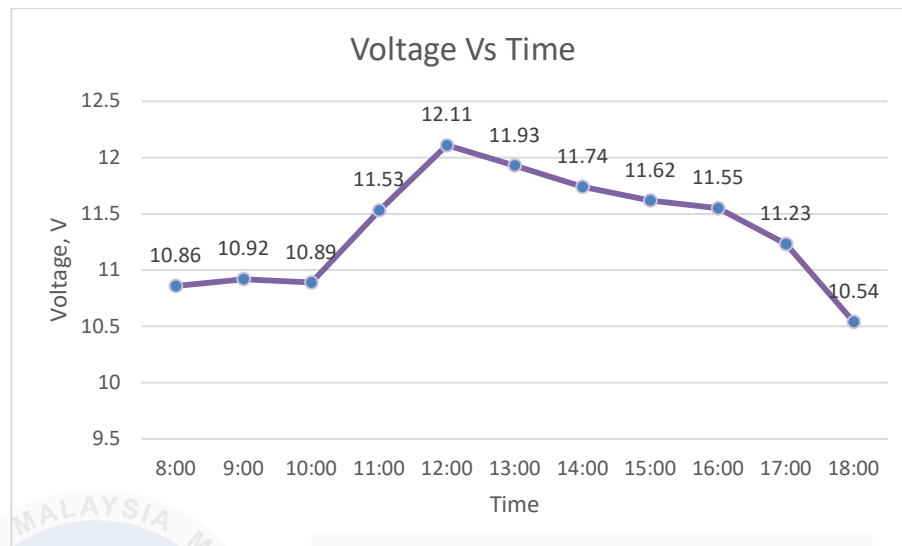


Figure 4.18 Voltage Vs Time

The graph illustrates the relationship between voltage and time. It shows that the voltage starts at around 11 volts at 8:00 and increases steadily to a peak of approximately 12.2 volts around 12:00. After this peak, the voltage gradually decreases, reaching a value of about 10.5 volts by 18:00. The overall trend suggests a pattern of increasing voltage followed by a decrease over the observed time period.



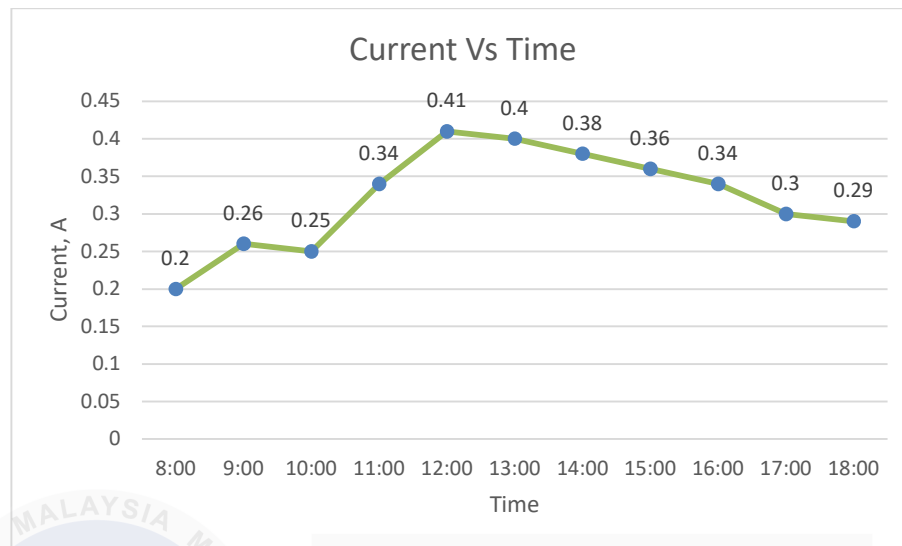


Figure 4.19 Current Vs Time

The graph illustrates the connection between time and current. The current starts off at about 0.2 amps at 8:00 and gradually rises to a high of about 0.42 amps at 12:00. The current steadily drops after this peak, reaching a value of around 0.3 amps at 18:00. Throughout the observed time, this general trend points to a pattern of rising current followed by falling current.

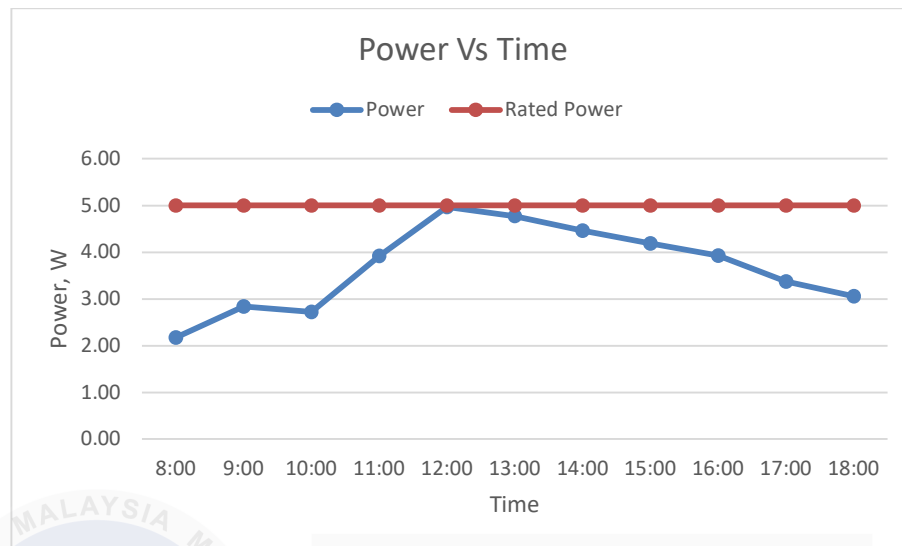


Figure 4.20 Power Vs Time

The graph illustrates the relationship between power and time throughout the day. The blue line represents the actual power generated, while the red line indicates the rated power of 5 W, which remains constant. Initially, the actual power increases steadily from 2 W at 8:00 to its peak of approximately 5 W at 12:00, matching the rated power. After 12:00, the actual power begins to decline gradually, falling below 4 W by 14:00 and continuing to decrease until reaching around 2 W by 18:00. This trend suggests that power generation is influenced by environmental factors, such as solar intensity, which peaks around midday and diminishes later in the afternoon.

#### 4.5 Data tested from Water Quality Sensor

This section will cover the test result obtained for each sensors used in water quality system. This result obtained from several type of water sample. First, the test is conducted on the DS18B20 temperature sensor. The test is conducted in different temperatures level of water from low to high. The measurements from the sensor and thermometer are compared in order to obtain the data. Table 4.4 Data collected for temperatureTable 4.4 and Figure 4.21 shows the temperature test result.

Table 4.4 Data collected for temperature

Different Temperature Level	Temp 1	Temp 2	Temp 3	Temp 4	Temp 5
Data from Thermometer	16.1	19.1	28.7	30.7	41.13
Data from Sensor	14.38	17.44	28.81	29.0	38.1
Difference	1.72	1.66	0.11	1.7	3.03
% Difference	10.68	8.69	0.38	5.54	7.37

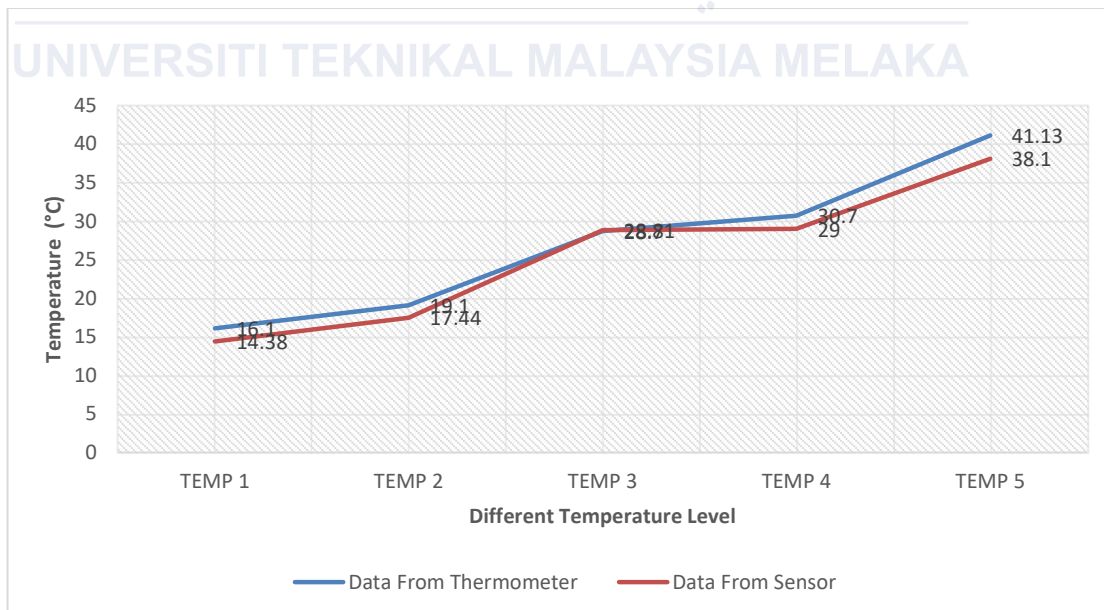


Figure 4.21 Temperature measurement graph

There are differences between sensor and thermometer measurements, as indicated by the data measurement in the table. The difference in sensitivity is the reason. Despite the discrepancies, this test is successful since the trend is followed by both graph lines. To obtain the measurement, both the thermometer and the sensor are submerged in the water simultaneously. Figure 4.22 Temperature test setup

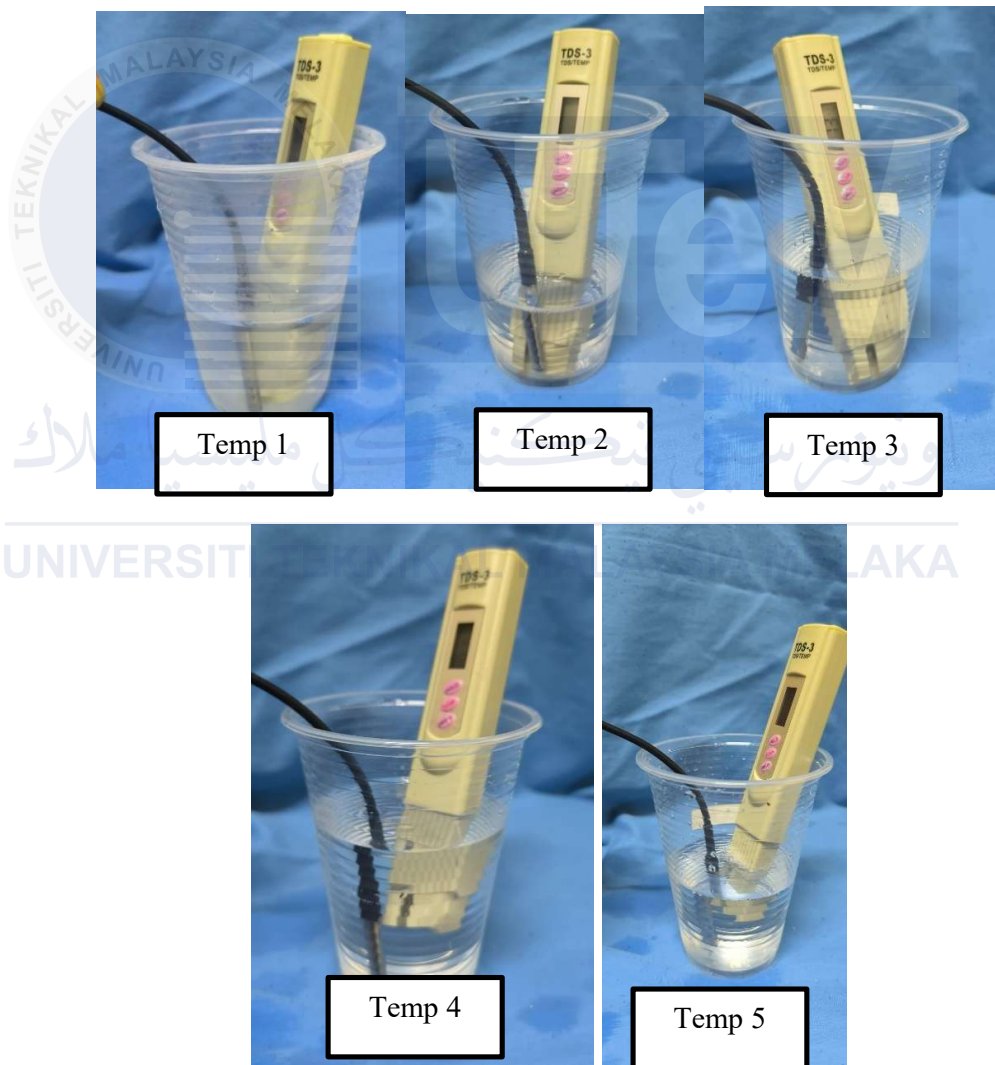


Figure 4.22 Temperature test setup

Next is tds sensor data measurement. There are 5 tests conducted to record the data measurement. The test was conducted by comparing tds sensor with tds meter. Table 4.3 and figure 4.13 show the result from the test.

Table 4.5 Data collected for TDS

Type of water	Tap	Muddy	Lake	Soap	Deionized
Data from TDS meter	62	161	204	1360	1750
Data from TDS sensor	58.2	154.78	195.56	1254.52	1647.01
Difference	3.8	6.22	8.44	105.48	102.99
% difference	6.13	3.86	4.14	7.76	5.89

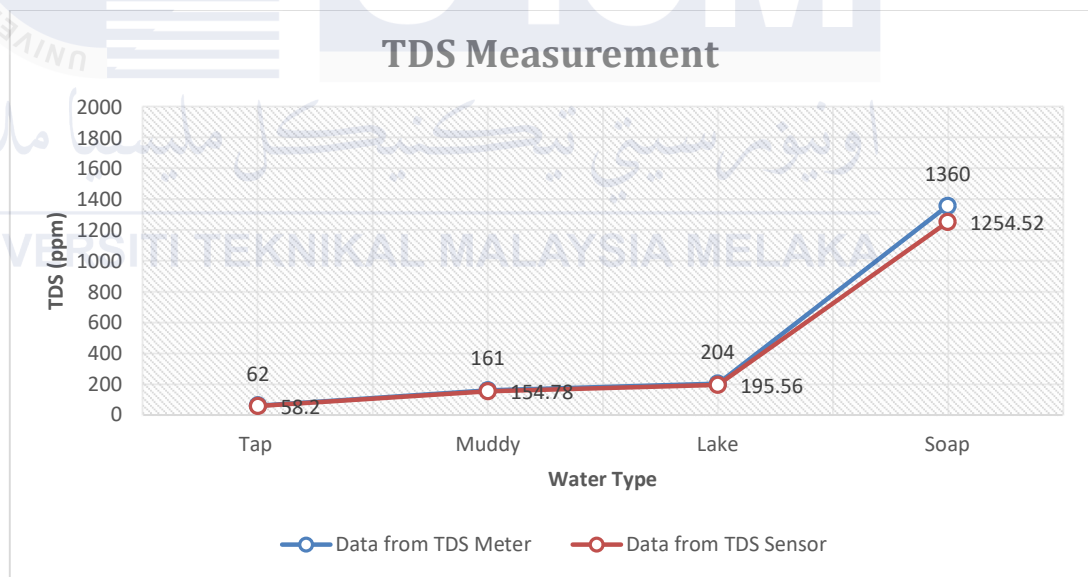


Figure 4.23 TDS measurement graph

Figure 4.23 contrasts TDS readings from a TDS sensor and a TDS meter for various kinds of water. The outcomes demonstrate consistent performance between the two devices and are closely matched. TDS levels are lowest in tap water (meter: 62 ppm, sensor:

58.2 ppm) and highest in deionized water (meter: 1750 ppm, sensor: 1647.01 ppm). Lake and muddy water have moderate TDS levels, which indicate their impurity concentration, but soap water also exhibits high amounts. Calibration or sensor sensitivity might be the cause of the little variations between the two devices. The test setup for TDS can be seen in Figure 4.24.

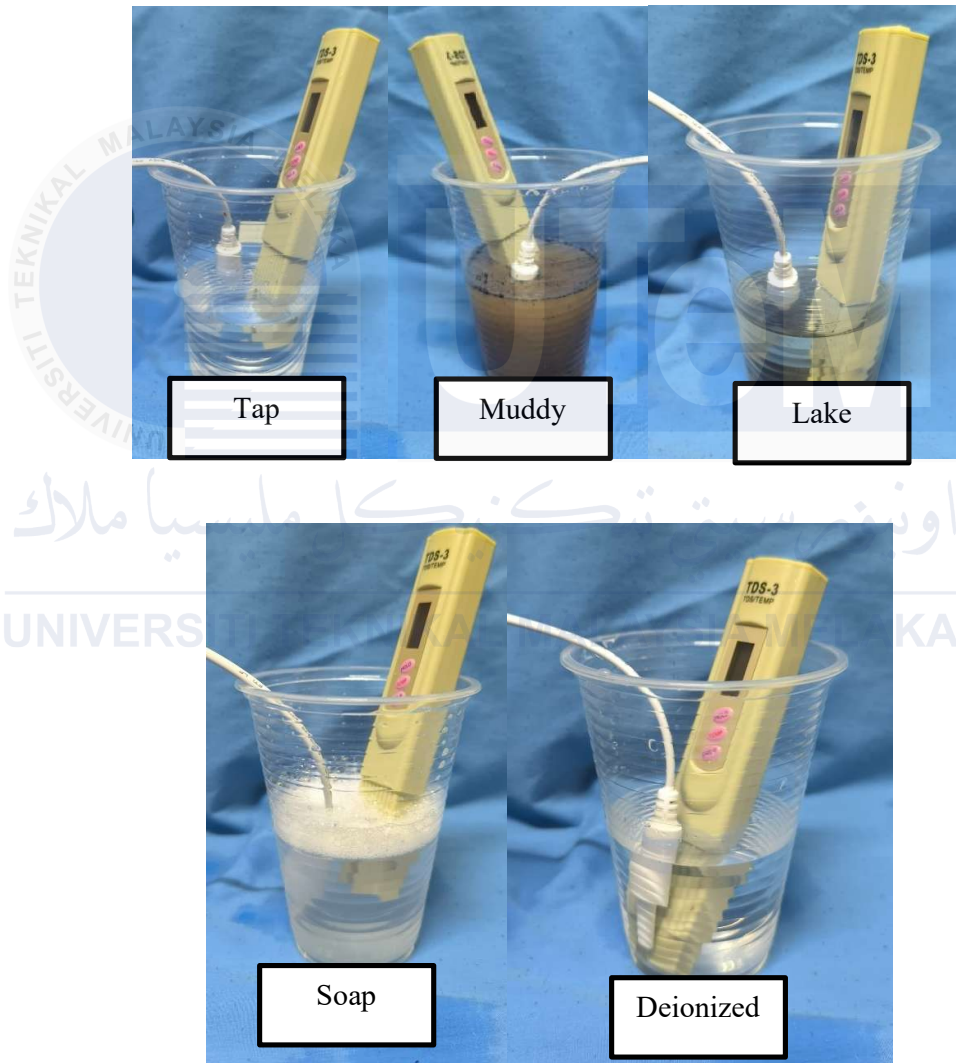


Figure 4.24 TDS test setup

Data from the pH sensor is then measured. To capture the data measurement, five tests are run. The test was carried out by contrasting a commercial pH meter with a pH sensor. Table 4.6 and Figure 4.26 shows the result from the test.

Table 4.6 Data collected for pH

Sample	Ginger	pH 4.01	Tap	pH 9.18	Soap
Data from pH meter	3.18	4.01	7.14	9.18	12.58
Data from pH sensor	2.65	3.88	6.95	9.06	12.03
Difference	0.53	0.13	0.19	0.12	0.55
% Difference	16.67	3.24	2.66	1.31	4.37

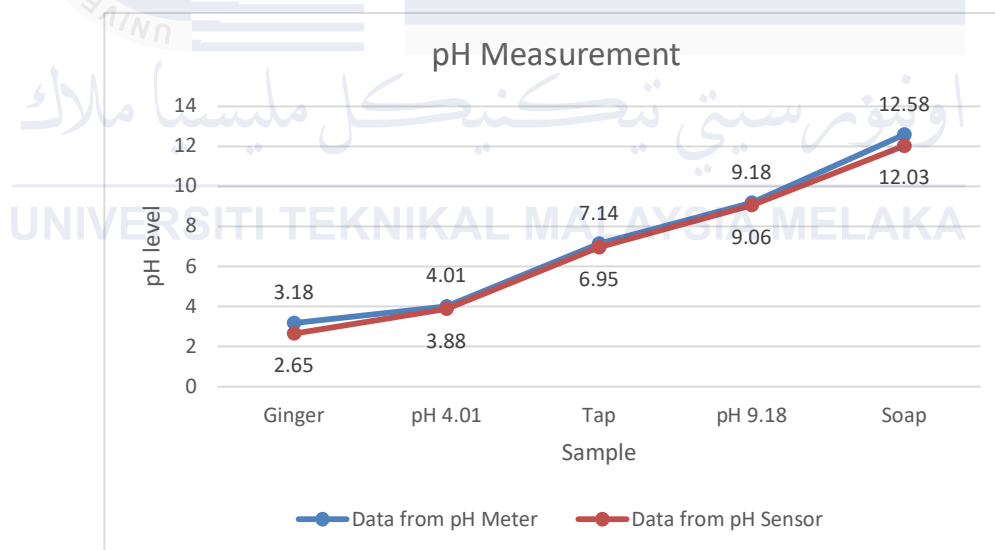


Figure 4.25 pH measurement graph

Figure 4.25 shows the pH values of several substances as determined by a pH sensor and a pH meter. Soap is highly alkaline, tap water is somewhat acidic to neutral, ginger and the pH 4.01 sample are acidic, and the pH 9.18 sample is mildly alkaline. Temperature



changes, measuring methods, and calibration variances are some possible causes of the discrepancies in measurements. Figure 4.26 shows the experimental setup

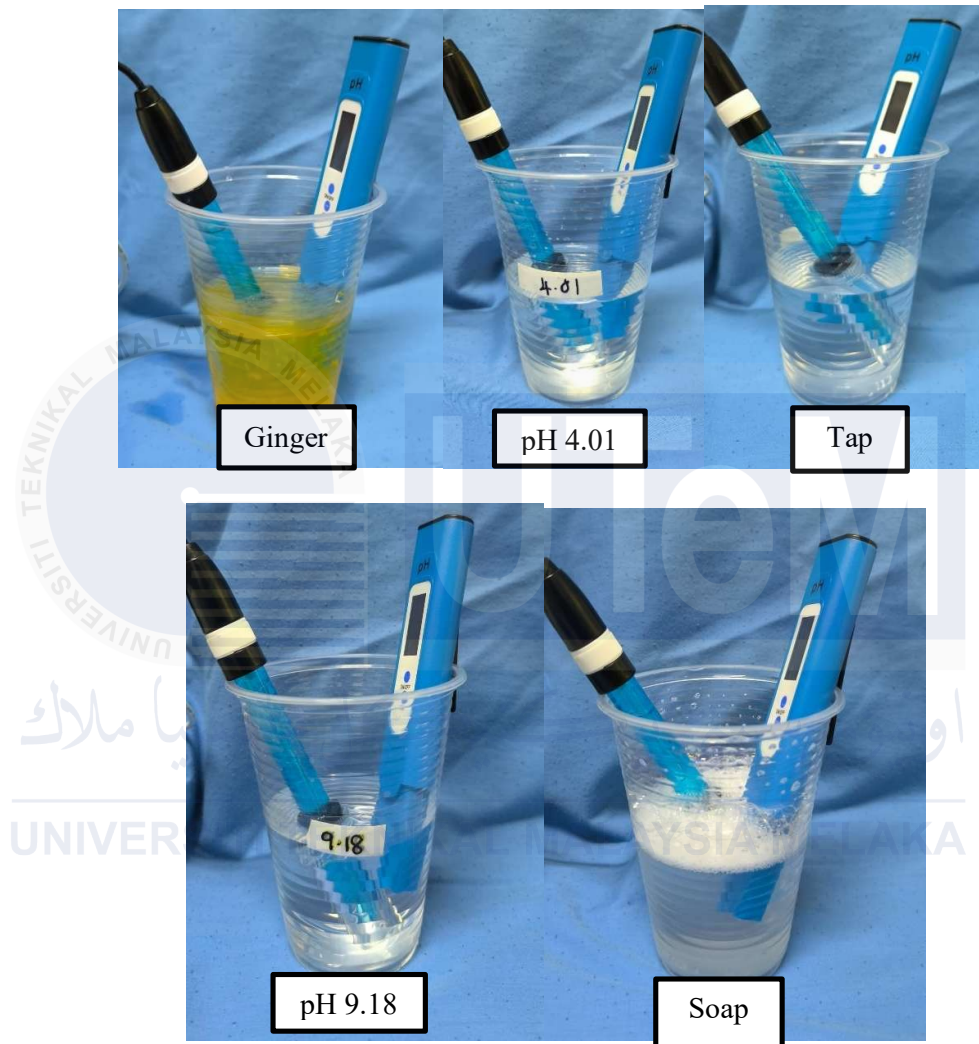


Figure 4.26 pH test setup



#### 4.6 Data collected at Location 1 (Urban Reforestation)

Table 4.7 Solar measurement at Location 1

Voltage, V	Current, A	Power, W
10.96	0.36	3.95
10.81	0.36	3.89
10.85	0.35	3.79
10.35	0.32	3.31
10.43	0.35	3.65

Table 4.7 shows the solar measurement at location 1 while collecting data for water sample. This is expected due to cloudy weather and the lack of full sunlight, leading to reduced energy generation by the floatovoltaics system. The data for the TDS (Total Dissolved Solids), pH, and temperature of a water sample were collected over 20 readings, with a 15-second interval between each measurement. This process ensured consistent monitoring of water quality parameters. The reading for each reading can be seen in Table 4.8.

Table 4.8 Water sample at Location 1

Bil.	pH	Tds (ppm)	Temperature (°C)
1.	6.8	450	22.1
2.	6.7	460	22.3
3.	6.9	455	22
4.	7	470	22.2
5.	6.8	475	22.1
6.	6.9	460	22.3
7.	7.1	445	22
8.	6.7	440	22.4
9.	6.8	465	22.1
10.	6.9	460	22.3
11.	7	470	22
12.	6.7	455	22.2
13.	6.8	460	22.3
14.	6.9	465	22
15.	6.8	450	22.2
16.	6.7	445	22.3
17.	6.9	460	22.1
18.	6.8	455	22.3
19.	6.9	445	22.4
20.	6.8	440	22.2
Average	6.85	456.25	22.19

Table 4.8 shows the water sample reading at location 1. The water quality is poor, as indicated by the consistently high TDS readings (around 450–475 ppm), suggesting an elevated level of dissolved solids, such as suspended particles, contaminants, or algae. This aligns with the observation of turbid water, which appears unclear and contains visible pollutants. The pH levels fluctuate between 6.7 and 7.1, which is slightly acidic to neutral. This range indicates that the water may not be ideal for most aquatic life, possibly due to organic waste or acidification from environmental factors like rain. The slight variation in pH is typical during cloudy weather and rainfall, as these conditions can dilute or alter pH levels. Temperature readings, ranging from 22.0°C to 22.4°C, suggest a stable, moderate water temperature, which is characteristic of calm waters. The overcast weather with impending rain likely prevented any significant temperature fluctuations caused by sunshine or wind, maintaining a stable environment.

#### 4.7 Data collected at Location 2 (Taman Rimba)

Table 4.9 Solar measurement at Location 2

Voltage, V	Current, A	Power, W
11.54	0.36	4.15
11.58	0.38	4.40
11.46	0.32	3.67
11.51	0.35	4.03
11.49	0.34	3.91

The solar measurement at location 2 during the data collection for the water sample is displayed in Table 4.9. This is to be expected as the floatovoltaics system generates less

energy when there is cloud cover and partial sunshine. Twenty measurements of a water sample's TDS (total dissolved solids), pH, and temperature were made, with a 15-second lag between each measurement. Consistent monitoring of water quality measures was guaranteed by this procedure. Table 4.10 shows the reading for each reading at location 2.

Table 4.10 Water sample at Location 2

<b>Bil.</b>	<b>pH</b>	<b>Tds (ppm)</b>	<b>Temperature (°C)</b>
1.	7.2	180	23
2.	7.3	175	23.1
3.	7.1	185	23.2
4.	7.2	190	23
5.	7.3	180	23.1
6.	7.2	185	23
7.	7.1	190	23.2
8.	7.3	175	23.3
9.	7.2	180	23.1
10.	7.1	185	23
11.	7.2	190	23.1
12.	7.3	175	23.2
13.	7.2	180	23.1
14.	7.1	185	23
15.	7.2	190	23.3
16.	7.3	175	23.2
17.	7.2	180	23.1

18.	7.1	185	23
19.	7.2	190	23.1
20.	7.3	175	23.2
Average	7.21	182.5	23.12

As seen in Table 4.10, TDS tests at Location 2 ranged from 175 to 190 ppm, showing lower levels of dissolved solids and clearer water, indicating higher water quality than at Location 1. This is consistent with the small-scale aquaculture system and the reported sunny weather, both of which probably help to create a cleaner environment. The aquaculture system benefited even more from the pH levels being steady and in the neutral range, which is optimal for most of the aquatic life. Furthermore, the water temperature was steady and mild between 23.0 to 23.3°C, which is ideal for aquatic life, especially in aquaculture settings. This steady temperature was probably maintained in part by the bright weather, which benefited the general well-being of the aquatic life there.

#### 4.8 Data collected at Location 3 (Tasik Ayer Keroh)

Table 4.11 Solar measurement at Location 3

Voltage, V	Current, A	Power, W
12.36	0.39	4.82
12.33	0.39	4.81
12.02	0.41	4.93
12.25	0.40	4.90
11.76	0.41	4.96

Despite the turbulent water conditions and human activity surrounding the location, Table 4.11 show that the floatovoltaics system is performing well. The sunny weather probably helped the system, which produced enough electricity to operate the large-scale aquaculture activities as well as the water quality monitoring. A water sample's temperature, pH, and TDS (total dissolved solids) were measured twenty times, with a 15-second interval between each measurement. This process ensured regular monitoring of water quality indicators. The reading for each reading at site 3 is displayed in Table 4.12.

Table 4.12 Water sample at Location 3

<b>Bil.</b>	<b>pH</b>	<b>Tds (ppm)</b>	<b>Temperature (°C)</b>
1.	7.6	250	24.5
2.	7.5	240	24.6
3.	7.7	260	24.7
4.	7.6	255	24.5
5.	7.5	250	24.6
6.	7.5	245	24.7
7.	7.6	250	24.6
8.	7.5	240	24.5
9.	7.5	245	24.7
10.	7.7	260	24.6
11.	7.6	255	24.5
12.	7.5	250	24.6
13.	7.5	240	24.7
14.	7.5	245	24.6

15.	7.6	250	24.5
16.	7.5	240	24.7
17.	7.5	245	24.6
18.	7.7	260	24.5
19.	7.6	255	24.6
20.	7.1	252	24.2
Average	7.54	249.35	24.58

Table 4.12 shows the data at Location 3. The data revealed TDS readings ranging from 240 to 260 ppm, indicating moderately good water quality. While slightly higher in dissolved solids compared to Location 2, likely due to increased human activity and the larger aquaculture operations, the water remained relatively clear, crucial for maintaining a healthy aquatic ecosystem. pH levels fluctuated between 7.5 and 7.7, slightly more alkaline than Location 2 but still within a range that supports aquatic life. This slightly higher pH is typical for larger aquaculture environments, where efforts are made to maintain a balanced pH for optimal fish health. Temperature readings were slightly higher than Location 2, ranging from 24.5 to 24.7°C, which is expected given the sunnier conditions. While rough water conditions may have introduced minor temperature fluctuations, the system maintained a stable range suitable for aquatic life, further contributing to a healthy environment for the aquaculture operations.

#### 4.9 Analysis for pH, TDS and Temperature

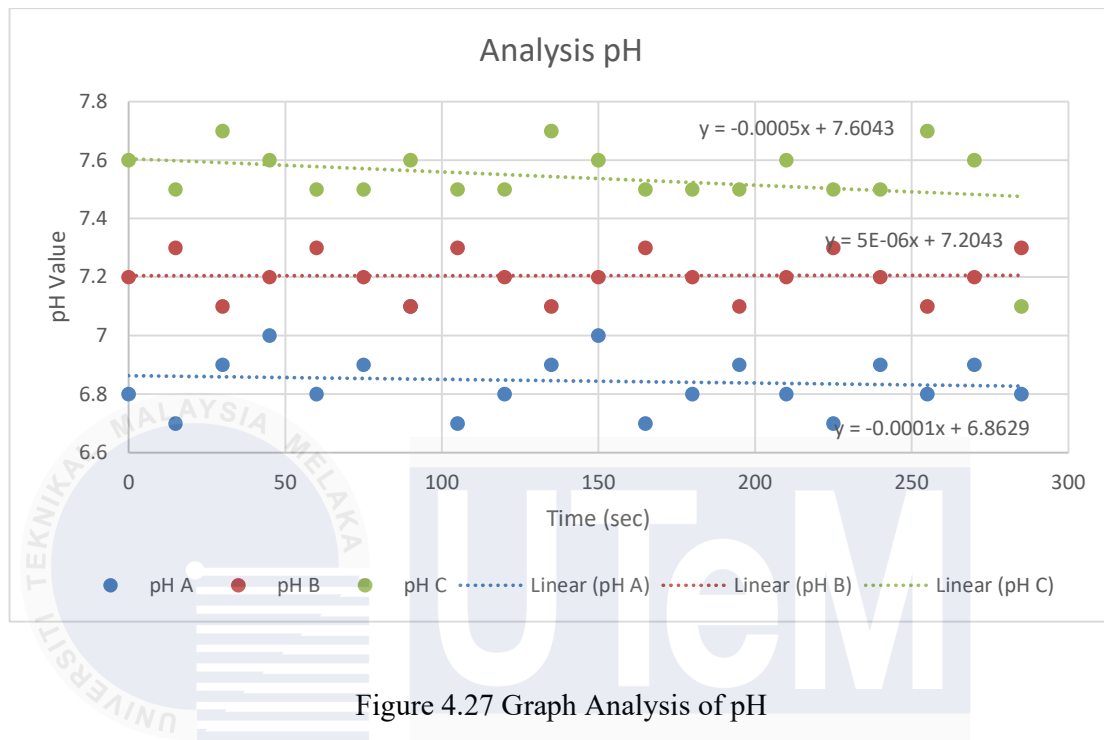


Figure 4.27 Graph Analysis of pH

Figure 4.27 shows the analysis for pH value at 3 different location. The linear trend displaying different slopes for each location. This indicates that the value of pH for each location changes over time. These changes may be due to various reasons, such as chemical reactions, biological activity and more. The summary of the pH analysis can be seen in Table 4.13.

Table 4.13 Summary of the pH analysis

SUMMARY				
Groups	Count	Sum	Average	Variance
pHA	20	136.9	6.845	0.01207895
pHB	20	144.1	7.205	0.00576316
pHC	20	150.8	7.54	0.01621053



Table 4.13 presents a summary of pH analysis. Each contains 20 data points, with their respective average pH values. All three groups have pH values within the recommended range for drinking water (6.5 to 8.5), suggesting acceptable water quality in terms of pH. pH A (6.845) is slightly acidic, while pH B (7.205) and pH C (7.54) are slightly alkaline. While these pH values are within the acceptable range, a comprehensive assessment of water quality requires considering other factors such as the source of water and the presence of other contaminants. Figure 4.28 shows the analysis of tds value for 3 location.

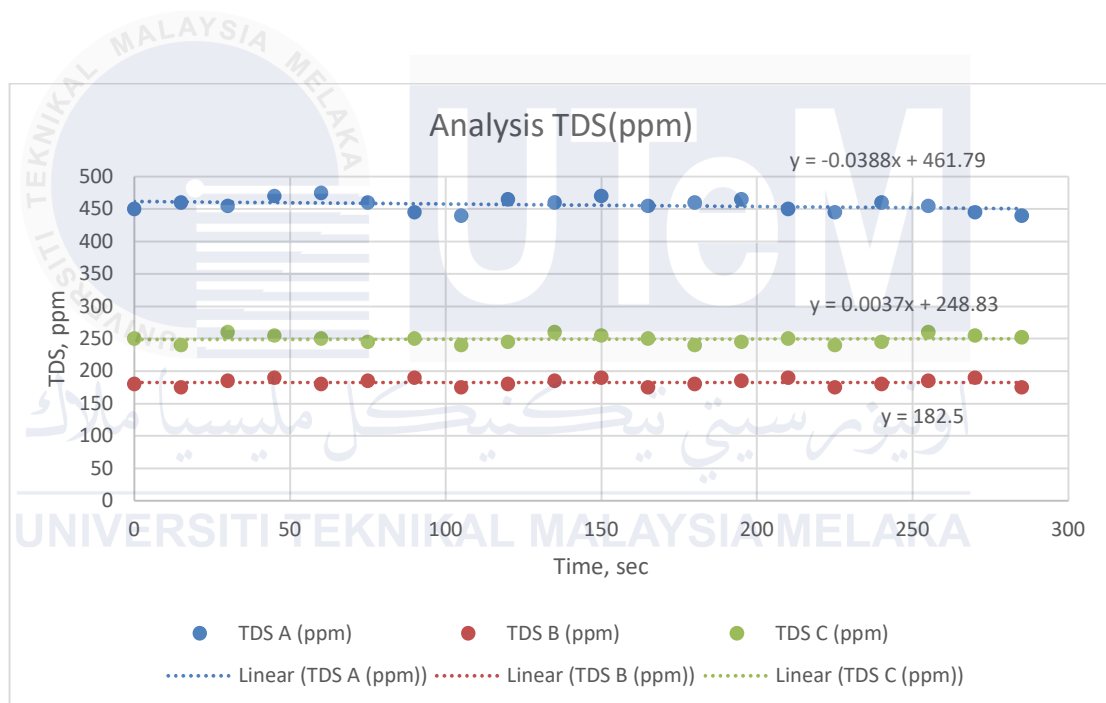


Figure 4.28 Graph Analysis for TDS

Figure 4.28 presents the tds analysis at 3 locations. TDS A shows a slight downward trend, indicating a gradual decrease in dissolved solids. TDS B exhibits a slight upward trend, suggesting an increase in dissolved solids. In contrast, TDS C remains relatively constant. While TDS levels within certain ranges are generally safe for drinking, higher levels can affect taste and may pose health concerns for some individuals. However, a

comprehensive assessment of water quality requires considering other parameters and the intended use of the water. Table 4.14 shows the summary of tds analysis.

Table 4.14 Summary of Tds analysis

<i>Groups</i>	<i>Count</i>	<i>Sum</i>	<i>Average</i>	<i>Variance</i>
TDS A (ppm)	20	9125	456.25	102.302632
TDS B (ppm)	20	3650	182.5	32.8947368
TDS C (ppm)	20	4987	249.35	45.8184211

From Table 4.14, TDS A has the highest average TDS value, which approaches the WHO recommended limit. TDS B has the lowest average TDS value and is considered safe for drinking. TDS C falls within the acceptable range for drinking water. However, further analysis and consideration of other water quality parameters are necessary for a complete evaluation of water quality. Figure 4.28 represent analysis of temperature at 3 location.

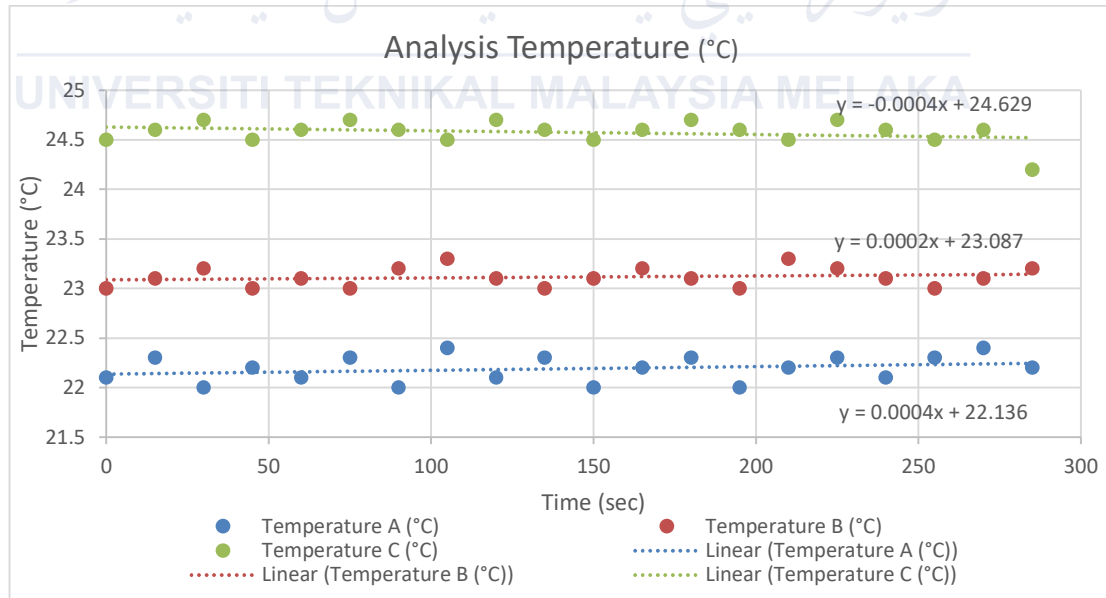


Figure 4.29 Graph Analysis of Temperature

Figure 4.29 presents three distinct data sets representing temperature over time. Temperature A shows a slight downward trend, indicating a gradual decrease in temperature. Temperature B exhibits a slight upward trend, suggesting a gradual increase in temperature. In contrast, Temperature C remains relatively constant. The slopes of the linear regression lines for each dataset are very small, indicating that the temperature changes are minor over time. Table 4.15 shows the summary of temperature analysis.

Table 4.15 Summary of Temperature analysis

SUMMARY				
<i>Groups</i>	<i>Count</i>	<i>Sum</i>	<i>Average</i>	<i>Variance</i>
Temperature A (°C)	20	443.8	22.19	0.017789474
Temperature B (°C)	20	462.3	23.115	0.009763158
Temperature C (°C)	20	491.5	24.575	0.013552632

Based on Table 4.15 , temperature A represents the coldest water, temperature C the warmest, and temperature B falls in between. While lower temperatures are generally more favorable for cold-water species, it's important to consider the specific temperature requirements of the target organisms and other water quality parameters for a comprehensive assessment of water temperature quality.

#### 4.10 Analysis for Solar

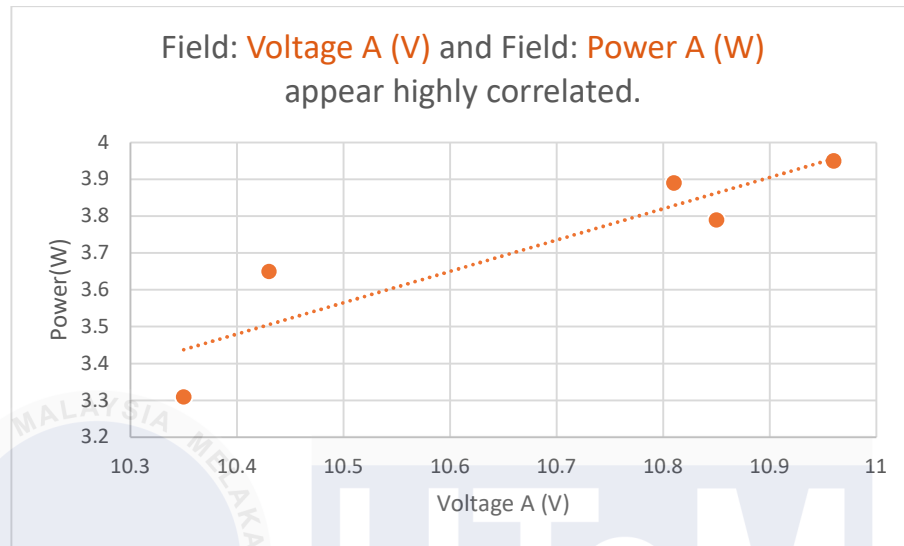


Figure 4.30 Graph Voltage A Vs Power A

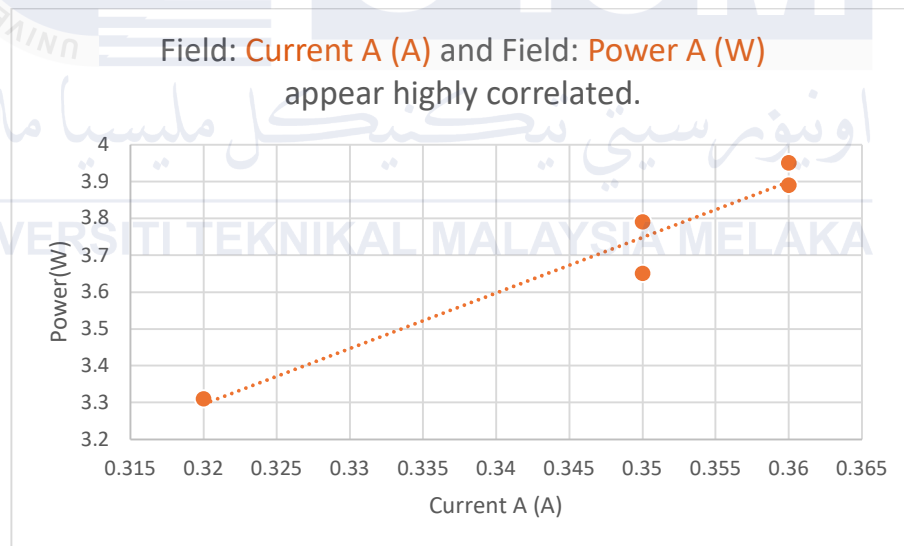


Figure 4.31 Graph Current A Vs Power A

The relationship between voltage, current, and power is shown in Figure 4.30 and Figure 4.31 . There is a clear positive link between the two plots, indicating that power rises in tandem with increases in either voltage or current. The fundamental electrical concept that power is directly proportional to both voltage and current is supported by this discovery. A

linear pattern is suggested by the dots drawn on both graphs, suggesting that a linear equation may be used to explain the relationship between these variables. The proportional constant between the variables is shown by the slope of the lines; a higher slope denotes a quicker rate of power change. Figure 4.32 and Figure 4.33 shows the correlation graph on voltage, current and power at location B.

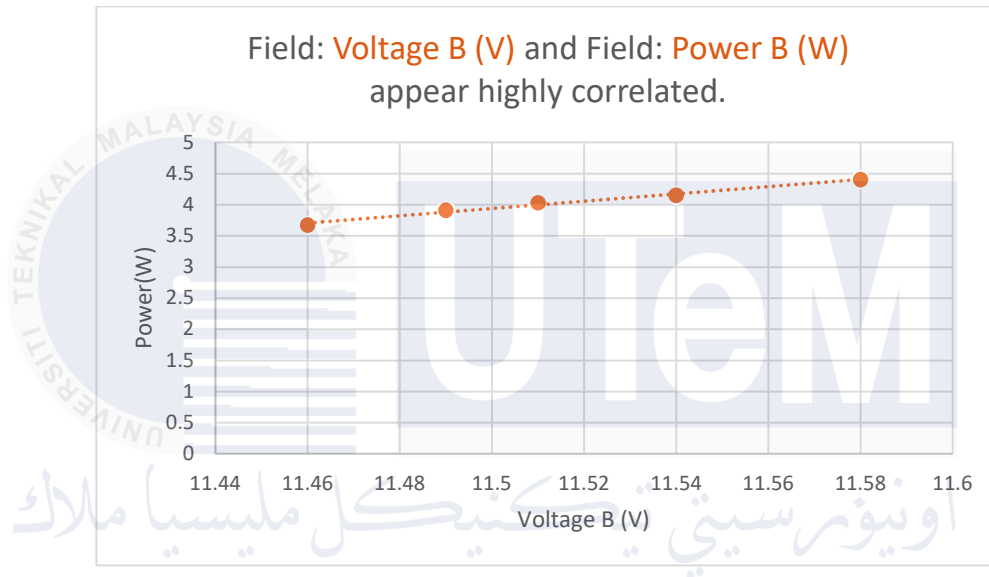


Figure 4.32 Graph Voltage B Vs Power B

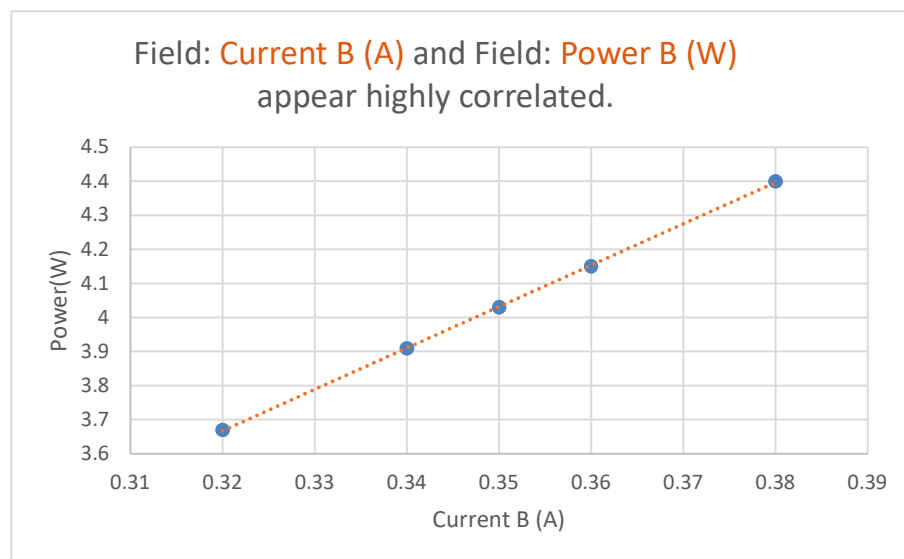


Figure 4.33 Graph Current B Vs Power B

Figure 4.32 and Figure 4.33 illustrate how voltage, current, and power are related for a different data set. Both plots reveal a strong positive correlation, meaning that increases in voltage (B) or current (B) lead to a rise in power (B). This observation is in accordance with the basic electrical principle that power is proportional to both voltage and current. The data points in the graphs suggest a linear pattern, indicating that the connection between these variables can be described by a linear equation. The slope of each line represents the proportional constant between the variables, with a steeper slope indicating a more significant change in power in response to voltage or current changes. Figure 4.34 and Figure 4.35 shows the graph for voltage, current and power at location C.

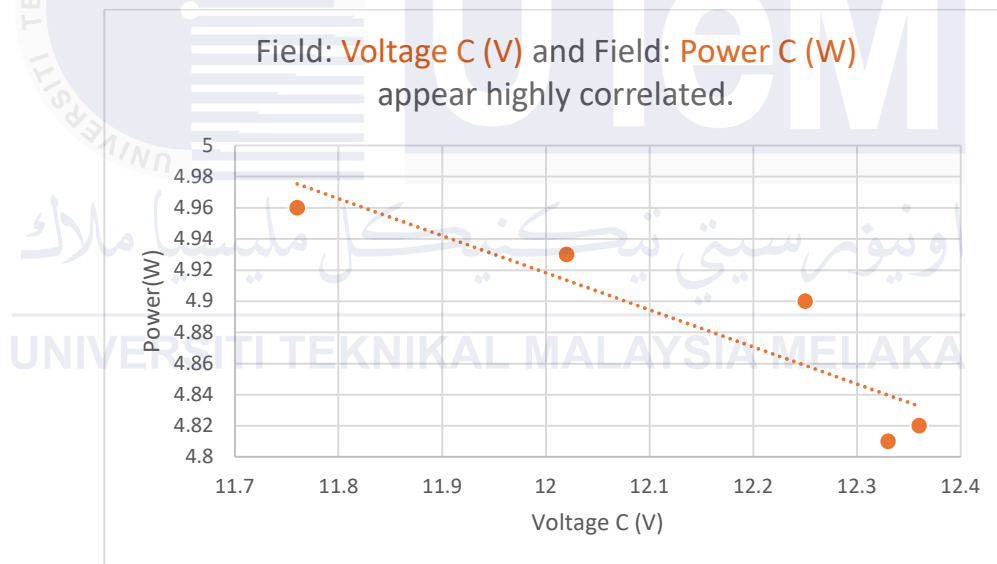


Figure 4.34 Graph Voltage C Vs Power C

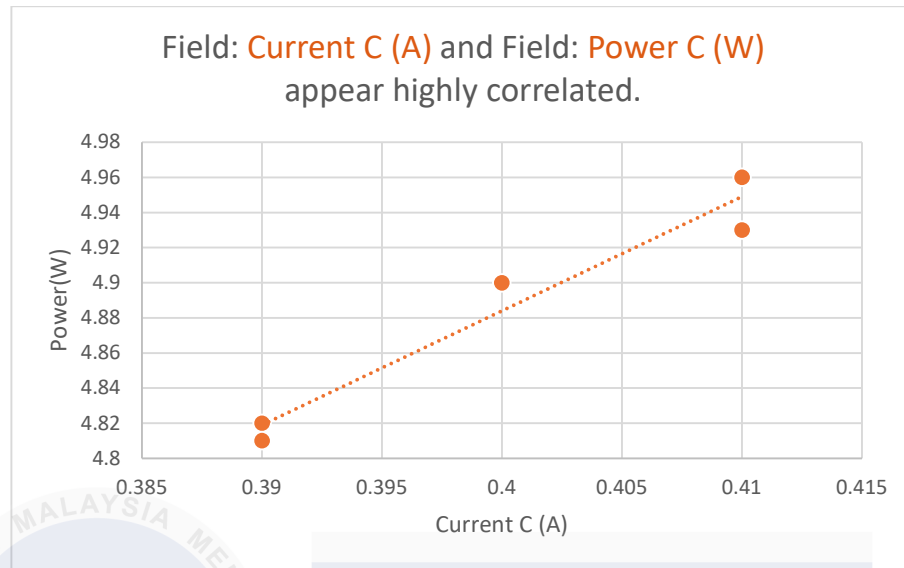


Figure 4.35 Graph Current C Vs Power C

Figure 4.34 and Figure 4.35 illustrate the connection between voltage, current, and power. The first chart, "Graph Voltage C Vs Power C," reveals an unexpected trend, showing a strong negative correlation between voltage (C) and power (C), which goes against the usual expectation in electrical circuits where power typically rises with voltage. On the other hand, the second chart, "Graph Current C Vs Power C," displays a strong positive correlation between current (C) and power (C), consistent with the fundamental principle that power is proportional to current. Both charts indicate a linear relationship between the variables, suggesting that the relationship can be modeled by a straight-line equation. The slope of the line represents the proportionality constant between the variables, with a steeper slope indicating a greater rate of change in power.

#### 4.11 Analysis of Battery Capacity

To estimate how long the battery can supply an ESP32 if the solar panel is disconnected or not charging the battery, a simple calculation for the runtime using the battery's capacity and the ESP32's power consumption had been done. The ESP32 chip consumes about 240 mA of power. The total energy stored in the supply can be calculated in watt-hours (Wh):

$$\text{Power consumption} = 240\text{mA} \times 3.3\text{V} = 0.792\text{W} \quad (4.1)$$

The power consumption of a 12V 7.2Ah sealed lead-acid (SLA) battery depends on how much energy it can provide over time. The specification can be seen in Appendix C. The energy capacity of the battery in watt-hours (Wh) is calculated as:

$$\text{Battery energy} = 7.2\text{Ah} \times 12\text{V} = 86.4\text{Wh} \quad (4.2)$$

The battery provides 12V, but the ESP32 operates at 3.3V using a step-down converter. Assuming 90% efficiency:

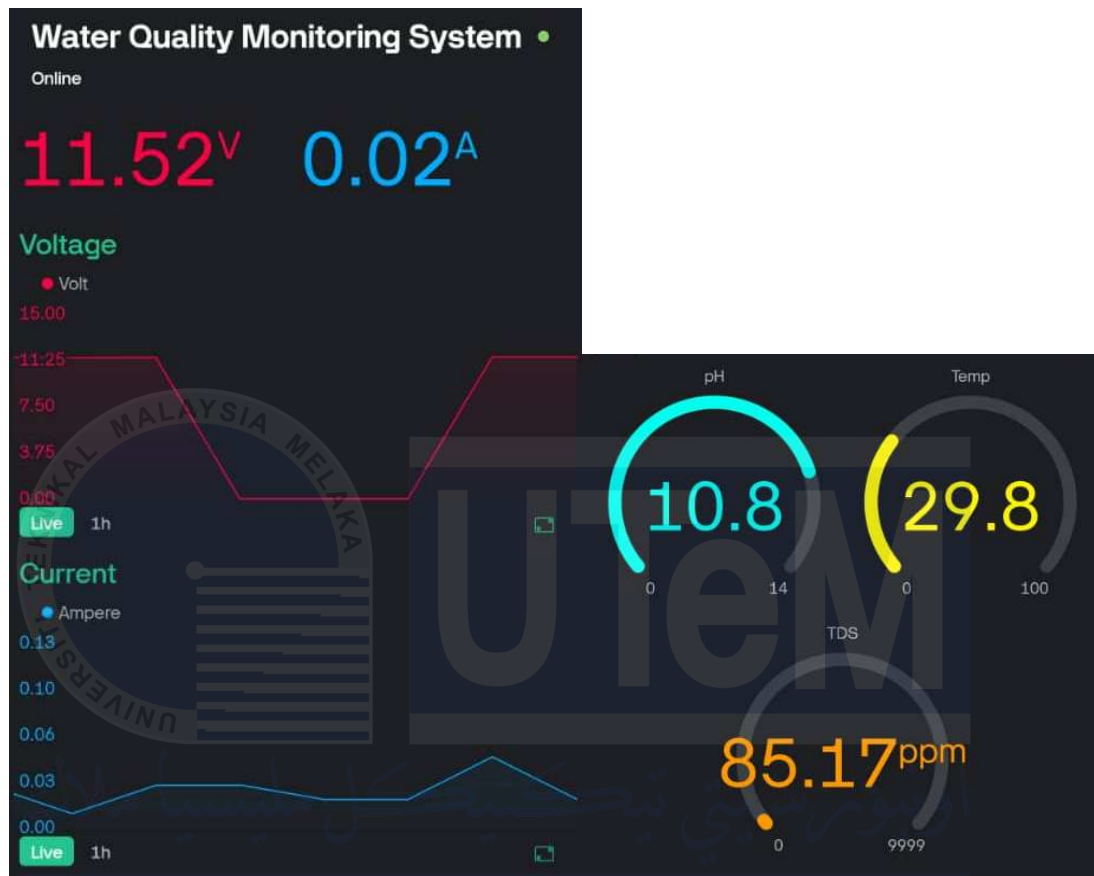
$$\text{Usable Energy for ESP32} = 86.4\text{Wh} \times 0.9 = 77.76\text{Wh} \quad (4.3)$$

$$\text{Runtime (hours)} = \frac{77.76\text{Wh}}{0.792\text{Wh}} = 98.2 \text{ hours} \approx 4.1 \text{ days} \quad (4.4)$$

From the calculation, an analysis of the battery capacity and esp32 power consumption had been proved. The battery can lasts 4days without charging by solar panel. With the monitoring system, an early detection for solar generation can seen for maintenance.



#### 4.12 Monitoring system



UNIVERSITI TEKNIKAL MALAYSIA MELAKA

Figure 4.36 Blynk app interface

Figure 4.36 presents the blynk app interface for monitoring the parameters measured. The voltage and current of the solar panel presented in standard display and super chart to monitor the solar generation over time. While the other 3 sensor of water quality only presented in gauge cause the value flactuate because of noise from the sensor.

#### 4.13 Summary

The analysis examined the weekly performance of a solar PV system, showing consistent voltage, current, and power fluctuations recorded at 8:00 AM, 12:00 PM, and 4:00 PM, with values generally rising and then falling. These fluctuations appear to be influenced by weather conditions. Voltage behavior, particularly at maximum power ( $V_{mp}$ ), typically peaked around midday and declined afterward, though one series showed a rise towards the end of the day. Current measurements mirrored this trend, with most days peaking at noon, except for one instance of increased current later in the day. Average power output consistently fell below the rated 5W.

The evaluation of a floatovoltaic system combined with water quality monitoring across three locations highlighted its adaptability. Location 1 demonstrated resilience despite poor conditions, Location 2 showed optimal performance under ideal conditions, and Location 3 proved effective in challenging environments like rough waters and heavy human activity. These findings emphasize the potential of this integrated system for sustainable environmental management in diverse aquatic settings, from small-scale to larger aquaculture systems.

## CHAPTER 5

### CONCLUSION AND RECOMMENDATIONS

#### 5.1 Conclusion

In conclusion, the project successfully achieved its objectives, demonstrating the effective integration of floating solar panels with a water quality monitoring system. The first objective, which focused on developing solar energy generation using floating solar panels, was successfully accomplished by utilizing renewable energy to power the entire monitoring system. Floating solar panels offer space efficiency, reduce land use, and improve energy generation, making them an ideal solution for water-based monitoring systems. The second objective, which involved implementing the water quality monitoring system using the ESP32 microcontroller and pH, TDS, and temperature sensors, was also successfully achieved. The sensors allowed for real-time monitoring of critical water parameters, ensuring accurate and reliable data for water quality analysis. The ESP32 provided seamless integration and control, ensuring the system's flexibility and scalability. The third objective, which involved analyzing the performance of the floating solar panels in the water quality monitoring system, was carried out through data experiments. The analysis confirmed that the floating solar panels were efficient in powering the system even under varying environmental conditions, ensuring the continuous operation of the monitoring setup. Overall, this project successfully integrated renewable energy with environmental monitoring, providing a sustainable and innovative solution for water quality assessment. The achievement of these objectives highlights the potential of combining solar

power with advanced monitoring technologies for more efficient and eco-friendly water quality management.

## **5.2 Future works**

For future work, several enhancements can be made to further improve the water quality monitoring system and its sustainability. One key improvement would be the addition of a data logger that stores water quality data locally when there is no Wi-Fi connection, ensuring continuous data collection and retrieval once connectivity is restored. Another potential enhancement is the integration of a self-cleaning mechanism for the floating solar panels. This would ensure optimal solar power generation by automatically removing dirt and debris that can accumulate on the panels, thus maintaining efficiency and extending their lifespan. Furthermore, additional sensors such as an oxygen sensor could be incorporated into the system to provide a more comprehensive analysis of water quality, enabling the monitoring of dissolved oxygen levels, which are critical for aquatic life. Additionally, the system could benefit from cloud-based solutions like MIT App Inventor or Firebase for data storage and remote monitoring, enabling real-time data access, enhanced user interaction, and data analytics. These future improvements would contribute to making the water quality monitoring system more robust, reliable, and scalable, offering better long-term performance and broader capabilities for environmental monitoring.

## REFERENCES

- [1] A. G. Olabi and M. A. Abdelkareem, 'Renewable energy and climate change', *Renewable and Sustainable Energy Reviews*, vol. 158, p. 112111, Apr. 2022, doi: 10.1016/J.RSER.2022.112111.
- [2] K. Ukoba, K. O. Yoro, O. Eterigho-Ikelegbe, C. Ibegbulam, and T. C. Jen, 'Adaptation of solar energy in the Global South: Prospects, challenges and opportunities', *Heliyon*, vol. 10, no. 7. Elsevier Ltd, Apr. 15, 2024. doi: 10.1016/j.heliyon.2024.e28009.
- [3] G. Wang, Z. Zhang, and J. Lin, 'Multi-energy complementary power systems based on solar energy: A review', *Renewable and Sustainable Energy Reviews*, vol. 199. Elsevier Ltd, Jul. 01, 2024. doi: 10.1016/j.rser.2024.114464.
- [4] A. Kudelin and V. Kutcherov, 'Wind ENERGY in Russia: The current state and development trends', *Energy Strategy Reviews*, vol. 34, Mar. 2021, doi: 10.1016/j.esr.2021.100627.
- [5] X. Costoya, M. deCastro, D. Carvalho, Z. Feng, and M. Gómez-Gesteira, 'Climate change impacts on the future offshore wind energy resource in China', *Renew Energy*, vol. 175, pp. 731–747, Sep. 2021, doi: 10.1016/j.renene.2021.05.001.
- [6] Kuan, J. Zhang, and T. Liu, 'Research on the environmental benefits of marine tidal energy and its impact on regional economic structure', *J Sea Res*, vol. 198, Apr. 2024, doi: 10.1016/j.seares.2024.102489.
- [7] V. Khare, C. J. Khare, and M. A. Bhuiyan, 'Prediction of tidal energy resources at Gulf of Kutch and Gulf of Khambhat by data mining', *Cleaner Energy Systems*, vol. 6, Dec. 2023, doi: 10.1016/j.cles.2023.100090.

- [8] E. Pasta, G. Papini, Y. Peña-Sanchez, F. D. Mosquera, F. Ferri, and N. Faedo, 'Data-based modelling of arrays of wave energy systems: Experimental tests, models, and validation', *Control Eng Pract*, vol. 148, Jul. 2024, doi: 10.1016/j.conengprac.2024.105949.
- [9] B. Joensen and H. B. Bingham, 'Economic feasibility study for wave energy conversion device deployment in Faroese waters', *Energy*, vol. 295, May 2024, doi: 10.1016/j.energy.2024.130869.
- [10] I. Martić, N. Degiuli, and C. G. Grlj, 'Scaling of wave energy converters for optimum performance in the Adriatic Sea', *Energy*, vol. 294, May 2024, doi: 10.1016/j.energy.2024.130922.
- [11] B. P. Singh, S. K. Goyal, and S. A. Siddiqui, 'Maximum power point estimation of MSX-60 poly-crystalline standalone solar PV system', *Mater Today Proc*, vol. 79, pp. 424–429, Jan. 2023, doi: 10.1016/j.matpr.2022.12.268.
- [12] A. Hassan, O. Bass, Y. M. Al-Abdeli, M. Masek, and M. A. S. Masoum, 'A novel approach for optimal sizing of stand-alone solar PV systems with power quality considerations', *International Journal of Electrical Power and Energy Systems*, vol. 144, Jan. 2023, doi: 10.1016/j.ijepes.2022.108597.
- [13] A. Niccolai, F. Grimaccia, G. Di Lorenzo, R. Araneo, F. Ughi, and M. Polenghi, 'A Review of Floating PV Systems With a Techno-Economic Analysis', *IEEE J Photovolt*, vol. 14, no. 1, pp. 23–34, Jan. 2024, doi: 10.1109/JPHOTOV.2023.3319601.
- [14] J. T. Dellosa, E. V. Palconit, and N. H. Enano, 'Risk Assessment and Policy Recommendations for a Floating Solar Photovoltaic (FSPV) System', *IEEE Access*, vol. 12, pp. 30452–30471, 2024, doi: 10.1109/ACCESS.2024.3368620.

- [15] A. Bhalkar, A. Wadekar, M. Wagh, and S. Dengle, 'Issues, challenges, and current lacunas in design, and installation of ground mounted solar PV module mounting structure (MMS)', *Mater Today Proc*, vol. 58, pp. 128–134, Jan. 2022, doi: 10.1016/j.matpr.2022.01.093.
- [16] O. Yemenici and M. O. Aksoy, 'An experimental and numerical study of wind effects on a ground-mounted solar panel at different panel tilt angles and wind directions', *Journal of Wind Engineering and Industrial Aerodynamics*, vol. 213, Jun. 2021, doi: 10.1016/j.jweia.2021.104630.
- [17] H. Y. Peng, S. S. Song, H. J. Liu, S. F. Dai, and F. L. Zhang, 'Investigation of wind loading characteristics of roof-mounted solar panels on tall buildings', *Sustainable Energy Technologies and Assessments*, vol. 54, Dec. 2022, doi: 10.1016/j.seta.2022.102800.
- [18] H. Alrawashdeh and T. Stathopoulos, 'Wind loads on solar panels mounted on flat roofs: Effect of geometric scale', *Journal of Wind Engineering and Industrial Aerodynamics*, vol. 206, Nov. 2020, doi: 10.1016/j.jweia.2020.104339.
- [19] C. Correa, D. Dujovne, and F. Bolano, 'Design and Implementation of an Embedded Edge-Processing Water Quality Monitoring System for Underground Waters', *IEEE Embed Syst Lett*, vol. 15, no. 2, pp. 81–84, Jun. 2023, doi: 10.1109/LES.2022.3184925.
- [20] A. Abu Sneineh and A. A. A. Shabaneh, 'Design of a smart hydroponics monitoring system using an ESP32 microcontroller and the Internet of Things', *MethodsX*, vol. 11, Dec. 2023, doi: 10.1016/j.mex.2023.102401.
- [21] L. E. Kane, J. J. Chen, R. Thomas, V. Liu, and M. McKague, 'Security and Performance in IoT: A Balancing Act', *IEEE Access*, vol. 8, pp. 121969–121986, 2020, doi: 10.1109/ACCESS.2020.3007536.

- [22] R. Muniz, J. Diaz, F. Nuno, M. J. Prieto, and A. M. Pernia, 'A smart power meter to recharge electric vehicles in communal parking areas', *IEEE Internet Things J*, vol. 6, no. 2, pp. 3448–3454, Apr. 2019, doi: 10.1109/JIOT.2018.2885171.
- [23] Y. Sangeetha, P. S. Sashank, C. V. Satyanarayana, and M. Geethika, 'Development of Weight System Embedded with Tracking System using Arduino UNO Rev3', in *Proceedings - 7th International Conference on Computing Methodologies and Communication, ICCMC 2023*, Institute of Electrical and Electronics Engineers Inc., 2023, pp. 1411–1416. doi: 10.1109/ICCMC56507.2023.10084100.
- [24] M. R. M. Veeramanickam, B. Venkatesh, L. A. Bewoor, Y. W. Bhowte, K. Moholkar, and J. L. Bangare, 'IoT based smart parking model using Arduino UNO with FCFS priority scheduling', *Measurement: Sensors*, vol. 24, Dec. 2022, doi: 10.1016/j.measen.2022.100524.
- [25] A. Ananthanarayanan, T. Sivasai, D. D. Gowda, G. H. T. Ganya, and K. S. Shreyas, 'Smart Mirror Using Rasberry Pi for Human Monitoring and Intrusion Detection', in *Proceedings - 2021 International Conference on Design Innovations for 3Cs Compute Communicate Control, ICDI3C 2021*, Institute of Electrical and Electronics Engineers Inc., Jun. 2021, pp. 207–210. doi: 10.1109/ICDI3C53598.2021.00049.
- [26] I. Binti, M. Syawal, F. Bin, and M. Khairul, 'Identification of Fruit Size and Maturity Through Fruit Images Using OpenCV-Python and Rasberry Pi'.
- [27] V. Lakshmikantha, A. Hiriyanagowda, A. Manjunath, A. Patted, J. Basavaiah, and A. A. Anthony, 'IoT based smart water quality monitoring system', *Global Transitions Proceedings*, vol. 2, no. 2, pp. 181–186, Nov. 2021, doi: 10.1016/J.GLTP.2021.08.062.



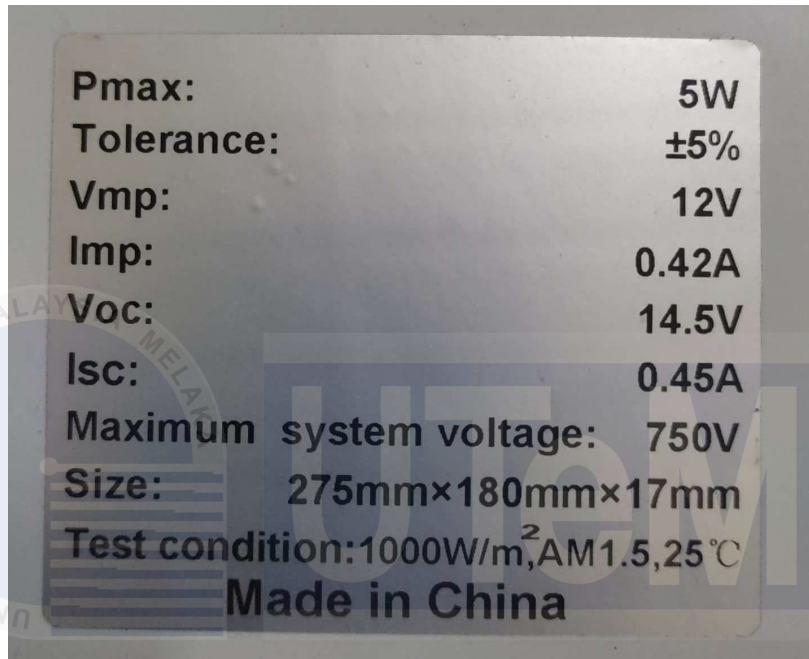
- [28] Y. Wen, Y. Mao, Q. Luo, and X. Wang, 'Smart pH Sensor Using Untreated Platinum Sheet Based on Chronopotentiometry and Long-Term Stability Analysis', *IEEE Sens J*, vol. 19, no. 10, pp. 3841–3845, May 2019, doi: 10.1109/JSEN.2019.2897073.
- [29] U. Mithra, A. Shrivastava, K. S. Devan, R. Bhaskar, V. Vijayakumar, and S. Sarveswari, 'Development of a pH sensor in range 7–11 using 9H-fluorene and its application in real samples', *Inorg Chem Commun*, vol. 166, Aug. 2024, doi: 10.1016/j.inoche.2024.112632.
- [30] H. Xu, W. Wang, W. Deng, and Z. Lun, 'Design of portable refrigerator based on DS18B20 temperature sensor', in *2023 2nd International Symposium on Sensor Technology and Control, ISSTC 2023*, Institute of Electrical and Electronics Engineers Inc., 2023, pp. 32–36. doi: 10.1109/ISSTC59603.2023.10281139.
- [31] D. Bora, D. Singh, and B. Negi, 'Utilization of DS18B20 Temperature Sensor for Predictive Maintenance of Reciprocating Compressor', in *2023 International Conference on Power Energy, Environment and Intelligent Control, PEEIC 2023*, Institute of Electrical and Electronics Engineers Inc., 2023, pp. 147–150. doi: 10.1109/PEEIC59336.2023.10450639.
- [32] L. Andraini, Styawati, and A. Surahman, 'Design and Implementation of 02244 TDS Meter Gravity Sensor and 4502C pH Sensor on Hydroponic', in *2022 International Conference on Information Technology Research and Innovation, ICITRI 2022*, Institute of Electrical and Electronics Engineers Inc., 2022, pp. 129–134. doi: 10.1109/ICITRI56423.2022.9970236.
- [33] B. Suwandi *et al.*, 'Development of a Low-Cost TDS Sensor Using an Electric Plug with The Curve Fitting Method Approaches', in *Proceeding - 2022 International Conference on Radar, Antenna, Microwave, Electronics, and Telecommunications: Emerging Science and Industrial Innovation in Electronics and Telecommunication*,

- ICRAMET 2022*, Institute of Electrical and Electronics Engineers Inc., 2022, pp. 83–87. doi: 10.1109/ICRAMET56917.2022.9991206.
- [34] J. Trevathan, W. Read, and S. Schmidtke, ‘Towards the development of an affordable and practical light attenuation turbidity sensor for remote near real-time aquatic monitoring’, *Sensors (Switzerland)*, vol. 20, no. 7, Apr. 2020, doi: 10.3390/s20071993.
- [35] S. H. Shovo and S. Karmarker, ‘Solar Based Smart Water Pump Control with Turbidity and pH Measuring System’, in *International Conference on Robotics, Electrical and Signal Processing Techniques*, Institute of Electrical and Electronics Engineers Inc., 2023, pp. 223–227. doi: 10.1109/ICREST57604.2023.10070048.
- [36] J. Fonseca-Campos, I. Reyes-Ramirez, L. Guzman-Vargas, L. Fonseca-Ruiz, J. A. Mendoza-Perez, and P. F. Rodriguez-Espinosa, ‘Multiparametric System for Measuring Physicochemical Variables Associated to Water Quality Based on the Arduino Platform’, *IEEE Access*, vol. 10, pp. 69700–69713, 2022, doi: 10.1109/ACCESS.2022.3187422.
- [37] P. Suwanno, P. Chansri, and Y. Joothong, ‘IoT Assisted Oxygen Control Monitoring in Microbial Propagation for Shrimp Ponds’, in *Proceeding - 2023 International Electrical Engineering Congress, iEECON 2023*, Institute of Electrical and Electronics Engineers Inc., 2023, pp. 285–288. doi: 10.1109/iEECON56657.2023.10127007.
- [38] M. M. Nabi and A. Kharaz, ‘Design and Deployment of Dissolved Oxygen Remote Monitoring and Control for The Environmental Agency Using IoT’, in *9th 2023 International Conference on Control, Decision and Information Technologies, CoDIT 2023*, Institute of Electrical and Electronics Engineers Inc., 2023, pp. 494–499. doi: 10.1109/CoDIT58514.2023.10284326.

- [39] Y. Wang, I. W. H. Ho, Y. Chen, Y. Wang, and Y. Lin, 'Real-Time Water Quality Monitoring and Estimation in AIoT for Freshwater Biodiversity Conservation', *IEEE Internet Things J*, vol. 9, no. 16, pp. 14366–14374, Aug. 2022, doi: 10.1109/JIOT.2021.3078166.
- [40] 'View of Real Time Monitoring for Smart Water Quality'.
- [41] O. O. Ajayi, A. B. Bagula, H. C. Maluleke, Z. Gaffoor, N. Jovanovic, and K. C. Pietersen, 'WaterNet: A Network for Monitoring and Assessing Water Quality for Drinking and Irrigation Purposes', *IEEE Access*, vol. 10, pp. 48318–48337, 2022, doi: 10.1109/ACCESS.2022.3172274.
- [42] A. Q. S. Bahri, Y. W. M. Yusof, and M. Kassim, 'Solar Powered Smart Water Monitoring System Based on IoT and Blynk Platform', in *2023 IEEE International Conference on Automatic Control and Intelligent Systems, I2CACIS 2023 - Proceedings*, Institute of Electrical and Electronics Engineers Inc., 2023, pp. 189–194. doi: 10.1109/I2CACIS57635.2023.10193008.
- [43] A. C. D. S. Junior, R. Munoz, M. D. L. A. Quezada, A. V. L. Neto, M. M. Hassan, and V. H. C. D. Albuquerque, 'Internet of water things: A remote raw water monitoring and control system', *IEEE Access*, vol. 9, pp. 35790–35800, 2021, doi: 10.1109/ACCESS.2021.3062094.

## APPENDICES

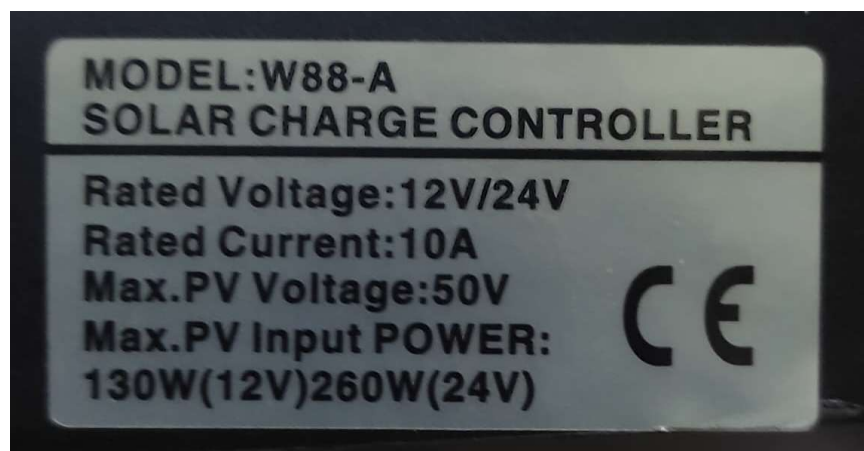
### Appendix A Solar panel specification



A photograph of a white rectangular label with black text, mounted on a solar panel. The label lists technical specifications for a 5W solar panel. A faint watermark of the University of Teknikal Malaysia Melaka is visible in the background.

<b>Pmax:</b>	<b>5W</b>
<b>Tolerance:</b>	<b>±5%</b>
<b>Vmp:</b>	<b>12V</b>
<b>Imp:</b>	<b>0.42A</b>
<b>Voc:</b>	<b>14.5V</b>
<b>Isc:</b>	<b>0.45A</b>
<b>Maximum system voltage:</b>	<b>750V</b>
<b>Size:</b>	<b>275mm×180mm×17mm</b>
<b>Test condition:</b>	<b>1000W/m<sup>2</sup>, AM1.5, 25°C</b>
<b>Made in China</b>	

### Appendix B Solar Charge Controller specification



A photograph of a white rectangular label with black text, mounted on a solar charge controller. The label lists technical specifications for a W88-A model. A CE mark is visible on the right side. A faint watermark of the University of Teknikal Malaysia Melaka is visible in the background.

<b>MODEL:W88-A</b>	
<b>SOLAR CHARGE CONTROLLER</b>	
<b>Rated Voltage:12V/24V</b>	
<b>Rated Current:10A</b>	
<b>Max.PV Voltage:50V</b>	
<b>Max.PV Input POWER:</b>	
<b>130W(12V)260W(24V)</b>	

**CE**

## Appendix C Battery specification

<b>GPP 1272</b> <b>12V 7.2AH</b>	<b>CONSTANT VOLTAGE CHARGING</b>	
	CYCLE USE	: 14.5 - 14.9V
	STANDBY USE	: 13.6 - 13.8V
	INITIAL CURRENT	: LESS THAN 2.1A

## Appendix D ESP32 Active Mode



## Appendix E TDS sensor arduino coding

```
#define TdsSensorPin A1
#define VREF 5.0      // analog reference voltage(Volt) of the ADC
#define SCOUNT 30      // sum of sample point
int analogBuffer[SCOUNT]; // store the analog value in the array, read
from ADC
int analogBufferTemp[SCOUNT];
int analogBufferIndex = 0,copyIndex = 0;
float averageVoltage = 0,tdsValue = 0,temperature = 25;

void setup()
{
    Serial.begin(115200);
    pinMode(TdsSensorPin,INPUT);
}

void loop()
{
    static unsigned long analogSampleTimepoint = millis();
    if(millis()-analogSampleTimepoint > 400) //every 400
    milliseconds,read the analog value from the ADC
    {
        analogSampleTimepoint = millis();
        analogBuffer[analogBufferIndex] = analogRead(TdsSensorPin); //read
the analog value and store into the buffer
        analogBufferIndex++;
        if(analogBufferIndex == SCOUNT)
            analogBufferIndex = 0;
    }
    static unsigned long printTimepoint = millis();
    if(millis()-printTimepoint > 800)
    {
        printTimepoint = millis();
        for(copyIndex=0;copyIndex<SCOUNT;copyIndex++)
            analogBufferTemp[copyIndex]= analogBuffer[copyIndex];
        averageVoltage = getMedianNum(analogBufferTemp,SCOUNT) * (float)VREF
/ 1024.0; // read the analog value more stable by the median filtering
algorithm, and convert to voltage value
        float compensationCoefficient=1.0+0.02*(temperature-
25.0); //temperature compensation formula: fFinalResult(25^C) =
fFinalResult(current)/(1.0+0.02*(fTP-25.0));
        float
compensationVolatge=averageVoltage/compensationCoefficient; //temperature
compensation
```

```

        tdsValue=(133.42*compensationVolatge*compensationVolatge*compensatio
nVolatge - 255.86*compensationVolatge*compensationVolatge +
857.39*compensationVolatge)*0.5; //convert voltage value to tds value
        Serial.print("voltage:");
        Serial.print(averageVoltage,2);
        Serial.print("V   ");
        Serial.print("TDS Value:");
        Serial.print(tdsValue,0);
        Serial.println("ppm");
    }
}
int getMedianNum(int bArray[], int iFilterLen)
{
    int bTab[iFilterLen];
    for (byte i = 0; i<iFilterLen; i++)
        bTab[i] = bArray[i];
    int i, j, bTemp;
    for (j = 0; j < iFilterLen - 1; j++)
    {
        for (i = 0; i < iFilterLen - j - 1; i++)
        {
            if (bTab[i] > bTab[i + 1])
            {
                bTemp = bTab[i];
                bTab[i] = bTab[i + 1];
                bTab[i + 1] = bTemp;
            }
        }
    }
    if ((iFilterLen & 1) > 0)
        bTemp = bTab[(iFilterLen - 1) / 2];
    else
        bTemp = (bTab[iFilterLen / 2] + bTab[iFilterLen / 2 - 1]) / 2;
    return bTemp;
}

```

## Appendix F pH sensor arduino coding

```

#include <Wire.h>
#include <LiquidCrystal_I2C.h>
LiquidCrystal_I2C lcd(0x3F, 16, 2);
float calibration_value = 21.34;
int phval = 0;
unsigned long int avgval;
int buffer_arr[10],temp;
void setup()

```

```

{
  Serial.begin(9600);
  lcd.init();
  lcd.begin(16, 2);
  lcd.backlight();
  lcd.setCursor(0, 0);
  lcd.print("  Welcome to      ");
  lcd.setCursor(0, 1);
  lcd.print(" Circuit Digest    ");
  delay(2000);
  lcd.clear();
}

void loop() {
  for(int i=0;i<10;i++)
  {
    buffer_arr[i]=analogRead(A0);
    delay(30);
  }
  for(int i=0;i<9;i++)
  {
    for(int j=i+1;j<10;j++)
    {
      if(buffer_arr[i]>buffer_arr[j])
      {
        temp=buffer_arr[i];
        buffer_arr[i]=buffer_arr[j];
        buffer_arr[j]=temp;
      }
    }
  }
  avgval=0;
  for(int i=2;i<8;i++)
  avgval+=buffer_arr[i];
  float volt=(float)avgval*5.0/1024/6;
  float ph_act = -5.70 * volt + calibration_value;
  Serial.print("pH Val:");
  Serial.print(ph_act);
  delay(1000);
}

```

## Appendix G Temperature sensor arduino coding

```

#include <OneWire.h>
#include <DallasTemperature.h>
const int SENSOR_PIN = 13; // Arduino pin connected to DS18B20 sensor's DQ
pin

```



```

OneWire oneWire(SENSOR_PIN);          // setup a oneWire instance
DallasTemperature tempSensor(&oneWire); // pass oneWire to
DallasTemperature library
float tempCelsius;    // temperature in Celsius
float tempFahrenheit; // temperature in Fahrenheit
void setup()
{
    Serial.begin(9600); // initialize serial
    tempSensor.begin(); // initialize the sensor
}
void loop()
{
    tempSensor.requestTemperatures(); // send the command to get
temperatures
    tempCelsius = tempSensor.getTempCByIndex(0); // read temperature in
Celsius
    tempFahrenheit = tempCelsius * 9 / 5 + 32; // convert Celsius to
Fahrenheit
    Serial.print("Temperature: ");
    Serial.print(tempCelsius); // print the temperature in Celsius
    Serial.print("°C");
    Serial.print(" ~ "); // separator between Celsius and
Fahrenheit
    Serial.print(tempFahrenheit); // print the temperature in Fahrenheit
    Serial.println("°F");
    delay(500);
}

```

UNIVERSITI TEKNIKAL MALAYSIA MELAKA

#### Appendix H Full system coding

```

#define BLYNK_TEMPLATE_ID "TMPL6R184pv7k"
#define BLYNK_TEMPLATE_NAME "Water Quality Monitoring System"
#define BLYNK_AUTH_TOKEN "LXznP1IIIf_hSnQn2iTZglJaa8-nzMr_8"

#include <Wire.h>
#include <LiquidCrystal_PCF8574.h>
#include <WiFi.h>
#include <BlynkSimpleEsp32.h>
#include <DallasTemperature.h>
#include <OneWire.h>

// WiFi and Blynk credentials
char auth[] = BLYNK_AUTH_TOKEN;
char ssid[] = "Hotspot Free";
char pass[] = "adibnordin";

```

```

#define REF_VOLTAGE 3.3
#define ADC_RESOLUTION 4096
#define PH_PIN 36
#define TDS_PIN 39
#define TEMP_PIN 33
#define VOLTAGE_PIN 34
#define CURRENT_PIN 32

//int pHValue = 0;
int tdsValue = 0;
int temperature = 0;
float calibrationFactor = 0.0014;

// Temperature Sensor
OneWire oneWire(TEMP_PIN);
DallasTemperature sensors(&oneWire);

// Voltage sensor
float R1 = 30000.0;
float R2 = 7500.0;

// ACS712 Current Sensor
const int mVperAmp = 185;

// Set the I2C address for the LCD (commonly 0x27 or 0x3F)
#define I2C_ADDR 0x27
LiquidCrystal_PCF8574 lcd(I2C_ADDR);

// Timers
BlynkTimer timer;

void setup() {
  Serial.begin(115200);
  delay(1000);

  lcd.begin(16,2);
  lcd.setBacklight(255);

  // Set ADC resolution
  analogReadResolution(12);
  analogSetAttenuation(ADC_11db); // Full range: 0 to 3.3V

  sensors.begin(); // Initialize DS18B20

  WiFi.begin(ssid, pass);

```

```

while (WiFi.status() != WL_CONNECTED) {
    delay(500);
    Serial.print(".");
}
Serial.println("\nWiFi connected!");

// Configure Blynk (non-blocking)
Blynk.config(auth);
Blynk.connect();

// Timer to send data to Blynk every 2 seconds
timer.setInterval(1000L, sendToBlynk);
}

void loop() {
    Blynk.run();
    timer.run();

    // Read pH sensor
    int phAnalogValue = analogRead(36);
    float phVoltage = phAnalogValue * (REF_VOLTAGE / ADC_RESOLUTION);
    float pHValue = phVoltage * REF_VOLTAGE ;

    // Read DS18B20 temperature sensor
    sensors.requestTemperatures();
    float temperature = sensors.getTempCByIndex(0);

    // Read TDs sensor
    int sensorValue = analogRead(39);
    float tdsVoltage = sensorValue * REF_VOLTAGE / ADC_RESOLUTION;
    float tdsValue = tdsVoltage / calibrationFactor;

    // Voltage sensor reading
    int adcValue = analogRead(34);
    float adcVoltage = adcValue * REF_VOLTAGE / ADC_RESOLUTION;
    float inputVoltage = adcVoltage / (R2 / (R1 + R2));

    // ACS712 Current Sensor reading
    int adc = analogRead(32);
    float voltage = adc * REF_VOLTAGE / ADC_RESOLUTION;
    float current = 0;
    if (voltage < 1.54) {
        current = (1.54 - voltage) / 0.185;
    } else {
        current = (voltage - 1.54) / 0.185;
    }
}

```

```

// Display results
Serial.print("\npH Value: ");
Serial.println(pHValue, 2);
Serial.print("TDS Value: ");
Serial.print(tdsValue, 2);
Serial.println(" ppm");
Serial.print("Temperature: ");
Serial.print(temperature, 2);
Serial.println(" °C");
Serial.print("Input Voltage:");
Serial.print(inputVoltage,2);
Serial.println(" V");
Serial.print("Current:");
Serial.print(current,2);
Serial.println(" A");
delay(50);

// Display on LCD
lcd.clear();
lcd.setCursor(0, 0);
lcd.print("pH:");
lcd.print(pHValue,2);
lcd.setCursor(0, 1);
lcd.print("TDS:");
lcd.print(tdsValue);
delay(2000);
lcd.clear();
lcd.setCursor(0, 0);
lcd.print("Temp:");
lcd.print(temperature,2);
lcd.setCursor(0, 1);
lcd.print("V:");
lcd.print(inputVoltage, 2);
lcd.setCursor(8, 1);
lcd.print("C:");
lcd.print(current, 2);
delay(2000);
}

void sendToBlynk() {

    // Read pH sensor
    int phAnalogValue = analogRead(36);
    float phVoltage = phAnalogValue * REF_VOLTAGE / ADC_RESOLUTION;

```

```

float pHValue = pHVoltage * REF_VOLTAGE ;

// Read DS18B20 temperature sensor
sensors.requestTemperatures();
float temperature = sensors.getTempCByIndex(0);

// Read TDS sensor
int sensorValue = analogRead(39);
float tdsVoltage = sensorValue * REF_VOLTAGE / ADC_RESOLUTION;
float tdsValue = tdsVoltage / calibrationFactor;

//Voltage Sensor reading
int adcValue = analogRead(34);
float adcVoltage = adcValue * REF_VOLTAGE / ADC_RESOLUTION;
float inputVoltage = adcVoltage / (R2 / (R1 + R2));

// ACS712 Current Sensor reading
int adc = analogRead(32);
float voltage = adc * REF_VOLTAGE / ADC_RESOLUTION;
float current = 0;
if (voltage < 1.54) {
    current = (1.54 - voltage) / 0.185;
} else {
    current = (voltage - 1.54) / 0.185;
}

// Send data to Blynk
Blynk.virtualWrite(V0, temperature);
Blynk.virtualWrite(V1, tdsValue);
Blynk.virtualWrite(V2, pHValue);
Blynk.virtualWrite(V3, inputVoltage);
Blynk.virtualWrite(V4, current);
}

```